INSTABILITY IN TWO ROTATING SYSTEMS: THERMAL CONVECTION AND LANGMUIR CIRCULATION

A Dissertation

Presented to the Faculty of the Graduate School

of Cornell University

in Partial Fulfillment of the Requirements for the Degree of

Doctor of Philosophy

by

Beverly Ann Thurber

May 2009

INSTABILITY IN TWO ROTATING SYSTEMS: THERMAL CONVECTION AND LANGMUIR CIRCULATION

Beverly Ann Thurber, Ph.D.

Cornell University 2009

In this dissertation, two related problems are considered: rotating Rayleigh-Bénard convection and Langmuir circulation with thermal effects. These two phenomena can be modeled using similar equation systems because convection rolls and Langmuir circulation windrows are physically similar, although the two driving processes differ.

The first part of this dissertation is concerned with rotating convection, for which fully three-dimensional amplitude equations are derived for both stationary and Hopf bifurcations. These take the form of one equation (stationary bifurcation) or two coupled equations (Hopf bifurcation) of the Ginzburg-Landau type, coupled to an additional equation for the mean drift. The coefficients of the Ginzburg-Landau type equation(s) are derived analytically for systems with stress-free boundaries that undergo stationary and Hopf bifurcations and numerically for systems with rigid boundaries that undergo stationary bifurcations. Criteria for the stability of a single traveling wave solution are given.

In the second part of this dissertation, the effect of thermal variations on Langmuir circulation is considered. Results of the linearized problem are presented and show how the critical values vary with latitude and wind direction. Stable temperature stratification, represented by a negative Rayleigh number, makes it more difficult for Langmuir circulations to form, as shown by an increase in the critical Reynolds number. However, in all cases considered, Langmuir circulations were able to form. Changes in latitude and wind direction do not significantly alter the critical values.

The patterns formed by Langmuir circulation are described using a multi-mode model based on the results of the linear problem. Slightly above critical, a band of unstable modes interacts to form patterns on the ocean surface. These patterns are shown to have Y-junctions at points where the temperature perturbation is zero. In the temperature field, the orientation of the Y-junctions is biased downwind.

BIOGRAPHICAL SKETCH

Bev Thurber received simultaneous Bachelor of Science degrees in Mathematics and Humanities from the Massachusetts Institute of Technology in 2001. The following year she received the degree of Master of Philosophy in Anglo-Saxon, Norse and Celtic from Cambridge University. In fall 2002 she joined Cornell's department of Theoretical and Applied Mechanics. From August 2007 to March 2009 she was in Heidelberg, Germany, learning amazing things unrelated to this dissertation.

ACKNOWLEDGEMENTS

I would like to acknowledge the substantial contributions of my excellent cats, Pi and George, and thank the following people:

- Sid Leibovich, for his good advice.
- Wayne Harbert and Kerry Cook, for being on my committee, and for teaching me lots of interesting things.
- Steve Colucci, for substituting for Kerry Cook in my B Exam.
- Bobby Piankian, for comments on a draft.
- Erik Martens, for help with some of the code.
- Cindy Twardokus, for her paperwork expertise.
- Emily Minturn, for her technological heroism right before my B Exam.

I was supported by a General Electric Foundation Fellowship, a National Science Foundation Graduate Research Fellowship, a Cornell University Provost's Diversity Fellowship, and a Cornell-Heidelberg Exchange Fellowship.

TABLE OF CONTENTS

LIST OF FIGURES

LIST OF TABLES

CHAPTER 1

INTRODUCTION

This dissertation is concerned with two related phenomena, rotating Rayleigh-Bénard convection and Langmuir circulation. Both occur as the result of instability in a fluid layer, and they are linked by their visual manifestations: both phenomena cause stripes to appear on the surface. Although the driving mechanisms differ, the physical results are similar and allow the two to be studied using similar models. The driving factor behind thermal convection is the temperature difference between the top and bottom boundaries. Langmuir circulation is driven by the wind, but the effects of rotation and thermal variation are investigated here, allowing its model to be linked to rotating convection.

Thermal convection is a well-studied problem in fluid mechanics because it is one of the simples pattern-forming systems. The addition of rotation is a natural way to extend the system, especially when geophysical applications are of interest. A typical experimental apparatus consists of a horizontal region of fluid with boundaries a distance d apart, as shown in figure 1.1. In the simplest configuration, the boundaries are kept at constant temperatures, with the top boundary cooler than the bottom. This produces a linear temperature gradient, $T = \bar{T}(z)$. A very basic version of this experiment is a pot of water on a stove. The bottom surface of the water is heated by the stove, and the top is cooled by evaporation. When the system becomes unstable, the warm, light fluid on the bottom of the container begins to rise, and the cool, heavy fluid on the top sinks. This leads to a system of vortices, which, when viewed from above, take the appearance of geometric patterns on the surface.

The first part of this dissertation, chapters two and three, is about rotating Rayleigh-Bénard convection. Since this is a simple physical system with a wide

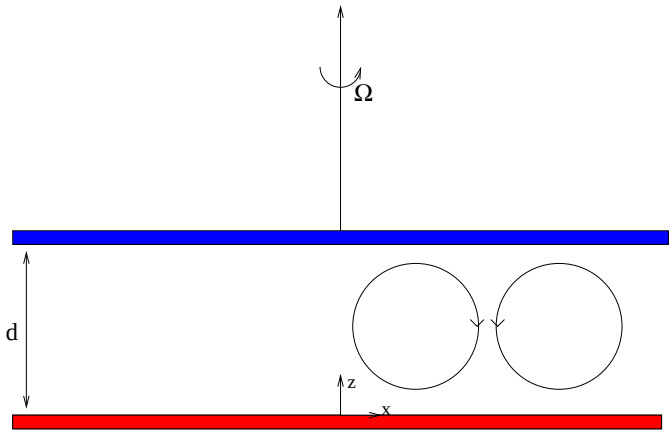

Figure 1.1: A diagram of rotating convection.

range of applications, it has received much attention over the years, and new results can be applied to a variety of real-world problems. Convection occurs in the rotating systems of the earth's atmosphere and mantle, as well as in the interior of stars, and is important in the Czochralski crystal growth method used in semiconductor physics [37]. In chapter two, I consider fully three-dimensional rotating convection, with finite Prandtl number and mean drift in both horizontal directions. As found by Siggia and Zippelius [63] and Zippelius and Siggia [73], a slow drift over large spatial scales is necessary for the problem to be solvable, and use the method of multiple scales to derive an amplitude equation reminiscent of of the well-known Ginzburg-Landau equation, coupled to an equation for the mean flow. This set of equations, an extension of the set derived by Zippelius and Siggia ([63] and [73]) for ordinary convection, describes nonlinear effects in the flow.

Several different boundary conditions are possible. Stress-free boundaries, though not realistic, have the advantage of producing a problem that can be solved analytically. Physically, a stress-free boundary is one across which no shear stresses are transmitted, like the surface of the water in an idealized pot. Rigid bound-

aries, such as the top and bottom of the container in the laboratory experiment described above, require numerical solution methods from the beginning, and I have assembled the computational tools needed to treat these problems. Solving the free-boundary case analytically permits the results of the numerical methods to be compared to exact solutions, developing confidence in the numerical solution of the rigid boundary case.

In chapter three, this analysis is extended to parameter regimes in which the onset of convection is in the form of a Hopf bifurcation. In this case, the solutions to the linearized system of governing equations take the form of two traveling waves, corresponding to the pair of complex conjugate eigenvalues which occurs at the bifurcation. This means that there are now two slowly-varying amplitudes, which lead to a pair of coupled equations of the Ginzburg-Landau type, as well as an extended mean-drift equation.

Finally, stability criteria for Stokes wave solutions to the amplitude equations for both bifurcation types are derived. For the case of a stationary bifurcation, the stability of a Stokes wave depends on the value of the perturbation wave-vector, $\vec{Q}$. When the system undergoes a Hopf bifurcation, the Stokes wave solution may take the form of a pair of waves traveling in opposite directions, or a composite solution. The stability of one traveling wave solution is analyzed.

The amplitude equations derived here may be used in theoretical models of experiments, which have applications to a variety of geophysical processes in the atmosphere, ocean, and mantle. The Ginzburg-Landau equations are of general interest in that they appear as amplitude equations for a variety of physical phenomena, not just convection. Scientists interested in these equations may use the coefficients derived here as a way to connect theoretical studies of the equation system to a physical system. The stability results derived here are general and may

be of use for other systems with the same type of symmetry as rotating convection.

In the future, it would be interesting to simulate the amplitude equations, then reconstruct the complete dimensional velocity and temperature fields from the perturbation solution. This reconstruction will show where upwelling and downwelling occur, leading to a description of the patterns which will form. It should be possible to use these methods to describe the patterns qualitatively as well as to compute the velocity and temperature perturbations quantitatively.

First described by Irving Langmuir in his 1938 paper [44], Langmuir circulation (figure 1.2) is a wind-driven mixing process in the surface layer of the ocean. The visible result of this process is a series of stripes, nearly aligned with the wind direction, on the surface of a body of water. These stripes are visible evidence of counter-rotating vortices that physically resemble thermally-driven convection rolls, but are mechanical in origin. The upper layer of the ocean absorbs nearly all of the incoming energy from the sun, because solar radiation does not penetrate water very well. Since sunlight is predominant in this layer, a great deal of organic matter lives in it. It is this organic matter, or any other impurity present in the water, that aligns along the convergence lines and produces the visible results.

The second part of this dissertation is about the effects of both stratification and the Coriolis force on the formation of Langmuir circulations in the oceanic mixed layer. The mixed (surface) layer of the ocean extends from the air-sea interface to depths ranging from a few to 500 meters in depth, with a global average of 70 meters [54, p.256–257]. It is characterized by its nearly-uniform temperature and density profiles, the result of mixing processes aided by the effects of the wind, which supplies both kinetic energy (by shearing the surface) and heat to the ocean [31, p.176–180].

Figure 1.2: Streaks on the surface of a body of water are signs of Langmuir circulation [71].

Mixing has important environmental implications. A large fraction of the carbon dioxide released into the atmosphere through natural and industrial processes is absorbed by the ocean. This absorption begins with molecular processes at the air-sea interface and continues with oceanic mixing processes, which transfer the gases downwards. Carbon dioxide uptake by the ocean is a major factor in determining the atmospheric concentration of carbon dioxide, which is responsible for long-wave radiation trapping in the atmosphere, which causes the greenhouse effect.

Langmuir circulation and much of the work done on it is described in the reviews [27], [45], [47], [56], and, most recently, [66]. The physics of this phenomenon is discussed in [20] and diagrammed in [45] and [47]. Recently, Haeusser [30] considered the effects of the Coriolis force due to the rotation of the earth on Langmuir circulation formation using the method of multiple scales to develop an

amplitude equation for the motions. Fluid density variations, which could be due to the inclusion of additional materials (i.e., salinity), or thermal expansion, and their effects on the formation of Langmuir circulations (without the Coriolis force) were investigated by Leibovich and Tandon [48], who performed a linear stability analysis.

In this context, heating is the dominant cause of stratification, as it is in thermal convection. Heat, due to sunlight and long-wave radiation trapped in the atmosphere, is transferred between the ocean surface and the atmosphere by evaporation, sensible heat transfer, and radiation. It may be possible to use the heat distribution revealed by infrared photography to determine physical properties of a set of Langmuir circulations. When thermal effects are included in the model, the wind shear becomes less important: "In fact, with weak winds and thermally unstable conditions, buoyancy may be the motive force," writes Leibovich [47, p.392]. Langmuir circulation is stronger than thermally induced stability, but convection can occur in an unstably stratified environment in the absence of Langmuir circulations.

Since the Coriolis force is also a factor in the formation of Langmuir circulations in the ocean, rotating thermal convection is used as a first approach to the problem. This classical physics problem involves a subset of the physics contained in the case of Langmuir circulation with thermal effects. The resulting rolls resemble the Langmuir case, but the number of physical parameters is smaller, and the driving force is thermal rather than mechanical.

In order to best model Langmuir circulation, it is sensible to use a slightly different nondimensionalization of the governing equations than that used for rotating convection. The effects of wind and surface waves are added to the model; thermal stratification is already included. Wind shear causes a current, which appears as

the basic flow, and surface waves, which cause the Stokes drift. These terms are added to the velocity vector, accompanied by a new upper boundary condition: constant stress instead of no stress. The horizontal component of the angular velocity is added by removing the assumption that this vector is perpendicular to the two plates and writing it in its proper form, given the latitude of the part of the ocean to be considered. The bottom boundary is assumed to be rigid, an idealized condition. At the bottom of the mixed layer, the pycnocline, a layer where the water's density varies strongly with depth, acts to inhibit vertical motion. The approach used here is to model the pycnocline as a rigid surface. A more involved approach, described by Cox and Leibovich [16], uses a mixed boundary condition to allow stress to be communicated to the abyss below.

A linearized stability analysis of this problem is the subject of chapter four, and an investigation of the patterns formed by several interacting modes fills chapter five. I find that stable stratification affects the formation of Langmuir circulations in the expected way: the critical Reynolds number is increased. An examination of the effects of latitude and wind direction on the stability criteria shows that they are minimal. The approach to pattern formation taken in chapter five is qualitative; the Landau coefficient is approximated and results from the linearized problem are used to compute the interacting modes. Y-junctions, places where a new roll is created, which take the shape of the letter Y on the ocean surface, appear at points where the temperature perturbation is zero. This result is related to the correspondence between defects (places where the slowly-varying amplitude A is zero) and Y-junctions analyzed by Haeusser [30] and Bhaskaran and Leibovich [5]. More Y-junctions open downwind than upwind, in agreement with the observations of Farmer and Li [28] and the calculations of Bhaskaran and Leibovich [5].

The results of the second part of this dissertation have important applications to the oceanic mixed layer in particular and climate science in general. Understanding oceanic mixing processes is a step towards understanding climate change. The results presented here are a basis for understanding the surface thermal signature of Langmuir circulation on large scales. This could then be used to interpret satellite images of the ocean surface. The two problems treated in the following chapters, convection and Langmuir circulation, are linked by their patterns as well as their environmental importance. This work may be applied to studies of the earth system, particularly climate change.

CHAPTER 2

AMPLITUDE EQUATIONS FOR ROTATING CONVECTION WITH A STATIONARY BIFURCATION

2.1 Introduction

Rotating Rayleigh-Bénard convection is a classical physics problem that can be modelled simply, yet has many applications and frequently appears in the natural world. The earth's movement supplies the rotation, and buoyancy differences in the atmosphere and ocean can result in convection. Convection also occurs in the earth's mantle, as well as in the interior of (rotating) stars. While buoyancy is usually due to thermal expansion, other density differences could also be responsible.

Since it is such a common phenomenon, convection, both ordinary and rotating, has seen a great deal of interest in the years since Bénard's first experiments in 1898, done as a part of his doctoral work in France [69]. Chandrasekhar's classic book [11] contains a thorough treatment of the linearized problems for both ordinary and rotating convection, and lays the groundwork for future research.

Much of the scientific literature concerning convection is referenced in the review article by Bodenschatz, Pesch and Ahlers [6]. The investigation of nonlinear effects in rotating convection is an area of research with many different methods currently in use; nonlinear theoretical models usually take the form of a Swift-Hohenberg equation or one or more coupled amplitude equations of the Ginzburg-Landau type. The review article includes a section on rotating convection, covering both experimental and theoretical results. The authors write,

> Over a wide parameter range, the bifurcation remains supercritical for $\Omega > 0$ [Ω is the rotation rate], i.e. the flow amplitudes still grow continuously from zero and the usual weakly nonlinear theories, for instance in the form of Ginzburg-Landau (GL) or Swift-Hohenberg equations, should remain applicable. Thus one may expect interesting new effects to occur in a theoretically tractable parameter range....
>
> This particular case [small Prandtl number] should be accessible to analysis by weakly nonlinear theories, and a theoretical description in terms of Ginzburg-Landau equations would be extremely interesting and could be compared with experimental measurements [6, p.759,766].

This is the type of analysis I will present in this dissertation. Ginzburg-Landau amplitude equations are typically formulated by expanding a set of governing equations in powers of a small parameter, ϵ, defined by $\epsilon^2 = \frac{\mathrm{Ra}-\mathrm{Ra}_c}{\mathrm{Ra}_c}$, where Ra is the Rayleigh number (the ratio of the buoyancy force to the viscous damping forces) and Ra_c is the critical Rayleigh number, at which the flow becomes unstable. It corresponds with a critical wave-number, k_c. Past analyses suggest some problems I may anticipate while providing a basis for comparison. In this chapter, the Prandtl number is finite, but above that required for a Hopf bifurcation. Small Prandtl number systems, which undergo Hopf bifurcations, are subject of the following chapter.

While the coefficients of a Ginzburg-Landau-type amplitude equation have not yet been calculated for fully three-dimensional rotating convection in the literature, a number of similar analyses have been undertaken. The complex Ginzburg-Landau equation, which describes the temporal and spatial variation of the ampli-

tude, A, of the perturbation quantities, is

$$\frac{\partial A}{\partial T} = (b + ic)\nabla^2 A + f|A|^2 A \tag{2.1}$$

An equation similar to this is the result of a perturbation expansion (using the method of multiple scales) of the governing equations for ordinary Rayleigh-Bénard convection.

Ginzburg-Landau-type models are generally applied to a region of infinite horizontal extent between parallel boundaries. Within this geometry, interest has been focussed around the derivation of amplitude equations describing the flow at higher order and the description of secondary instabilities. A domain of infinite horizontal extent is popular among theorists because of its simplicity. In this geometry, two parallel plates of infinite extent are placed a specified distance apart. The plates could be rigid (ordinary plates; this is a common experimental configuration), free (boundaries which apply no stress to the fluid between them, a theoretically useful but physically unrealistic model), or one of each (representing a fluid in a horizontally-infinite container with no top). The effects of sidewalls are assumed to be of secondary importance, an assumption which must be examined on a case-by-case basis.

The derivation of a Ginzburg-Landau amplitude equation from first principles has been an important area of study for some time. The first amplitude equation calculations for ordinary convection were performed by Newell and Whitehead [53] and Segel [61]. Of note are their (independent) calculations showing that while the length parallel to the wave-vector scales like ϵ, the length perpendicular to it scales like $\sqrt{\epsilon}$. Their equation is

$$\frac{2}{3\pi^2}\frac{\partial A}{\partial T} = A + \frac{8}{3\pi^2}\left(\frac{\partial}{\partial X} + \frac{1}{2ik_c}\frac{\partial^2}{\partial Y^2}\right)^2 A - \frac{8}{3\pi^2}|A|^2 A \tag{2.2}$$

the derivation of which is also presented by Cross and Hohenberg [21, p.1081–1085]. The need for a horizontal mean flow, which is not included in this equation,

was subsequently discovered by Davey, Hocking, and Stewartson [23].

Rotation is important for some geophysical and astrophysical problems, and new analyses including it were soon completed. In their important theoretical paper, Küppers and Lortz consider the case of free boundary conditions and infinite Prandtl number [42]. Using the vertical component of the single and double curls of the momentum equation, and neglecting the part of the momentum equation that is proportional to the inverse Prandtl number, they consider small perturbations. At third order in ϵ, Küppers and Lortz determine that the nonlinear part of the equation, when combined with the first-order solution, restricts the manifold of first-order solutions. They follow the calculation to a system of equations and conclude that, for sufficiently large angular velocity, no neutrally stable eigenmode can grow when the stability threshold is crossed. This is a remarkable finding, quite different from all previously studied hydrodynamic stability problems.

Clune and Knobloch [15] focus on linear stability and explicitly describe how to derive a Ginzburg-Landau equation at third order. Details of the calculation, performed using a Mathematica package, are in an unpublished paper by T. Clune [14]. They find that for large Taylor number, the boundary layer on no-slip boundaries thins, allowing the boundary conditions to approach those of stress-free boundaries. In the case of free boundaries, they find a critical Prandtl number of 0.676605 above which there is no oscillatory convection, in agreement with the results of Chandrasekhar [11].

One important part of the flow, which is not included in these analyses, is the mean drift. This term, first derived by Davey, Hocking, and Stewartson [23] in the form of a secular pressure term, arises in the three-dimensional theory because its slow spatial dependence means it can not be eliminated. Siggia and Zippelius [63] were the first to describe mean flow effects in ordinary convection. Cross and

Newell [22] describe the effects of the mean drift in more detail. They explain that there is a horizontal velocity field, driven by wave-vector inhomogeneities, which is undamped and constant in depth. It transports the roll pattern, making its inclusion in the amplitude equation system essential. Chiam, Paul, Cross, and Greenside [13] show that the mean flow is responsible for the appearance of spiral-defect chaos in stationary Rayleigh-Bénard convection. They numerically construct a velocity field which lacks a mean flow, and then perform direct numerical simulations, which lead to patterns of bending stripes instead of the expected spiral-defect chaos. This shows that the mean flow is physically important, even though it is difficult to observe experimentally.

Cox and Matthews derive an amplitude equation for a restricted case of non-oscillatory rotating convection from first principles [17]. While their goal is to study rotating magneto-convection, they present rotating convection as a special case. They restrict convection to two dimensions, with free boundaries, and find that a slowly-varying velocity component, V, in the direction of the neglected spatial variable is required. Eventually, they arrive at a pair of coupled equations, with analytically-computed coefficients:

$$\frac{\partial A}{\partial T} = a_5 A + a_6 \frac{\partial^2 A}{\partial X^2} - a_7 A|A|^2 - a_8 A \frac{\partial V}{\partial X} \tag{2.3}$$

$$\frac{\partial V}{\partial T} = \mathrm{Pr} \frac{\partial^2 V}{\partial X^2} + \frac{\pi^2 \mathcal{T}}{a_c^2} \frac{\partial |A|^2}{\partial X} \tag{2.4}$$

where k_c is the critical wavenumber, $\mathrm{Ra} = \mathrm{Ra_c} + \epsilon^2 R_2$, $\mathcal{T}$ is the square root of the Taylor number, and a_{5--7} are constants that depend on these parameters. a_7 must be positive for their assumption of a stationary bifurcation to hold.

V is a slowly-varying mean drift term perpendicular to the wave vector that arises at order ϵ in Cox and Matthews' analysis [17]. Siggia and Zippelius had previously shown that such a term is necessary in ordinary three-dimensional convection with finite Prandtl number [63], [73]. Their second-order drift term comes

from vertical vorticity generated as the rolls bend, resulting in a term proportional to AU in the amplitude equation, where U is the mean drift parallel to the wave vector. Zippelius and Siggia's equations for free-slip boundaries are

$$\left(\left(\frac{\partial}{\partial X}-\frac{i}{2q_0}\frac{\partial^2}{\partial Y^2}\right)^2+\frac{3\pi^2\epsilon^2}{8}-\frac{1+\mathrm{Pr}}{4\mathrm{Pr}}\frac{\partial}{\partial T}\right)A=\frac{1}{8}|A|^2A+iq_0\frac{1+\mathrm{Pr}}{4\mathrm{Pr}}AU \quad (2.5)$$

$$\left(\frac{\partial}{\partial T}-\mathrm{Pr}\left(\frac{\partial^2}{\partial X^2}+\frac{\partial^2}{\partial Y^2}\right)\right)\Omega=2\frac{\partial}{\partial Y}\left(A^*\left(\frac{\partial}{\partial X}-\frac{i}{2q_0}\frac{\partial^2}{\partial Y^2}\right)A+c.c.\right) \quad (2.6)$$

$$\frac{\partial\Omega}{\partial Y}=-\left(\frac{\partial^2}{\partial X^2}+\frac{\partial^2}{\partial Y^2}\right)U \quad (2.7)$$

with critical wavenumber q_0. The second equation arises from selecting the slowly-varying parts of the vorticity equation at order $\epsilon^{7/2}$. This is a more general derivation than that of Cox and Matthews [17], who average the horizontal Navier-Stokes equations to find their second equation. Bernoff [3] uses center manifold theory to add a higher-order term to Zippelius and Siggia's second equation, bringing their stability results into quantitative agreement with the results of Busse and Bolton [9].

Similarly, Young and Riecke [72] derive an extended Ginzburg-Landau equation. Their system of equations for stress-free boundaries is

$$\frac{\partial A}{\partial t}=\left(\mu+\left(\frac{\partial}{\partial x}-i\lambda\frac{\partial^2}{\partial y^2}\right)^2-|A|^2\right)A-is_1A\frac{\partial Q}{\partial y} \quad (2.8)$$

$$q_2\left(\nabla^2\frac{\partial Q}{\partial t}-\nabla^4Q\right)=\left(\frac{\partial}{\partial x}-i\lambda\frac{\partial^2}{\partial y^2}\right)^2\frac{\partial|A|^2}{\partial y} \quad (2.9)$$

where q_c is the critical wavenumber and Q is a potential function representing the mean flow.

Scheel [60] derives amplitude and mean flow equations for three-dimensional rotating convection with rigid boundaries using the full set of governing equations. Two equations, a Ginzburg-Landau-type equation at order ϵ^3 and another equation at order $\epsilon^{7/2}$ appear. The first of these depends only on the amplitude A (A_0 in

her formulation), and the second of which depends on A_0 and a second amplitude, A_1.

There are some analyses in which the Ginzburg-Landau equation is used as a model, but is not derived by a weakly nonlinear analysis. These examples have an experimental component, as the coefficients of the equation are tuned to match experimental results. The most frequent topic of discussion in these papers is traveling waves. Rotating convection is a natural system in which to study traveling wave solutions to the complex Ginzburg-Landau equation.

Liu and Ecke [50] find that the one-dimensional Ginzburg-Landau equation is a good model for the results of their experiments on traveling waves. They determine the relevant coefficients experimentally, but find that higher order corrections to the Ginzburg-Landau equation may be necessary to completely model the experimental results. This is because rotation breaks the symmetry of the problem, making it likely that third derivative terms or terms proportional to $|A|^4 A$ appear in the amplitude equation.

Van Hecke and van Saarloos [32] start with a pair of coupled Ginzburg-Landau equations, then show that rotating convection is an example of a system which can be used to perform experiments for a new parameter regime. Their interest is primarily in the equations, not in rotating convection, but experimental rotating convection allows them to understand the equations better. They select the coefficients they would like to study, which happen to fall into the rotating convection regime, and use a one-dimensional Ginzburg-Landau equation to model bulk modes. For Prandtl numbers between 0.1 and 0.2, they find that traveling waves are an "experimental realization" of the Ginzburg-Landau equation, with coefficients which scan through the chaotic part of the phase diagram when the rotation rate number is changed. Van Hecke [67] produced an unpublished account

of the details of their calculations.

The papers described in the last two paragraphs make the connection between Ginzberg-Landau amplitude equations and experiments apparent. They show that a perturbation expansion derivation leading to the coefficients of such an amplitude equation is the first step towards a complete theoretical understanding of the system. Reconstruction of the velocity field from the perturbation expansion results and simulations of the amplitude equations is expected to lead to results which are quantitatively as well as qualitatively correct. However, higher-order terms may be necessary for quantitative accuracy in some regimes.

I shall consider fully three-dimensional rotating convection, with finite Prandtl number and mean drift in both horizontal directions. A slow drift is required at second order, in agreement with the results of Zippelius and Siggia. From first principles, I derive an amplitude equation of the Ginzburg-Landau type, coupled to an equation for the mean flow. Numerical values for the coefficients for rigid boundaries are given in this chapter, as are analytical values for the case of stress-free boundaries. The same system, in the Hopf bifurcation parameter regime, is the subject of the following chapter.

2.2 Governing Equations

The governing equations, given in equations 2.10, 2.11, and 2.12, are the usual continuity, momentum (with terms for buoyancy and Coriolis forces), and energy equations, respectively. The continuity equation,

$$\nabla \cdot \vec{u} = 0 \tag{2.10}$$

utilizes the Boussinesq approximation: small changes in density are negligible in the inertial term, but important in the buoyancy term. Changes in fluid properties

are also neglected.

The momentum equation is

$$\frac{D\vec{u}}{Dt} = -\nabla P + \nu\nabla^2\vec{u} + \beta g\theta\hat{z} - 2\Omega\hat{z}\times\vec{u} \tag{2.11}$$

where $\hat{z}$ is a unit vector opposite in direction to gravity. The left hand side of the momentum equation is the material derivative. Terms on the right hand side are the pressure gradient force, dissipation due to viscosity, buoyancy (upwards only), and the Coriolis force due to rotation. ν is the kinematic viscosity, β is the coefficient of thermal expansion ($-\frac{1}{\rho}\frac{\partial\rho}{\partial T}$ for a fluid with density ρ), g represents gravity, and Ω is the rotation speed. The pressure P in this equation is a modified pressure that includes both pressure and the centrifugal force $\vec{\Omega}\times(\vec{\Omega}\times\vec{r})$, where r is the position vector.

The energy equation,

$$\frac{D\theta}{Dt} + w\frac{\partial\bar{T}}{\partial z} = \kappa\nabla^2\theta \tag{2.12}$$

shows how the temperature evolves. κ is the thermal diffusivity (heat conductivity χ divided by heat capacity per unit volume C). θ is the perturbation temperature and $T = \bar{T}(z) + \theta$ is the temperature distribution, with equilibrium temperature $\bar{T} = (T_{top} - T_{bottom})z/d + T_{bottom}$, where d is the distance between the upper and lower boundaries and z measures the depth.

This system of equations is nondimensionalized using the following scales:

- Time scale $\frac{d^2}{\kappa}$
- Length scale d
- Velocity scale $\frac{\kappa}{d}$
- Temperature scale $\Delta T = T_{bottom} - T_{top}$

The dimensionless groups that appear as a result of the nondimensionalization are $\mathrm{Ra} = \frac{\beta g\Delta T d^3}{\kappa\nu}$ (the Rayleigh number, the ratio of the buoyancy force to the viscous

damping forces), $\mathrm{Pr} = \frac{\nu}{\kappa}$ (the Prandtl number, the ratio of the viscosity to the heat conductivity), $\mathcal{T} = \frac{2\Omega d^2}{\nu}$ (the square root of the Taylor number, a measure of the rotation frequency). A frequently-used alternative nondimensionalization has ν in the velocity and time scales instead of κ. This makes energy stability calculations work out more cleanly, and is what Chandrasekhar used in his analysis [11].

In this analysis, small perturbations around an initial motionless state ($T = \bar{T}$, $\vec{u} = \vec{0}$) are considered. These perturbations will grow when the Rayleigh number is above its critical value, Ra_c, which will be calculated in the next section. The nondimensional perturbation equations follow.

$$\nabla \cdot \vec{u} = 0 \tag{2.13}$$

$$\frac{\partial \vec{u}}{\partial t} + \vec{u} \cdot \nabla \vec{u} = -\nabla P + \mathrm{Pr}(\nabla^2 \vec{u} + \mathrm{Ra}\theta \hat{z} - \mathcal{T}\hat{z} \times \vec{u}) \tag{2.14}$$

$$\frac{\partial \theta}{\partial t} + \vec{u} \cdot \nabla \theta = \vec{u} \cdot \hat{z} + \nabla^2 \theta \tag{2.15}$$

In order to reduce the size of the system, the custom of using the vorticity equation and its curl, along with the energy equation, is followed. This results in the final system,

$$\begin{pmatrix} \frac{\partial}{\partial t} - \mathrm{Pr}\nabla^2 & 0 & -\mathrm{Pr}\mathcal{T}\frac{\partial}{\partial z} \\ 0 & \frac{\partial}{\partial t} - \nabla^2 & -1 \\ \mathrm{Pr}\mathcal{T}\frac{\partial}{\partial z} & -\mathrm{PrRa}\nabla_h^2 & \nabla^2 \frac{\partial}{\partial t} - \mathrm{Pr}\nabla^4 \end{pmatrix} \begin{pmatrix} \zeta \\ \theta \\ w \end{pmatrix} = \begin{pmatrix} -\nabla \times (\vec{v} \cdot \nabla \vec{v}) \cdot \hat{z} \\ -\vec{v} \cdot \nabla \theta \\ \nabla \times \nabla \times (\vec{v} \cdot \nabla \vec{v}) \cdot \hat{z} \end{pmatrix} \tag{2.16}$$

The left-hand side matrix is called L. ∇_h^2 is the horizontal Laplacian ($\frac{\partial^2}{\partial x^2} + \frac{\partial^2}{\partial y^2}$), ζ is the $\hat{z}$ component of the vorticity, and w is the $\hat{z}$ component of the velocity. The boundaries are at first considered to be stress-free and isothermal, with $w = w'' = \theta = \zeta' = 0$ at $z = 0$ and $z = 1$. More realistic rigid boundaries have $w = w' = \theta = \zeta = 0$.

The methods used to solve this problem are those of normal modes and multiple scales. Due to symmetry in the problem, the axes can be oriented so that the wave vector is in the x direction: $\vec{k} = k\hat{x}$. The solution is assumed to be periodic in x, as in the method of normal modes: $\vec{v}_1 = \hat{v}_1(z)Ae^{\sigma t}e^{ikx}$, $\zeta_1 = \hat{\zeta}_1(z)Ae^{\sigma t}e^{ikx}$, $\theta_1 = \hat{\theta}_1(z)Ae^{\sigma t}e^{ikx}$. A is a slowly-varying amplitude that will be discussed later. The linearized problem for rotating convection was first solved by Chandrasekhar [11], who based the normal-modes analysis presented in his book on two earlier papers by himself [10] and with Donna D. Elbert [12]. This method was originally used for ordinary convection by Lord Rayleigh [65].

Following the method of multiple scales,the system is expanded in powers of a small parameter, ϵ, defined so that $\mathrm{Ra} = \mathrm{Ra}_c + \epsilon^2 R_2$: ϵ measures the distance away from the critical Rayleigh number. Space and time variables are separated into fast and slow parts by expanding as follows: $x \to x + \epsilon X$, $y \to \sqrt{\epsilon}Y$, and $t \to t + \epsilon^2 T$, which leads to $\frac{\partial}{\partial x} \to \frac{\partial}{\partial x} + \epsilon\frac{\partial}{\partial X}$, $\frac{\partial}{\partial y} \to \sqrt{\epsilon}\frac{\partial}{\partial Y}$. The two slow lengths appear at different orders of ϵ because of the rotational symmetry of the problem, which allows the wave-vector $\vec{k}$ to be aligned with the x-axis. This was first noticed by Newell and Whitehead [53] and Segel [61]. The scaling for Y comes from solving $-\nabla_h^2 = -k^2 = \left(ik + \epsilon\frac{\partial}{\partial X}\right)^2 + \delta^2\frac{\partial^2}{\partial Y^2}$, where ik is equivalent to $\frac{\partial}{\partial x}$ because of the normal modes definition of $\vec{v}$ and θ.

The slow time T is proportional to ϵ^2 for reasons to be discussed later. In the following sections, I will solve the problem at each order in $\sqrt{\epsilon}$ individually. The fast variables (x, y, z, and t) and the slow variables (X, Y, and T) are regarded as independent in the perturbation process in the well-known method of multiple scales, and their connections may be restored later. I treat both stress-free and rigid boundaries, with each section split into general considerations and specific results for each type of boundary.

2.3 Linearized Problem (Order ϵ)

The first step in the perturbation expansion is to solve the linearized problem. While the lowest-order scale in the problem is $\sqrt{\epsilon}$, with which Y scales, there is nothing of interest at that order. The linearized system is:

$$\begin{pmatrix} \sigma - \mathrm{Pr}\nabla^2 & 0 & -\mathrm{Pr}\mathcal{T}\frac{\partial}{\partial z} \\ 0 & \sigma - \nabla^2 & -1 \\ \mathrm{Pr}\mathcal{T}\frac{\partial}{\partial z} & -\mathrm{PrRa}\nabla_h^2 & \sigma\nabla^2 - \mathrm{Pr}\nabla^4 \end{pmatrix} \begin{pmatrix} \zeta \\ \theta \\ w \end{pmatrix} = \begin{pmatrix} 0 \\ 0 \\ 0 \end{pmatrix} \tag{2.17}$$

I have assumed that the solution is exponential in time, with all three variables proportional to $e^{\sigma t}$. For a stationary bifurcation, σ is zero on the neutral stability curve, along which perturbations such as these neither grow nor decay. Above this curve, when the real part of σ is positive, perturbations grow and the solution is unstable. Below it, perturbations decay and the solution is stable. A Hopf bifurcation, in which $\sigma = i\omega$, is also possible for Prandtl numbers less than approximately 0.67, as shown by Chandrasekhar [11]. In this chapter I assume the bifurcation is stationary.

A solution to the linear problem can be found by substituting the assumed normal mode solution form and finding out when the minimum of (the real part of) the eigenvalue of the operator matrix, L, vanishes. This provides the critical Rayleigh number in terms of the wave-number and other constants. The critical Rayleigh number, Ra_c, is the minimum value of the Rayleigh number on this curve. The corresponding eigenfunctions are solutions for ζ, θ, and w at first order. The horizontal velocity components can be found from these three dependent variables: u from continuity, $w' = -\frac{\partial u}{\partial x}$; v from the definition of ζ, $\zeta = \frac{\partial v}{\partial x}$, since there is no y dependence. At higher orders these two formulae have additional terms due to the slow length scales, X and Y.

Since u and v are defined using derivatives, an arbitrary constant (the mean drift, $\vec{U}$) may be added to them. As Zippelius and Siggia show, the mean drift is a function of the slow space and time variables for free boundaries, but must vary with depth for rigid boundaries. I will expand this mean drift in powers of $\sqrt{\epsilon}$: $\vec{U} = \epsilon\vec{U}_1 + \epsilon^{3/2}\vec{U}_1 + \epsilon^2\vec{U}_2 + \cdots$.

If the mean drift is included in the first order velocity, I find a second-order amplitude equation,

$$\frac{\partial A}{\partial T_1} = cAU_1 \tag{2.18}$$

where T_1 is a first-order timescale and c is a nonzero constant. Since the original system is invariant under the transformation $x \to -x$, this equation must also be invariant under $A \to -A$, $U_1 \to -U_1$, but it is not, which means that U_1 must be identically zero by symmetry considerations. In addition, averaging the Navier-Stokes equations at second order yields $\frac{\partial V_1}{\partial T_1} = \mathrm{Pr}\frac{\partial^2 V_1}{\partial Y^2}$ and a similar equation for U_1. These equations are satisfied by $U_1 = V_1 = 0$.

2.3.1 Results for Stress-free Boundaries

In this case, the matrix L has a determinant of zero when $k_c^2\mathrm{Ra}_c = \mathcal{T}^2\pi^2 + a_c^6$ and $\omega = 0$ (with $a_c^2 = k_c^2 + \pi_c^2$ throughout this chapter), in agreement with Chandrasekhar's classic result [11]. Figure 2.1 depicts Ra as a function of k. The critical Rayleigh number, Ra_c, and wavenumber, k_c, are at the minimum of this curve. They can be found analytically by setting $\frac{\partial \mathrm{Ra}}{\partial k}$ to zero. The eigenfunctions are

$$\zeta_1 = \frac{ik_c\mathcal{T}\pi}{a_c^2 C}\cos\pi z(A(\vec{X},T)e^{ik_c x} - c.c.) \tag{2.19}$$

$$\theta_1 = \frac{ik_c}{a_c^2 C}\sin\pi z(A(\vec{X},T)e^{ik_c x} - c.c.) \tag{2.20}$$

$$w_1 = \frac{ik_c}{C}\sin\pi z(A(\vec{X},T)e^{ik_c x} - c.c.) \tag{2.21}$$

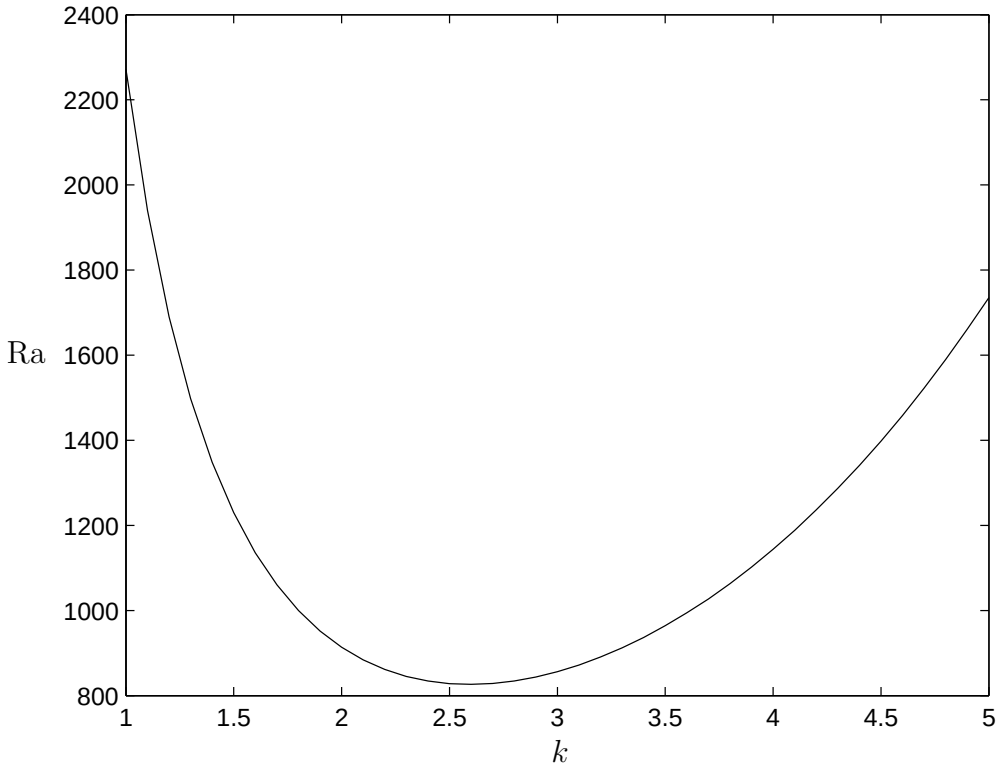

Figure 2.1: The neutral Rayleigh number versus the wave number, for $\mathcal{T} = 10$ (free boundaries). The critical values (k_c, Ra_c) are the minimum of this curve.

$$u_1 = -\frac{\pi}{C} \cos \pi z (A(\vec{X}, T) e^{ik_c x} + c.c.) \tag{2.22}$$

$$v_1 = \frac{\mathcal{T}\pi}{a_c^2 C} \cos \pi z (A(\vec{X}, T) e^{ik_c x} + c.c.) \tag{2.23}$$

in agreement with the results of Cox and Matthews [17]. *c.c.* stands for complex conjugate and C is an arbitrary constant used to normalize the solutions.

2.3.2 Results for Rigid Boundaries

The linearized problem with two rigid boundaries is solved using the numerical methods described in appendix C. Critical values are given numerically in table D.1 and shown graphically in figures 2.2 and 2.3. Sample eigenfunctions are shown

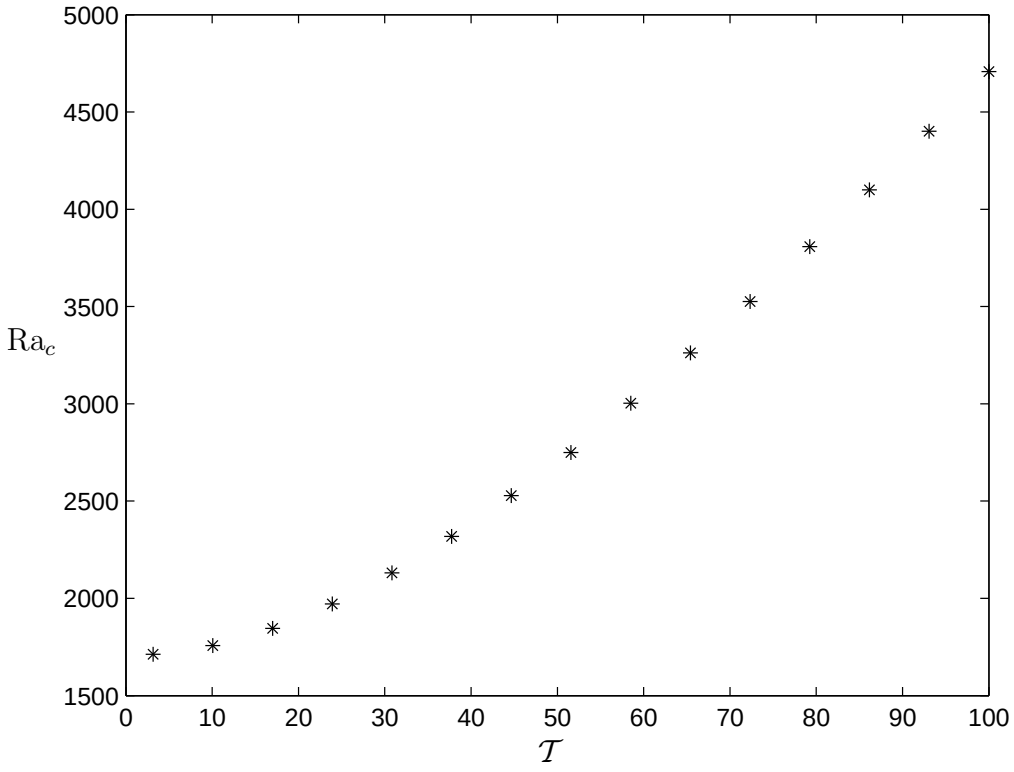

Figure 2.2: Critical Rayleigh number versus $\mathcal{T}$, with Pr = 1 and rigid boundaries.

in figures 2.4 through 2.6. The numerical solutions for the linear eigenfunctions are normalized so that the maximum of $\hat{w}_1(z)$ is ik_c, to agree with the analytic solutions when $C = 1$ and the boundaries are stress-free.

2.4 Adjoint Problem

The adjoint of an operator L is the operator L_A such that $(\vec{x}, L\vec{y}) = (L_A\vec{x}, \vec{y})$. For a complex matrix, L_A is the transpose of the complex conjugate of L. An adjoint differential operator can be calculated using integration by parts from

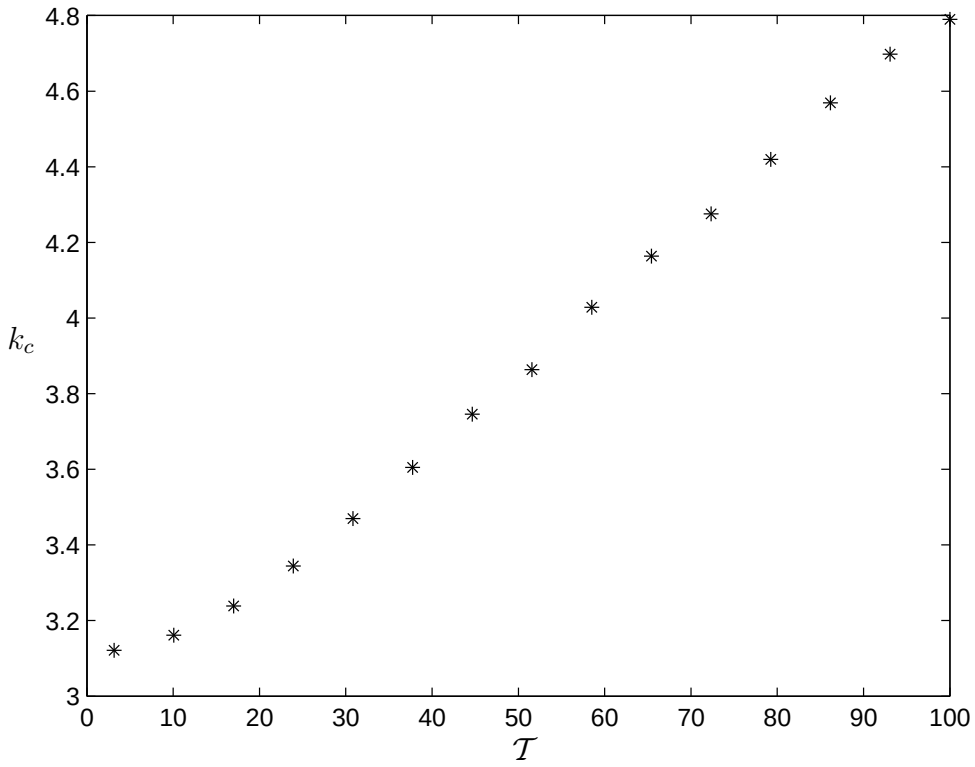

Figure 2.3: Critical wavenumber number versus $\mathcal{T}$, with Pr = 1 and rigid boundaries.

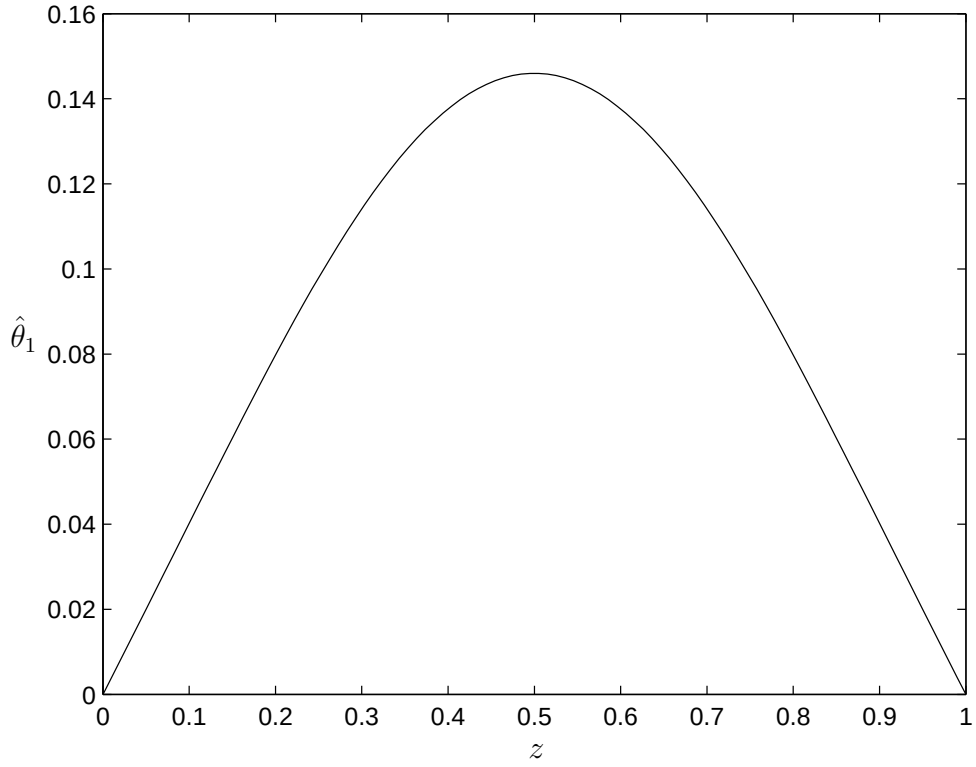

Figure 2.4: $\hat{\theta}_1(z)$ for the linearized problem with rigid boundaries, $\mathcal{T} = \sqrt{10}$ and $\mathrm{Pr} = 1$ (imaginary part).

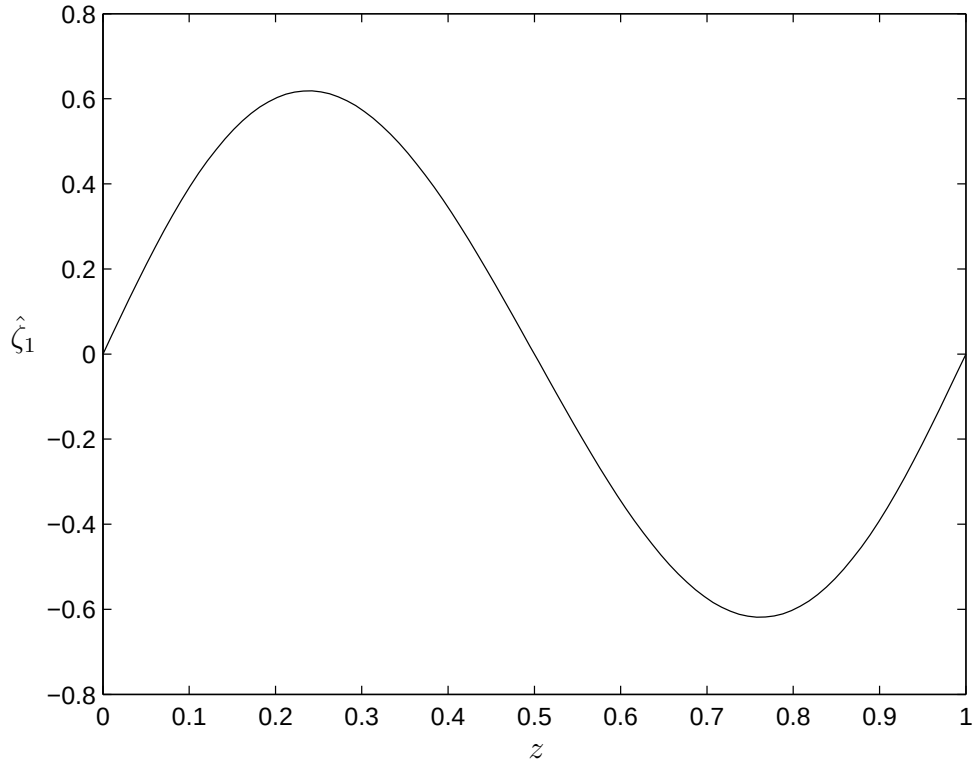

Figure 2.5: $\hat{\zeta}_1(z)$ for the linearized problem with rigid boundaries, $\mathcal{T} = \sqrt{10}$ and $\mathrm{Pr} = 1$ (imaginary part).

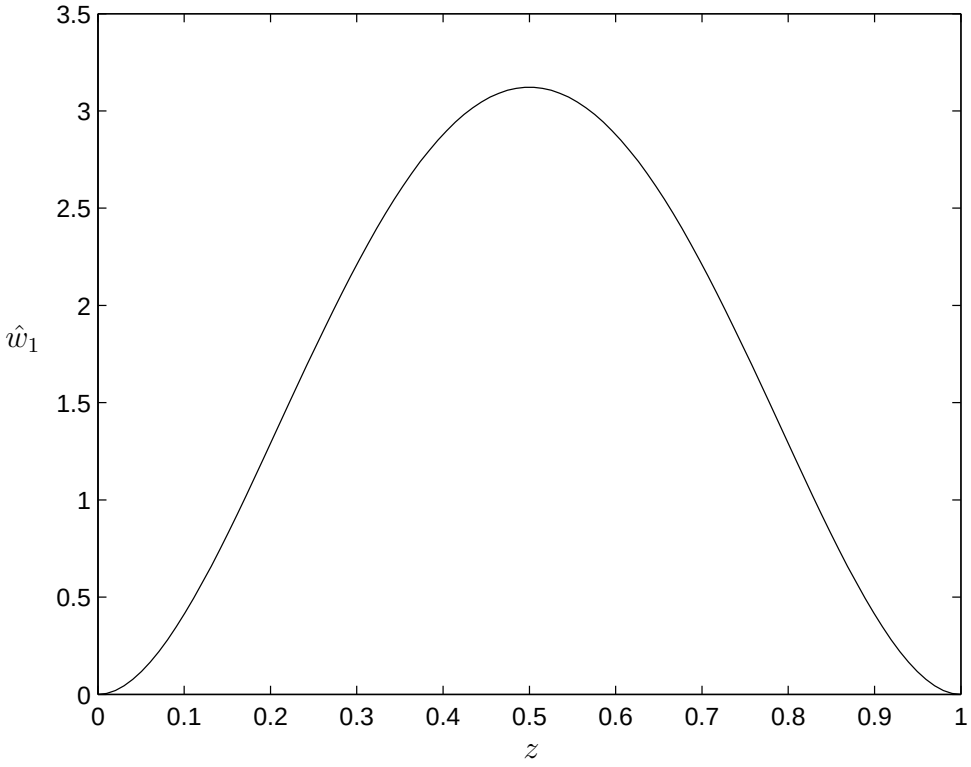

Figure 2.6: $\hat{w}_1(z)$ for the linearized problem with rigid boundaries, $\mathcal{T} = \sqrt{10}$ and $\mathrm{Pr} = 1$ (imaginary part).

$(\vec{f},\vec{g}) = \int_V \vec{f}\cdot\vec{g}^* dV$.[1] The eigenvalues of $L_A$are the complex conjugates of the eigenvalues of L. This provides a good numerical check, and is used to establish the solvability conditions which produce the amplitude equation at third order.

Assuming a stationary bifurcation, the adjoint problem is

$$\begin{pmatrix} -\mathrm{Pr}\nabla^2 & 0 & -\mathrm{Pr}\mathcal{T}\frac{\partial}{\partial z} \\ 0 & -\nabla^2 & -\mathrm{PrRa_c}\nabla_h^2 \\ \mathrm{Pr}\mathcal{T}\frac{\partial}{\partial z} & -1 & -\mathrm{Pr}\nabla^4 \end{pmatrix} \begin{pmatrix} \zeta_A \\ \theta_A \\ w_A \end{pmatrix} = \begin{pmatrix} 0 \\ 0 \\ 0 \end{pmatrix} \tag{2.24}$$

The adjoint boundary conditions appear during the integration by parts, and turn out to be the same as those for the linear problem.

The solution for free boundaries is:

$$\zeta_A = -\mathcal{T}\pi\cos\pi z(e^{ik_c x} + c.c.)$$

$$\theta_A = \mathrm{PrRa_c}k_c^2\sin\pi z(e^{ik_c x} + c.c.)$$

$$w_A = -a_c^2\sin\pi z(e^{ik_c x} + c.c.)$$

using the same methods as the linear problem. Numerical solutions for rigid boundaries are shown in figures 2.7 through 2.9. No normalization constant is given here; such a constant is unnecessary for deriving the amplitude equations because it will simply cancel out when the solvability condition is applied.

2.5 Order $\epsilon^{3/2}$

The right hand side of the equation system 2.16 is zero at this order, which means that there is no necessary contribution at this order: $w_{3/2} = \zeta_{3/2} = \theta_{3/2} = 0$ for both sets of boundary conditions. However, the horizontal velocity components

[1]The observations that the adjoint of a constant is its complex conjugate, and the adjoint of a derivative is the negative of that derivative may make the calculation easier.

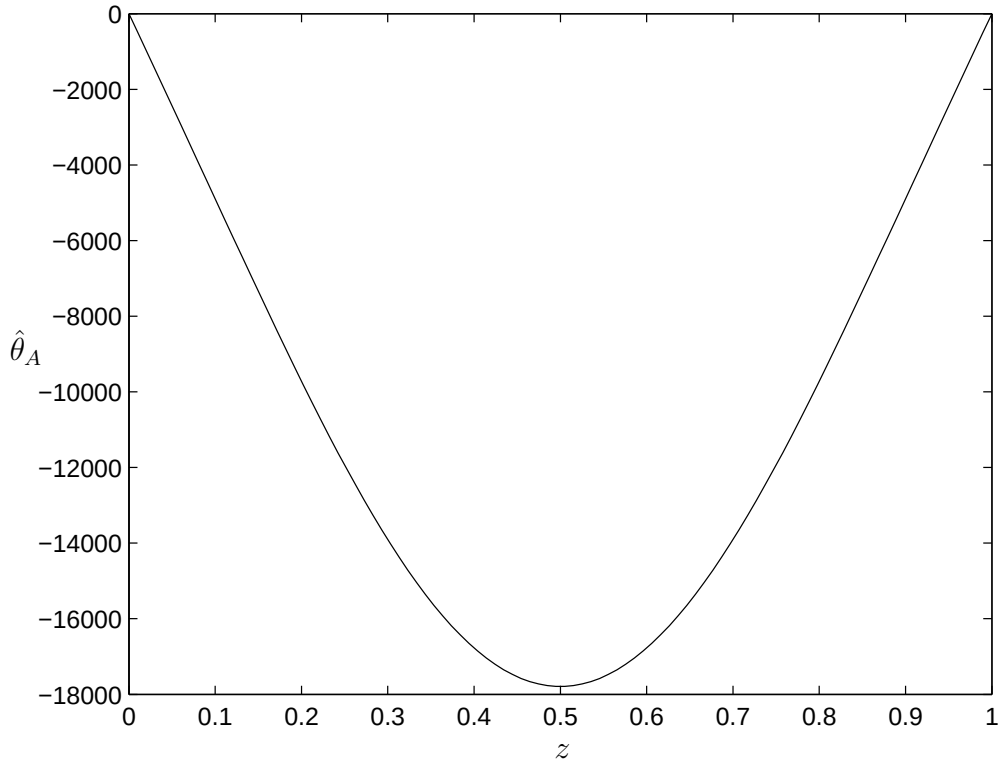

Figure 2.7: $\hat{\theta}_A(z)$ for the adjoint problem with rigid boundaries, $\mathcal{T} = \sqrt{10}$ and $\mathrm{Pr} = 1$ (real part).

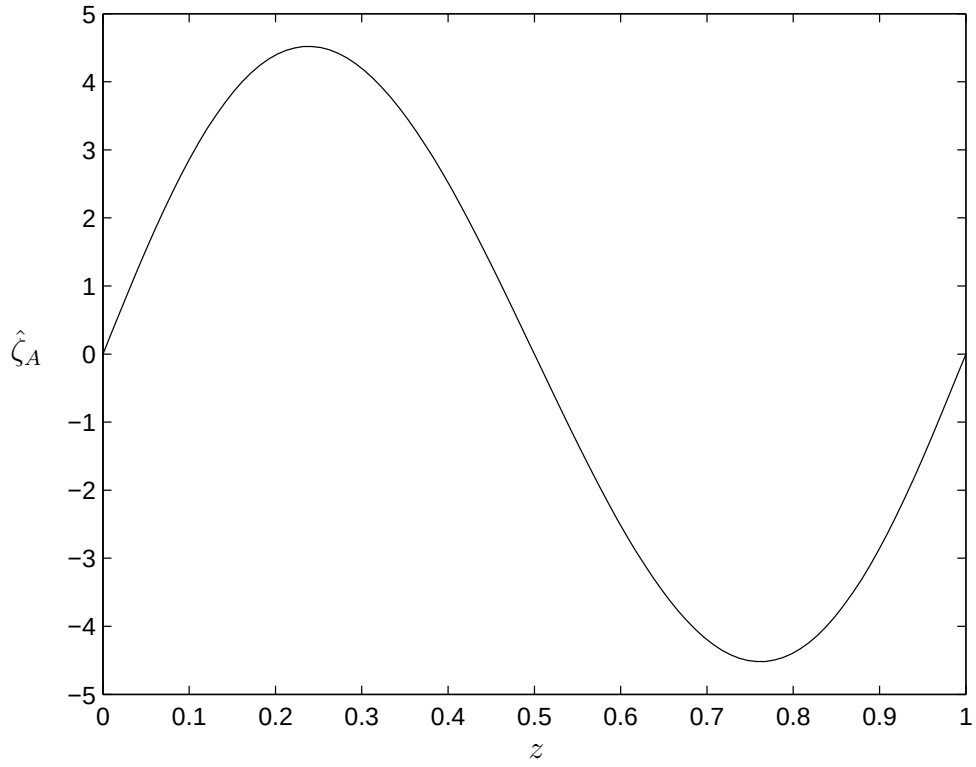

Figure 2.8: $\hat{\zeta}_A(z)$ for the adjoint problem with rigid boundaries, $\mathcal{T} = \sqrt{10}$ and $\mathrm{Pr} = 1$ (real part).

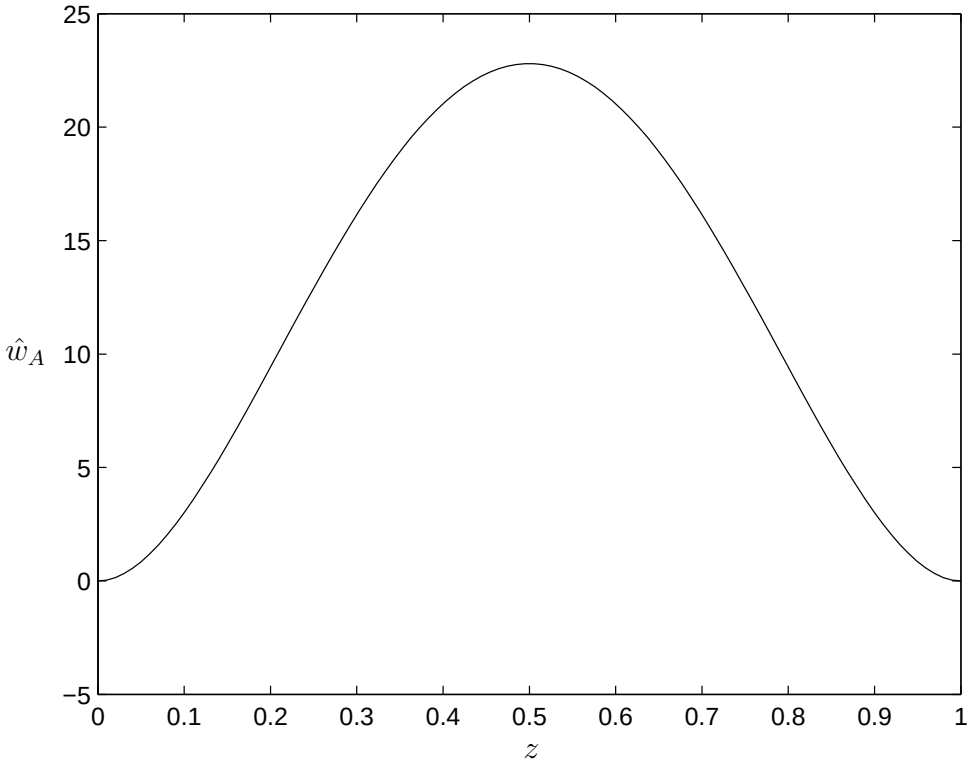

Figure 2.9: $\hat{w}_A(z)$ for the adjoint problem with rigid boundaries, $\mathcal{T} = \sqrt{10}$ and $\mathrm{Pr} = 1$ (real part).

are nonzero at this order. Continuity requires

$$\frac{\partial u_{3/2}}{\partial x} + \frac{\partial v_1}{\partial Y} = 0 \tag{2.25}$$

and the definition of ζ is

$$\frac{\partial v_{3/2}}{\partial x} = \frac{\partial u_1}{\partial Y} \tag{2.26}$$

For free boundaries, these two equations lead to the horizontal velocity components

$$u_{3/2} = -\frac{\mathcal{T}\pi}{ik_c a_c^2 C}\cos\pi z\left(\frac{\partial A}{\partial Y}e^{ik_c x} - c.c.\right) \tag{2.27}$$

$$v_{3/2} = -\frac{\pi}{ik_c C}\cos\pi z\left(\frac{\partial A}{\partial Y}e^{ik_c x} - c.c.\right) \tag{2.28}$$

For rigid boundaries, the horizontal velocities at this order can be found using the numerical results from the first-order problem.

2.6 Order ϵ^2

At order ϵ^2, the original problem (2.16) becomes

$$\begin{aligned} L\begin{pmatrix}\zeta_2\\ \theta_2\\ w_2\end{pmatrix} = &\begin{pmatrix}0\\ 2(\hat{w}_1\hat{\theta}_1' - ik_c\hat{\theta}_1\hat{u}_1)\\ 0\end{pmatrix}|A|^2 + \begin{pmatrix}-2(\hat{w}_1\hat{\zeta}_1' + ik_c\hat{u}_1\hat{\zeta}_1)\\ -(\hat{\theta}_1'\hat{w}_1 + ik_c\hat{\theta}_1\hat{u}_1)\\ 2ik_c\hat{u}_1''\hat{w}_1 - 2k_c^2\hat{u}_1\hat{u}_1'\end{pmatrix}A^2e^{2ik_cx} \\ &+ \begin{pmatrix}\mathrm{Pr}\hat{\zeta}_1\\ \hat{\theta}_1\\ \mathrm{Pr}(\mathrm{Ra}_c\hat{\theta}_1 + 2(\hat{w}_1'' - k_c^2\hat{w}_1))\end{pmatrix}2ik_c\left(\frac{\partial}{\partial X} + \frac{1}{2ik_c}\frac{\partial^2}{\partial Y^2}\right)Ae^{ik_cx} \end{aligned} \tag{2.29}$$

Additional complex conjugate terms have not been printed here because they are quite similar to these, and do not contribute to the final system of amplitude equations. This problem can be separated into three different inhomogeneous

problems to be solved individually. For free boundaries, the first of these problems is proportional to $|A|^2 \sin 2\pi z$ (for θ_2 and w_2; $|A|^2 \cos 2\pi z$ for ζ_2), the second is independent of z and the third is proportional to $\left(\frac{\partial}{\partial X} + \frac{1}{2ik_c}\frac{\partial^2}{\partial Y^2}\right) A \sin \pi z$ ($\left(\frac{\partial}{\partial X} + \frac{1}{2ik_c}\frac{\partial^2}{\partial Y^2}\right) A \cos \pi z$ for ζ_2).

It is important to note that the wave-number of the normal modes representation of each part of the second-order solution is different. The operator L still depends only on the fast variables, but the wave-number is 0, k_c, or $2k_c$, and the trigonometric functions may be of $2\pi z$ instead of πz. This results in an operator that is non-singular for the first and second problems, implying that L has different eigenvalues for these different problems. The part of the problem proportional to $\left(\frac{\partial}{\partial X} + \frac{1}{2ik}\frac{\partial^2}{\partial Y^2}\right) A$ is also proportional to $e^{ik_c x}$ and therefore has the same singular matrix operator as the linear problem. This leads to a secular term at second order, which would have to be eliminated by applying the solvability condition. However, this turns out to be unnecessary, as shown in appendix A.

At second order, the continuity equation becomes:

$$\frac{\partial v_{3/2}}{\partial Y} + \frac{\partial w_2}{\partial z} + \frac{\partial u_2}{\partial x} + \frac{\partial u_1}{\partial X} = 0 \tag{2.30}$$

and the definition of ζ becomes

$$\zeta_2 = \frac{\partial v_2}{\partial x} - \frac{\partial u_{3/2}}{\partial Y} + \frac{\partial v_1}{\partial X} \tag{2.31}$$

I use these expressions to calculate the horizontal velocity components, and add the mean drift terms $(U_2, V_2, 0)$ at this order following the example of Siggia and Zippelius [63] The y-component at second order, V_2, is shown to be zero in the next section, in agreement with their results.

2.6.1 Results for Stress-free Boundaries

Each of the three second-order problems can be solved analytically. The results are:

$$\theta_2 = -\frac{k_c^2}{2\pi a_c^2 C^2}\sin 2\pi z|A|^2 - \frac{2k_c^2}{a_c^4 C}\sin \pi z(\left(\frac{\partial}{\partial X} + \frac{1}{2ik_c}\frac{\partial^2}{\partial Y^2}\right) Ae^{ik_c x} + c.c.) \quad (2.32)$$

$$\zeta_2 = -\frac{\pi^2 \mathcal{T}}{2a_c^2 C^2 \mathrm{Pr}}\left(A^2 e^{2ik_c x} + c.c.\right) - \frac{2k_c^2 \mathcal{T}\pi}{a_c^4 C}\cos \pi z \left(\left(\frac{\partial}{\partial X} + \frac{1}{2ik_c}\frac{\partial^2}{\partial Y^2}\right) Ae^{ik_c x} + c.c.\right) \quad (2.33)$$

$$w_2 = 0 \quad (2.34)$$

$$u_2 = \frac{\pi}{ik_c C}\cos \pi z \left(\frac{\partial A}{\partial X}e^{ik_c x} - c.c.\right) - \frac{\pi}{k_c^2 C}\cos \pi z \left(\frac{\partial^2 A}{\partial Y^2}e^{ik_c x} + c.c.\right) + U_2 \quad (2.35)$$

$$v_2 = \frac{i\pi^2 \mathcal{T}}{4k_c a_c^2 C^2 \mathrm{Pr}}\left(A^2 e^{2ik_c x} - c.c.\right) + \frac{\pi \mathcal{T}}{k_c^2 a_c^2 C}\cos \pi z \left(\frac{\partial^2 A}{\partial Y^2}e^{ik_c x} + c.c.\right)$$
$$+\frac{2ik_c \mathcal{T}\pi}{a_c^4 C}\cos \pi z(\left(\frac{\partial}{\partial X} + \frac{1}{2ik_c}\frac{\partial^2}{\partial Y^2}\right) Ae^{ik_c x} - c.c.) + \frac{\mathcal{T}\pi}{ik_c a_c^2 C}\cos \pi z \left(\frac{\partial A}{\partial X}e^{ik_c x} - c.c.\right) \quad (2.36)$$

These results are in agreement with those of Cox and Matthews [17] when $\frac{\partial A}{\partial Y} = 0$ and the mean drift is neglected.

2.6.2 Results for Rigid Boundaries

At second order, Matlab's boundary value problem solver, `bvp4c`, described by Shampine, Kierzenka, and Reichelt [62], is used to solve each problem separately. Each right hand side is computed numerically from the first-order solution. All the parameters are known from the linear results, making each a straightforward boundary value problem. Sample numerical solutions to the second order problems with rigid boundaries, $\mathcal{T} = 10$, and $\mathrm{Pr} = 1$ are shown in figures 2.10 through 2.15. The parts not depicted are zero.

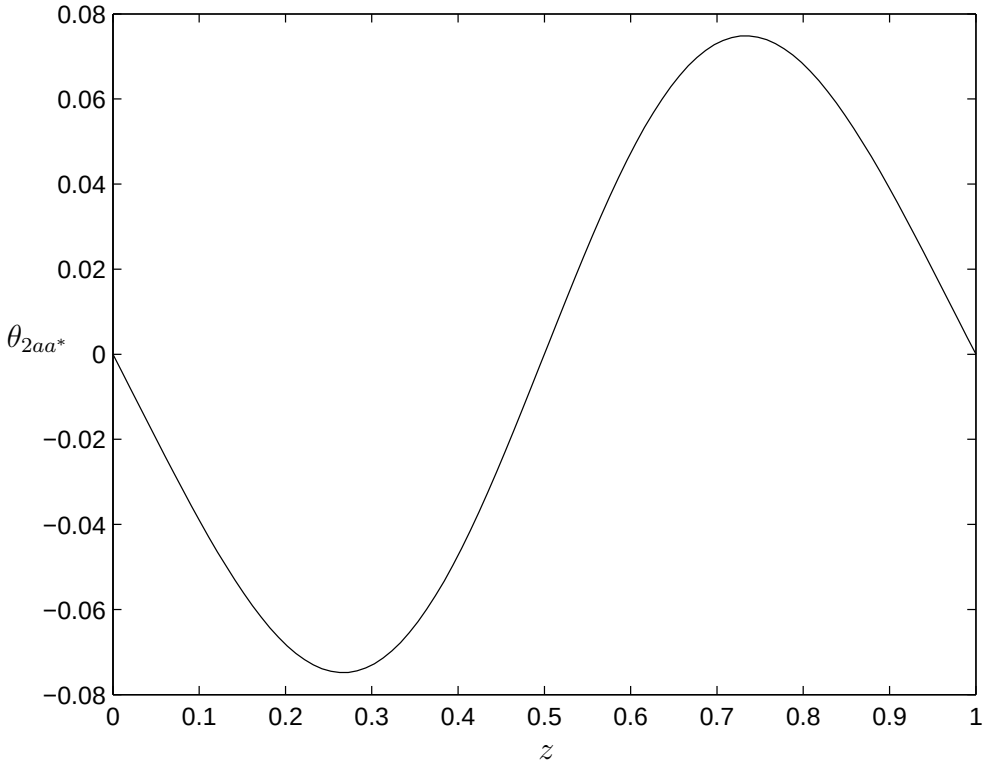

Figure 2.10: The part of θ_2 proportional to $|A|^2$ with rigid boundaries (real part).

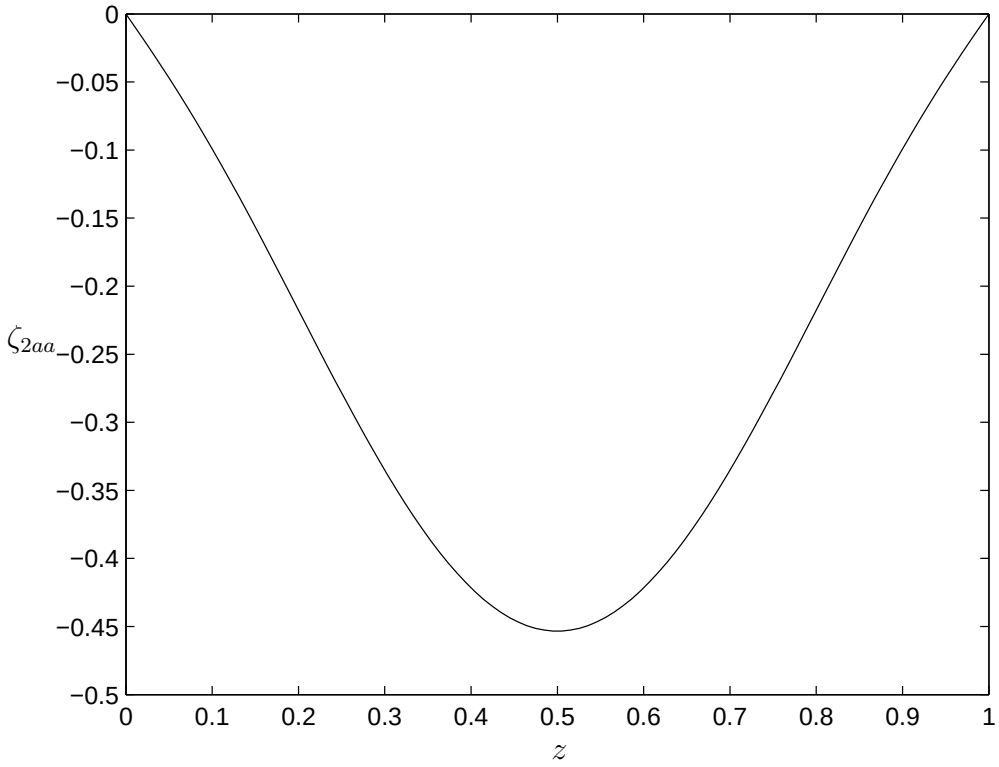

Figure 2.11: The part of ζ_2 proportional to A^2 with rigid boundaries (real part).

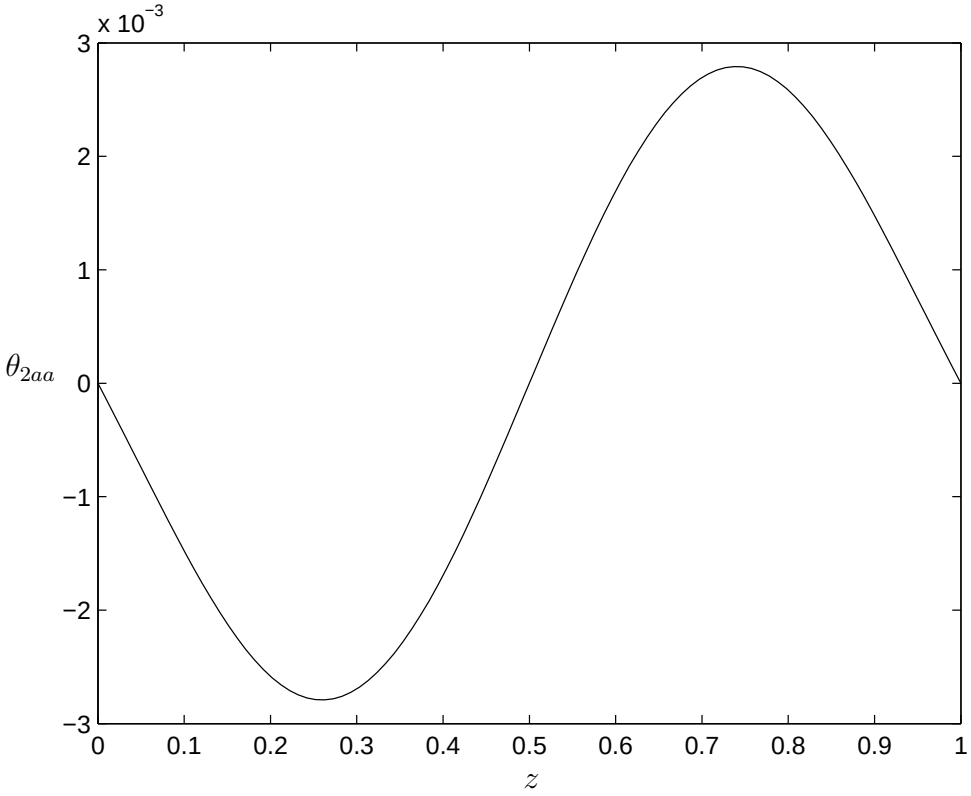

Figure 2.12: The part of θ_2 proportional to A^2 with rigid boundaries (real part).

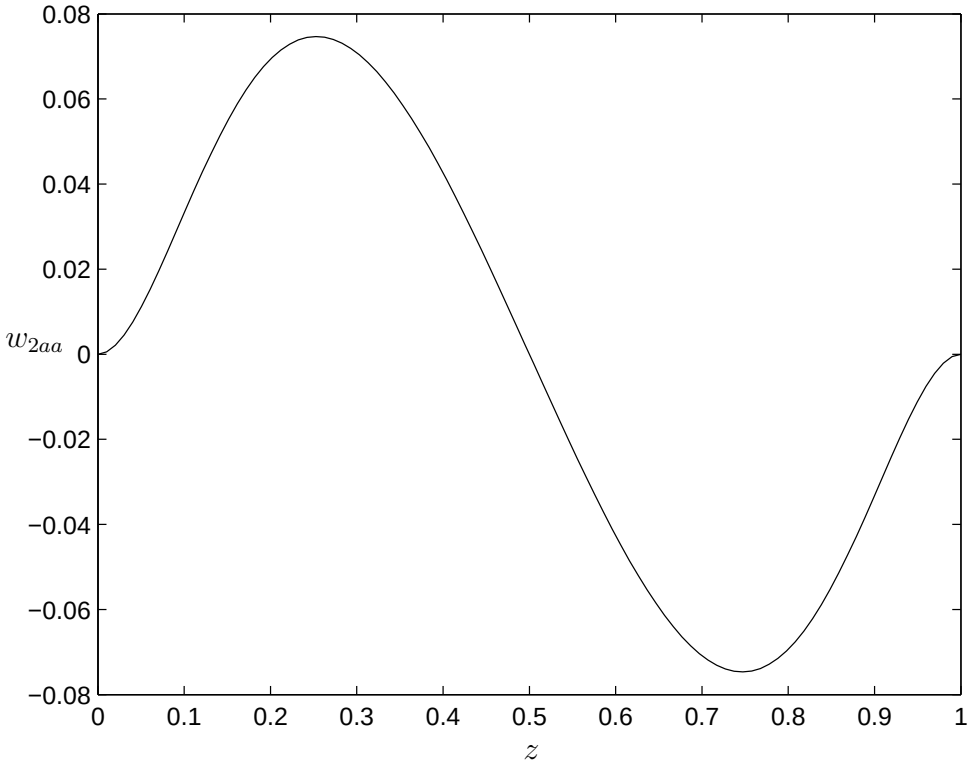

Figure 2.13: The part of w_2 proportional to A^2 with rigid boundaries (real part).

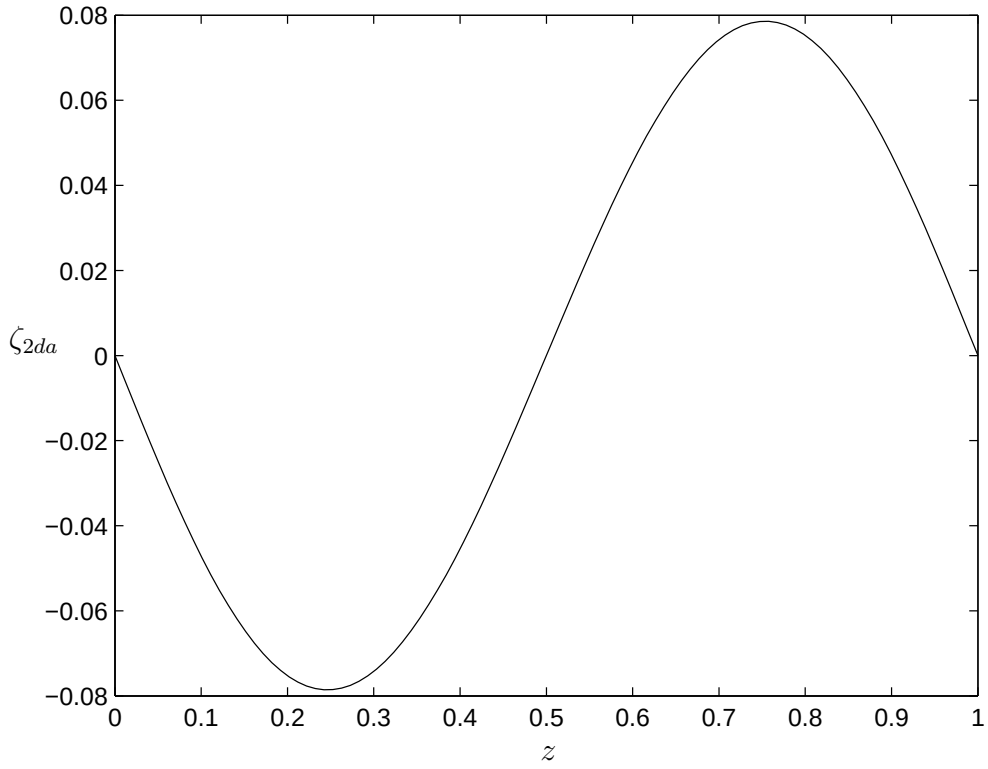

Figure 2.14: The part of ζ_2 proportional to $\left(\frac{\partial}{\partial X} + \frac{1}{2ik}\frac{\partial^2}{\partial Y^2}\right) A$ with rigid boundaries (real part).

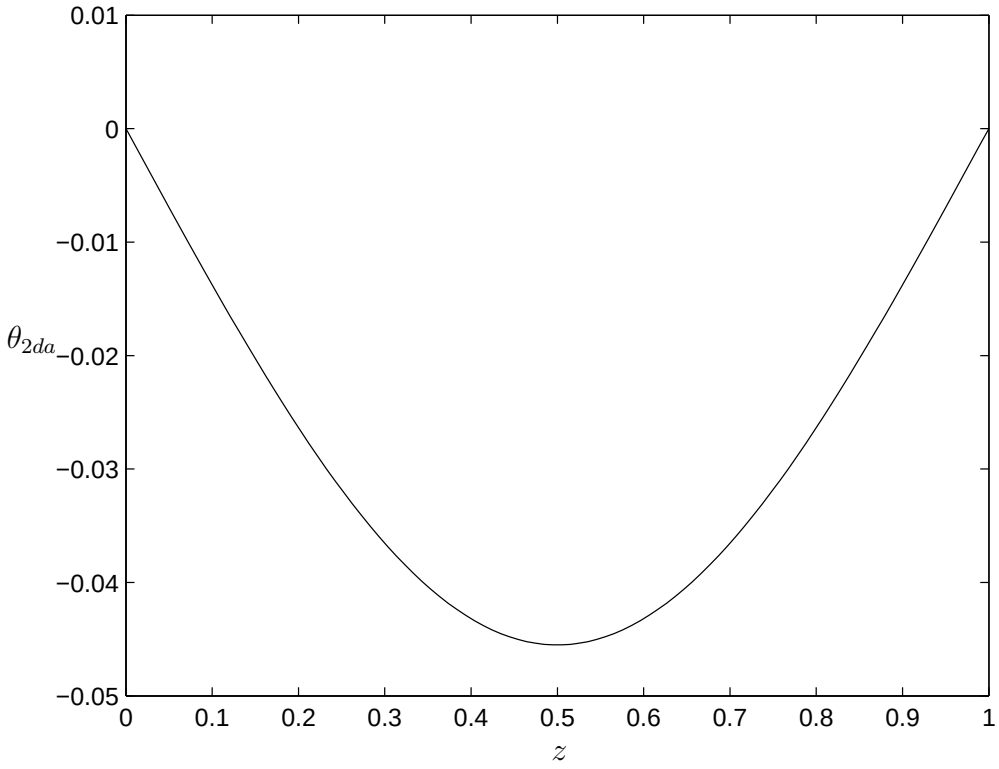

Figure 2.15: The part of θ_2 proportional to $\left(\frac{\partial}{\partial X} + \frac{1}{2ik}\frac{\partial^2}{\partial Y^2}\right) A$ with rigid boundaries (real part).

For rigid boundaries, the horizontal mean drift $\vec{U}$ is a function of z, as it must be zero on both boundaries. Following the example of Zippelius and Siggia [73], I assume that the quantity that appears in the amplitude equation is actually the vertically integrated velocity,

$$\vec{U}(X,Y) = \int_0^1 \vec{U}_{rigid}(X,Y,z)dz \tag{2.37}$$

Zippelius and Siggia emphasize that this is not exact, but does result in amplitude equations which are qualitatively realistic. As they remark,

> "...the generation of vertical vorticity by a modulation of the basic roll pattern is expected to be of higher order in ϵ and a systematic treatment of the effects would require an additional order in the amplitude expansion."

Using the vertical average of the mean drift is a way of avoiding this complexity, while maintaining the qualitative features of the flow. This assumption becomes important when the solvability condition is applied and the amplitude equation coefficients computed. If it is not made and U is left at second order, the amplitude equation term containing U involves an integral with respect to z.

2.7 Order $\epsilon^{5/2}$

At this order, the system (2.16) becomes

$$L\begin{pmatrix}\zeta_{5/2}\\ \theta_{5/2}\\ w_{5/2}\end{pmatrix} = \begin{pmatrix}\frac{2i}{k_c}\hat{\zeta}_1^2 + 2\hat{u}_1'\hat{w}_1 + 2ik_c\hat{u}_1^2\\ \frac{i}{k_c}\hat{\theta}_1\hat{\zeta}_1\\ \aleph\end{pmatrix}\left(A\frac{\partial A}{\partial Y}e^{2ik_cx} - c.c.\right) + \begin{pmatrix}0\\ \frac{i}{k_c}\hat{\theta}_1\hat{\zeta}_1\\ 0\end{pmatrix}\left(A^*\frac{\partial A}{\partial Y} - c.c.\right) \quad (2.38)$$

with

$$\aleph = -\frac{2}{k_c}(i\hat{w}_1\hat{\zeta}_1'' + i\hat{w}_1'\hat{\zeta}_1' - 2k_c\hat{u}_1\hat{\zeta}_1' + 2ik_c^2\hat{w}_1\hat{\zeta}_1 - 2k_c\hat{u}_1'\hat{\zeta}_1) \quad (2.39)$$

Continuity becomes

$$\frac{\partial u_{5/2}}{\partial x} + \frac{\partial u_{3/2}}{\partial X} + \frac{\partial v_2}{\partial Y} + \frac{\partial w_{5/2}}{\partial z} = 0 \quad (2.40)$$

The part of this equation that is not proportional to an exponential in x is

$$\frac{\partial V_2}{\partial Y} = 0 \quad (2.41)$$

which suggests that V_2 is zero, in agreement with Zippelius and Siggia's result [73]. There may be a horizontal mean flow term perpendicular to the wave-vector at order $\epsilon^{5/2}$, as they posit. The slowly-varying part of the continuity equation at third order is

$$\frac{\partial U_2}{\partial X} + \frac{\partial V_{5/2}}{\partial Y} = 0 \quad (2.42)$$

showing that the $\hat{y}$ mean drift at order $\epsilon^{5/2}$ instead of order ϵ^2. Because of this, V_2 can be set to zero, as Zippelius and Siggia [73] have done.

The definition of ζ states

$$\zeta_{5/2} = \frac{\partial v_{5/2}}{\partial x} + \frac{\partial v_{3/2}}{\partial X} - \frac{\partial u_2}{\partial Y} \tag{2.43}$$

To avoid a velocity that grows without bound when this equation is integrated, it is necessary to add a slowly-varying vorticity term $-\frac{\partial U}{\partial Y}$ to $\zeta_{5/2}$.

2.7.1 Results for Stress-free Boundaries

The solution to the system is:

$$\zeta_{5/2} = \frac{i\pi^2}{4a_c^4 C^2 k_c \mathrm{Pr}}(2a_c^4 - \mathcal{T}^2)\left(A\frac{\partial A}{\partial Y}e^{2ik_c x} - c.c.\right) + \zeta_{5/2A}\cos 2\pi z\left(A\frac{\partial A}{\partial Y}e^{2ik_c x} - c.c.\right) - \frac{\partial U}{\partial Y} \tag{2.44}$$

with

$$\zeta_{5/2A} = -\frac{ik_c\pi^2(k_c^2\mathrm{Ra}_c\mathcal{T}^2(\mathrm{Pr}-1) + 20a_c^6\mathcal{T}^2 + k_c^2a_c^4\mathrm{Ra}_c - 16a_c^{10})}{4C^2a_c^6\mathrm{Pr}(\mathcal{T}^2\pi^2 - k_c^2\mathrm{Ra}_c + 16a_c^6)} \tag{2.45}$$

$$w_{5/2} = w_{5/2A}\sin 2\pi z\left(A\frac{\partial A}{\partial Y}e^{2ik_c x} - c.c.\right) \tag{2.46}$$

$$\theta_{5/2} = \theta_{5/2A}\sin 2\pi z\left(A\frac{\partial A}{\partial Y}e^{2ik_c x} - c.c.\right) - \frac{i\pi k_c\mathcal{T}}{8\pi^2a_c^4C^2}\sin 2\pi z\left(A^*\frac{\partial A}{\partial Y} - c.c.\right) \tag{2.47}$$

$w_{5/2A}$ and $\theta_{5/2A}$ are constants which do not contribute to the final system of amplitude equations. The horizontal velocity component perpendicular to the wavevector is

$$\frac{\partial v_{5/2}}{\partial x} = \zeta_{5/2} - \frac{\pi}{ik_cC}\cos\pi z\left(\frac{\partial^3 A}{\partial Y^3}e^{ikx} + c.c.\right) + \frac{\partial U_2}{\partial Y} \tag{2.48}$$

from the definition of ζ.

2.8 Order ϵ^3

At third order I calculate the right hand side of 2.16 and apply the solvability condition. The problem is

$$L\begin{pmatrix}\zeta_3\\ \theta_3\\ w_3\end{pmatrix} = \begin{pmatrix}(-\nabla\times(\vec{v}\cdot\nabla\vec{v})\cdot\hat{z} + \mathrm{Pr}\nabla^2\zeta)_3 - \frac{\partial\zeta_1}{\partial T}\\ (-\vec{v}\cdot\nabla\theta + \nabla^2\theta)_3 - \frac{\partial\theta_1}{\partial T}\\ (\nabla\times\nabla\times(\vec{v}\cdot\nabla\vec{v})\cdot\hat{z} + \mathrm{Pr}\nabla^4 w + \mathrm{PrRa}_c\nabla_h^2\theta)_3 - \frac{\partial\nabla^2 w_1}{\partial T} + \mathrm{Pr}R_2\nabla_h^2\theta_1\end{pmatrix} \tag{2.49}$$

The subscript 3 refers to the order ϵ^3 parts of this that do not involve the third-order solutions, such as $\frac{\partial}{\partial X}$ and $\frac{\partial}{\partial Y}$ terms.

For this problem to have a solution, the right hand side of the third order system must be orthogonal to the adjoint eigenvector:

$$\int_0^1\int_{-\pi}^{\pi}\vec{R}_3\cdot\vec{S}_A dxdz = 0 \tag{2.50}$$

This well-known solvability condition is discussed, for example, in Joseph's monograph [36, p.39–41]. $\vec{R}_3$ is the right-hand side at order ϵ^3, as given in equation 2.49, and $\vec{S}_A$ is the solution to the adjoint problem, given in section 2.4.

Applying the solvability condition leads to the amplitude equation

$$\alpha\frac{\partial A}{\partial T} = \sigma A - \lambda|A|^2 A + \delta\left(\frac{\partial}{\partial X} + \frac{1}{2ik_c}\frac{\partial^2}{\partial Y^2}\right)^2 A - i\eta AU \tag{2.51}$$

where $U(X,Y,T)$ is the mean drift at order ϵ^2. The growth rate, $\frac{\sigma}{\alpha}$, is the eigenvalue of the linear operator L with the largest real part at the chosen Rayleigh number. It can be obtained from the linear problem at first order, or through the solvability condition.

2.8.1 Results for Stress-free Boundaries

For stress-free boundaries, the coefficients can be found analytically. They are:

$$\alpha = -\frac{ik_c}{2a_c^2 C}\left(\mathcal{T}^2\pi^2 - a_c^6 - k_c^2 \mathrm{PrRa}_c\right) \tag{2.52}$$

$$\sigma = \frac{ik_c^3 \mathrm{Pr} R_2}{2C} \tag{2.53}$$

$$\lambda = -\frac{ik_c}{4a_c^2 \mathrm{Pr} C^3}\left(\pi^4\mathcal{T}^2 - \mathrm{Pr}^2 k_c^4 \mathrm{Ra}_c\right) \tag{2.54}$$

$$\delta = \frac{2ik_c^3 \mathrm{Pr}}{a_c^4 C}(\pi^2(\mathcal{T}^2 + \mathrm{Ra}_c) + a_c^6) \tag{2.55}$$

$$\eta = -\frac{ik_c^2}{2a_c^2 C}\left(\pi^2\mathcal{T}^2 - a_c^6 - k_c^2 \mathrm{PrRa}_c\right) \tag{2.56}$$

2.8.2 Results for Rigid Boundaries

For rigid boundaries, it is necessary to compute the amplitude equation coefficients numerically. Each part of the right hand side is calculated and the solvability condition, equation 2.50, is applied. Numerical integration is performed using Matlab's `trapz` function. The values of the amplitude equation coefficients for rigid boundaries are shown in figures 2.16 through 2.18 and given in tabular form in appendix D. The coefficient of the mean drift term, η/α, is not shown because the numerically computed value of η is equal to $k_c\alpha$.

The derivation of the system of amplitude equations follows the methods of Zippelius and Siggia [73], who stress that

> "Certainly other nonlinearities are present to the same order in ϵ. We have not calculated these terms but merely tried to account qualitatively for the effects of vorticity in low Prandtl number convection."

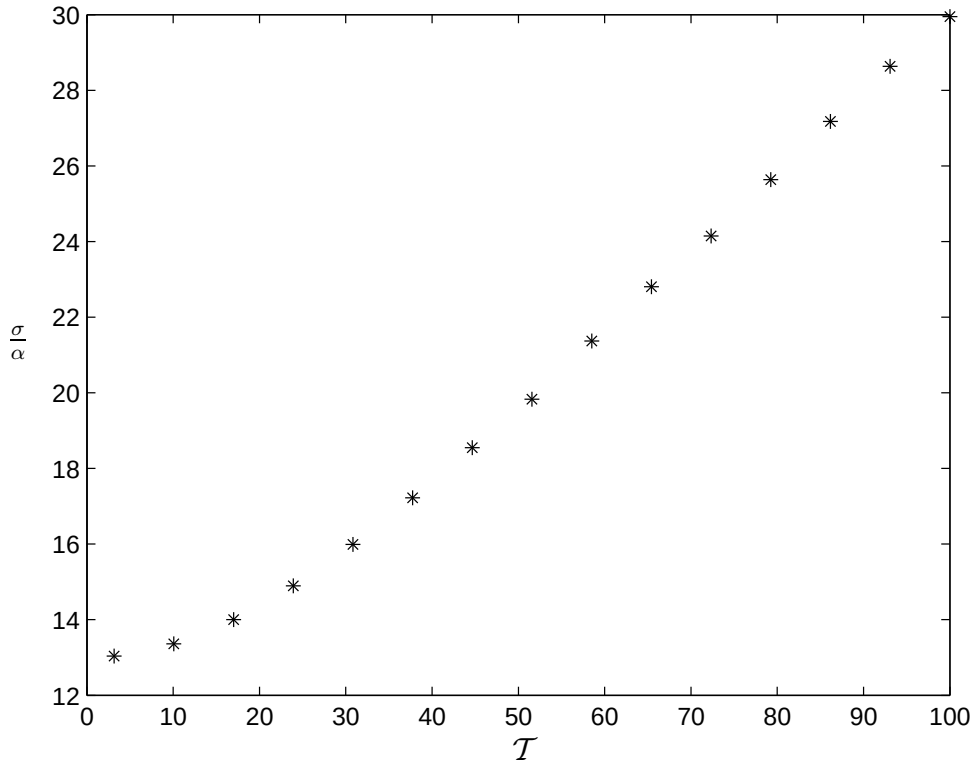

Figure 2.16: Growth rate, $\frac{\sigma}{\alpha}$ versus $\mathcal{T}$, with $\mathrm{Pr} = 1$ and rigid boundaries.

While the present analysis is careful in the calculation of the coefficients, the additional nonlinearities and variation with depth of the mean drift have been neglected. Decker and Pesch [24] seek to remedy these oversimplications for the case of ordinary Rayleigh-Bénard convection with rigid boundaries. Their analysis, based on order parameter equations, results in a pair of very complicated amplitude equations, the first of which simplifies to the usual Ginzburg-Landau equation with the mean drift term presented here when higher-order derivatives are neglected.

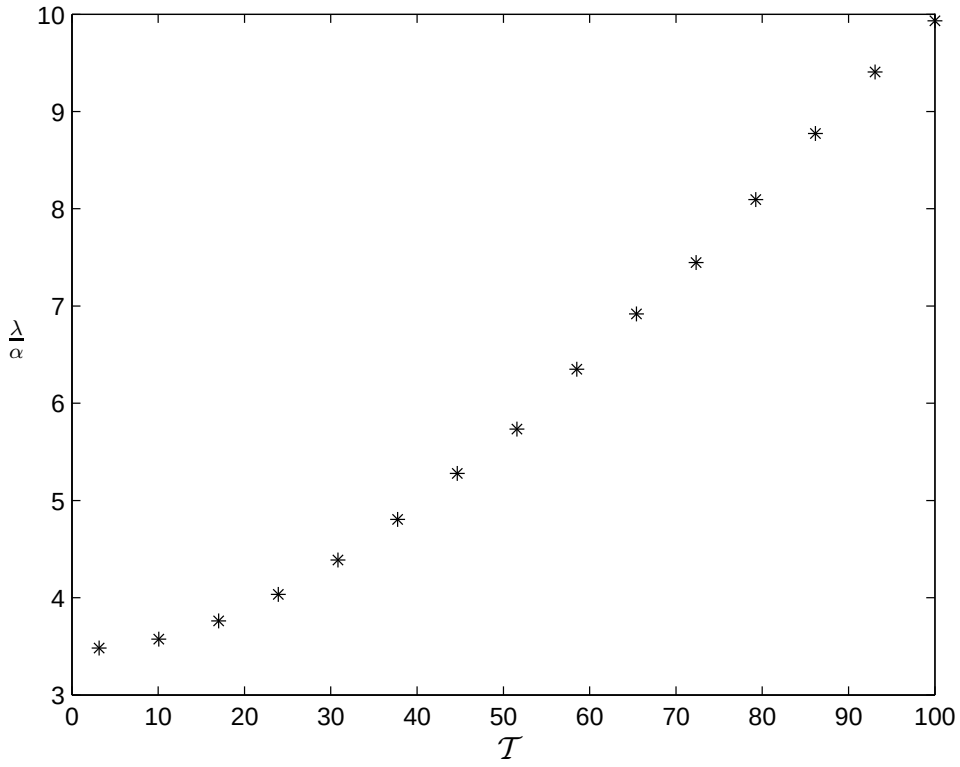

Figure 2.17: Landau coefficient, $\frac{\lambda}{\alpha}$ versus $\mathcal{T}$, with $\mathrm{Pr} = 1$ and rigid boundaries.

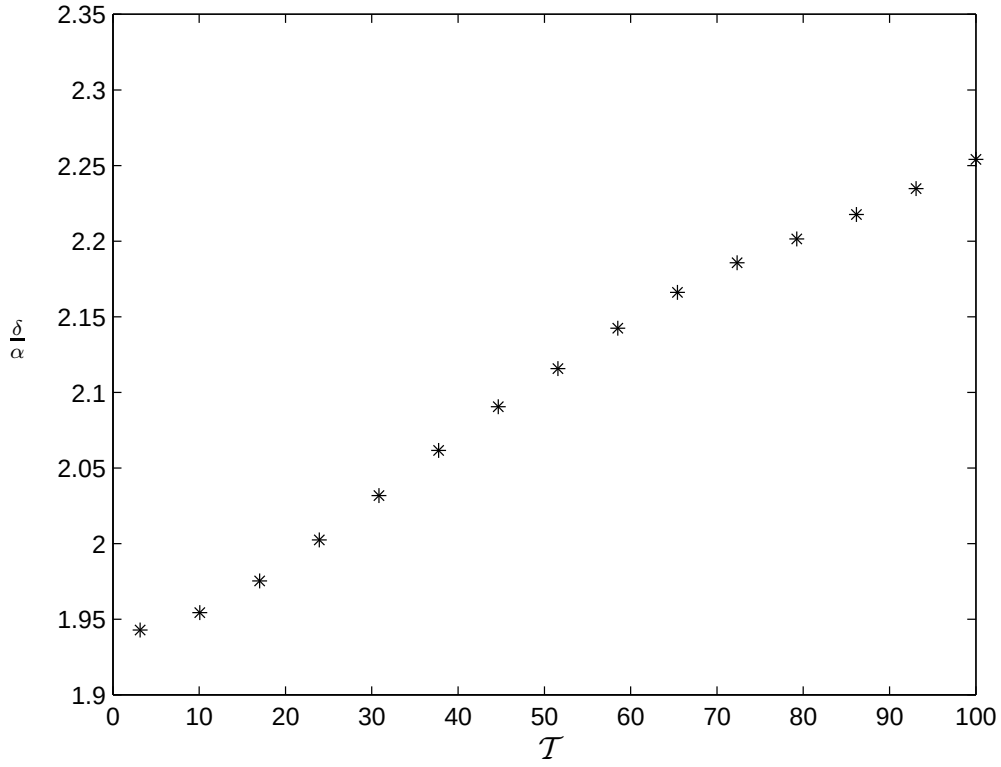

Figure 2.18: The coefficient $\frac{\delta}{\alpha}$ versus $\mathcal{T}$, with $\mathrm{Pr} = 1$ and rigid boundaries.

2.9 Order $\epsilon^{7/2}$

At this order, there is a slow vorticity equation that functions as a second equation, coupled to the Ginzburg-Landau amplitude equation derived at third order. Zippelius and Siggia [63], [73] derive this equation analytically for ordinary convection with stress-free boundaries, and describe its form for rigid boundaries. The following calculations agree with theirs when the Taylor number is zero and their different choices of nondimensionalization and normalization are accounted for.

2.9.1 Results for Stress-free Boundaries

Zippelius and Siggia use the slow part of $\zeta_{5/2}$ in the vorticity equation at order $\epsilon^{7/2}$ to derive their second equation. Following their method results in the equation:

$$-\mathrm{Pr}\frac{\partial^2\Omega}{\partial Y^2} = \left(\frac{\mathcal{T}^2}{a_c^4} - 1\right)\frac{\pi^2}{C^2}\frac{\partial}{\partial Y}\left(A^*\left(\frac{\partial}{\partial X} - \frac{i}{2k_c}\frac{\partial^2}{\partial Y^2}\right)A + c.c.\right) \tag{2.57}$$

where $\Omega = -\frac{\partial U}{\partial Y}$ is Zippelius and Siggia's [73] $\zeta_{5/2}$, and U is U_2, the mean drift at second order. In order to derive this equation, it is necessary to drop all fast terms, and any slow terms that may appear in the third or higher order solutions. Zippelius and Siggia choose to keep the (higher-order) $\frac{\partial\Omega}{\partial T}$ and $\frac{\partial^2\Omega}{\partial X^2}$ terms as a part of their second equation. In their analysis, these terms change quantitative aspects of the flow, but have no qualitative effects. Details of the derivation are given in appendix B and in the appendix of [73].

2.9.2 Results for Rigid Boundaries

Following the same methods, with the assumption that the relevant horizontal velocity is actually the vertical average velocity, an equation similar to 2.57 results

(see appendix B):

$$\mathrm{Pr}\frac{\partial^3 U}{\partial Y^3} = g\frac{\partial}{\partial Y}\left(A^*\left(\frac{\partial}{\partial X} - \frac{i}{2k_c}\frac{\partial^2}{\partial Y^2}\right)A + c.c.\right) \tag{2.58}$$

In this case, the constant g must be computed numerically. It is, according to Zippelius and Siggia [73], of order ϵ, to account for the higher-order vertical vorticity due to the depth-dependent mean flow introduced by rigid boundaries.

Zippelius and Siggia's second equation is quite similar:

$$\Omega = \epsilon g\frac{\partial}{\partial Y}\left(A^*\left(\frac{\partial}{\partial X} - \frac{i}{2k_c}\frac{\partial^2}{\partial Y^2}\right)A + c.c.\right) \tag{2.59}$$

with

$$\frac{\partial \Omega}{\partial Y} = -\left(\frac{\partial^2}{\partial Y^2} + \nu\frac{\partial^2}{\partial X^2}\right)U \tag{2.60}$$

where ν is a constant.

Decker and Pesch [24] also derive amplitude and mean drift equations for rigid boundaries, using order parameter equations. Unlike Zippelius and Siggia [73], who make assumptions about the final form of the equation based on the physics behind the system, Decker and Pesch complete the general calculation for non-rotating convection with rigid boundaries. Their (simplified) drift equation is:

$$\left(\frac{\partial^2}{\partial X^2} + \frac{\partial^2}{\partial Y^2}\right)B = g\frac{\partial}{\partial Y}\left(A\left(\frac{\partial}{\partial X} - \frac{i}{2k}\frac{\partial^2}{\partial Y^2}\right)A^* + c.c.\right) \tag{2.61}$$

where U is equivalent to $\frac{\partial B}{\partial Y}$. They assumed that the time derivative is zero, and kept the X-derivative despite its higher order. They also present a much more complex version of this equation, in which they keep higher-order derivative terms and calculate g as a rational function in terms of the Prandtl number.

The left hand side of 2.58 is proportional to the third derivative of U, while Zippelius and Siggia [73] and Decker and Pesch [24] have a left hand side which is proportional to U's first derivative. This is because the mean drift for rigid boundaries is actually assumed to be the vertically integrated version of the actual

drift, $U(X, Y, z)$. Both Zippelius and Siggia [73] and Decker and Pesch [24] try to correct the second equation to account for this averaging; I simply accept it, keeping the assumption to the end.

2.10 Stability of Stokes Wave Solutions

The stability analysis performed here follows the example of Matkowsky and Volpert [52]. The system of 2.51 and 2.57 has solutions in the form of Stokes waves, $A_s = Fe^{i\vec{Q}\cdot\vec{X}}$, where F and Q are constants. These waves are of interest because they are the simplest nontrivial solution to the amplitude equations, and because their instability leads to the well-known Küppers-Lortz instability [42]. Substituting this solution form into equation 2.51 yields the equation

$$0 = \sigma - \lambda|F|^2 - \delta P^2 - i\eta U \tag{2.62}$$

where $P = Q_x + \frac{Q_y^2}{2k_c}$. When this solution form is substituted into equation 2.57, the right hand side is zero, giving

$$\frac{\partial^3 U}{\partial Y^3} = 0 \tag{2.63}$$

showing that U is a function of X and T only, because otherwise U would be unbounded as $|Y| \to \infty$. However, since equation 2.62 has no spatial or time-dependence in any term except possibly U, U must be a constant when A is a Stokes wave. This constant is assumed to be zero for the rest of this analysis. Since the mean drift arises due to the curvature of the rolls, zero mean drift corresponds to ideal straight rolls.

The first step is to rescale equation 2.51 in order to simplify the coefficients. I choose the following new variables:

$$T' = \sigma T \tag{2.64}$$

$$Y' = \left(\frac{\sigma}{\delta}\right)^{\frac{1}{4}} \frac{Y}{\sqrt{2k_c}} \qquad X' = X\sqrt{\frac{\sigma}{\delta}} \tag{2.65}$$

$$A' = A\sqrt{\frac{\lambda}{\sigma}} \tag{2.66}$$

Substituting these expressions into this new equation and equation 2.51 (with $U = 0$), then dropping primes yields the new equation:

$$\frac{\partial A}{\partial T} = A - |A|^2 A + \left(\frac{\partial}{\partial X} - i\frac{\partial^2}{\partial Y^2}\right)^2 A \tag{2.67}$$

Next the solution form $A_s = Fe^{i\vec{Q}\cdot\vec{X}}$ is substituted. Solving for F gives the trivial solution $F = 0$, as well as

$$F = \pm\sqrt{1 - (Q_y^2 + Q_x)^2} \tag{2.68}$$

To determine the stability of each solution, I perturb the Stokes wave by substituting the form

$$A = (F + f(\vec{X}, T))e^{i\vec{Q}\cdot\vec{X}} \tag{2.69}$$

into equation 2.67 and linearize in the perturbation amplitude f:

$$\begin{aligned}\frac{\partial f}{\partial T} = -F^2(f + f^*) + 4iQ_y(Q_y^2 + Q_x)\frac{\partial f}{\partial Y} + 2i(Q_y^2 + Q_x)\frac{\partial f}{\partial X} + 2(3Q_y^2 + Q_x)\frac{\partial^2 f}{\partial Y^2} \\ - 4iQ_y\frac{\partial^3 f}{\partial Y^3} + 4Q_y\frac{\partial^2 f}{\partial Y \partial X} - \frac{\partial^4 f}{\partial Y^4} + \frac{\partial^2 f}{\partial X^2} - 2i\frac{\partial^3 f}{\partial Y^2 \partial X}\end{aligned} \tag{2.70}$$

If the trivial solution is chosen, equation 2.70 simplifies to

$$\frac{\partial f}{\partial T} = -\frac{\partial^4 f}{\partial Y^4} + \frac{\partial^2 f}{\partial X^2} - 2i\frac{\partial^3 f}{\partial Y^2 \partial X} \tag{2.71}$$

and separating the perturbation $f = u + iv$ into its real and imaginary parts leads to a pair of equations. Substituting the solution form $u = \hat{u}e^{\Omega T + i\vec{\kappa}\cdot\vec{X}}$ and $v = \hat{v}e^{\Omega T + i\vec{\kappa}\cdot\vec{X}}$ leads to the system of equations

$$\begin{pmatrix} \Omega\hat{u} \\ \Omega\hat{v} \end{pmatrix} = \begin{pmatrix} C_0 & -C_1 \\ C_1 & C_0 \end{pmatrix} \begin{pmatrix} \hat{u} \\ \hat{v} \end{pmatrix} \tag{2.72}$$

with $C_0 = -\kappa_y^4 - \kappa_x^2$ and $C_1 = 2i\kappa_x\kappa_y^2$. The characteristic equation for this system is $\Omega^2 - 2\Omega C_0 + C_1^2 + C_0^2$, with solution $\Omega = -(\kappa_y^2 \pm \kappa_x)^2 < 0$. Therefore the trivial solution is stable.

For the nontrivial solution, the system becomes

$$\begin{pmatrix} \Omega\hat{u} \\ \Omega\hat{v} \end{pmatrix} = \begin{pmatrix} C_0 - 2F^2 & -C_1 \\ C_1 & C_0 \end{pmatrix} \begin{pmatrix} \hat{u} \\ \hat{v} \end{pmatrix} \tag{2.73}$$

with

$$C_0 = -6\kappa_y^2 Q_y^2 - 4\kappa_x\kappa_y Q_y - 2\kappa_y^2 Q_x - \kappa_y^4 - \kappa_x^2 \tag{2.74}$$

$$C_1 = 4i\kappa_y Q_y^3 + 2i\kappa_x Q_y^2 + 4i\kappa_y Q_x Q_y + 4i\kappa_y^3 Q_y + 2i\kappa_x Q_x + 2i\kappa_x\kappa_y^2 \tag{2.75}$$

The characteristic equation is

$$\Omega^2 - 2\beta\Omega + \gamma = 0 \tag{2.76}$$

with

$$\beta = -F^2 + C_0 \tag{2.77}$$

$$\gamma = -2F^2 C_0 + C_1^2 + C_0^2 \tag{2.78}$$

The maximum real part of the growth rate $\Omega = \beta \pm \sqrt{\beta^2 - \gamma}$ determines whether a perturbation grows (positive value, unstable) or decays (negative value, stable). Figure 2.19 shows regions where at least one perturbation with $|\kappa_x|$ and $|\kappa_y|$ less than or equal to one is unstable. The maximum growth rate for $|\kappa_x|$ and $|\kappa_y|$ less than 2.5 is $\Omega = 1$, which occurs for the points $\vec{Q} = (0, -1)$ with $\vec{\kappa} = (-2.25, -0.5)$, $\vec{Q} = (0.75, -0.5)$ with $\vec{\kappa} = (-1.75, -0.5)$, $\vec{Q} = (-1, 0)$ with $\vec{\kappa} = (-1.25, 1.5)$, $\vec{Q} = (1, 0)$ with $\vec{\kappa} = (-2, 1)$, $\vec{Q} = (0.75, 0.5)$ with $\vec{\kappa} = (-1.75, 0.5)$, and $\vec{Q} = (0, 1)$ with $\vec{\kappa} = (-2.25, 0.5)$.

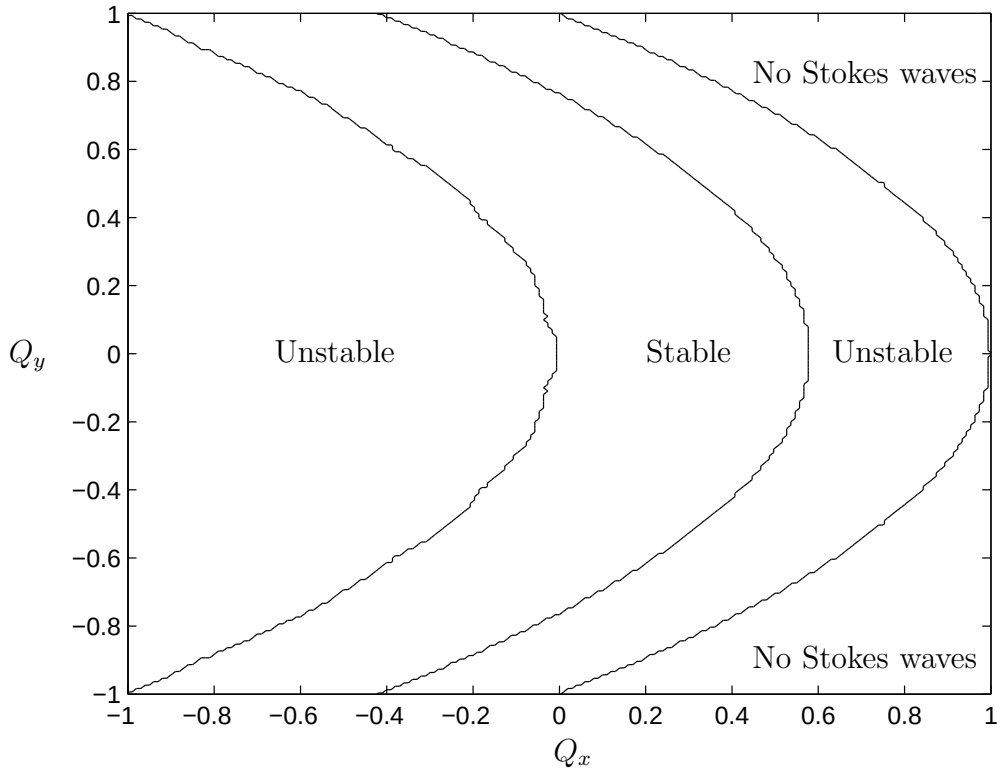

Figure 2.19: Stability of Stokes waves for any $\vec{\kappa}$ with $|\kappa_x|$ and $|\kappa_y|$ less than or equal to one. In the unstable regions, at least one perturbation grows. In the stable region, Stokes waves are (neutrally) stable for all perturbations. The regions labeled "No Stokes waves" are where $F^2 < 0$.

2.11 Conclusion

A fully three-dimensional system of amplitude equations (2.51 and 2.57) has been derived for rotating thermal convection, using the method of multiple scales. It has been shown that it is necessary to carry out the perturbation analysis in orders of $\epsilon^{1/2}$, because the velocity has horizontal components at non-integer orders. Analytic coefficients for free boundaries were derived, and numerical coefficients for rigid boundaries were calculated. This system of equations is the main result of this chapter. All of this analysis assumed a stationary bifurcation; with a Hopf bifurcation, the analysis is more complex, and is the subject of the following chapter.

A slowly-varying mean drift parallel to the wave-vector was found at second order in ϵ, and its perpendicular component was found at order $\epsilon^{5/2}$. The mean drift, resulting from roll curvature, is physically important because it advects the rolls. A mean drift equation, equation 2.57, coupled to the amplitude equation, was derived for free boundaries without using averaging, and described for rigid boundaries. A stability analysis revealed that, except in certain special cases, Stokes wave solutions to the amplitude equations without mean drift are stable.

There is some additional research to be done into the system of amplitude equations for rigid boundaries. The second equation could be better understood and its coefficient calculated. The variation of the horizontal mean drift with depth was neglected. Including such variation in the analysis could produce some interesting, and more realistic, results. The next step in this analysis is to simulate the amplitude equations. Once numerical simulations have been completed, it will be possible to reconstruct the physical velocity field by piecing the components at each order back together.

CHAPTER 3

AMPLITUDE EQUATIONS FOR ROTATING CONVECTION WITH A HOPF BIFURCATION

3.1 Introduction

The analysis of the previous chapter assumes that the convective system undergoes a stationary bifurcation. A Hopf bifurcation is also possible, if the Prandtl number is sufficiently small. When this type of bifurcation occurs, the eigenvalue with the largest real part is purely imaginary, equal to $i\omega$, resulting in a system which oscillates in time. Mathematically, the time-derivative term in each equation of the system 2.17 must be be kept, as σ, the eigenvalue, is now $\pm i\omega$, a complex conjugate pair. This change leads to some important changes in the amplitude equation system. In this chapter I consider only stress-free boundaries, but include slow spatial dependence and the mean drift.

At higher order, a Hopf bifurcation means that there are actually two traveling waves, corresponding to two slowly-varying amplitudes:

$$w_1 = w_{1a}(z)Ae^{i(k_c x+\omega_c t)} + w_{1a}^* A^* e^{-i(k_c x+\omega_c t)} + w_{1b}Be^{i(k_c x-\omega_c t)} + w_{1b}^* B^* e^{-i(k_c x-\omega_c t)} \tag{3.1}$$

with similar expressions for the other variables. The multiple-scales expansion is expected to lead to a pair of coupled equations, similar to those derived by Knobloch and De Luca [41] for double-diffusive convection. Bajaj, Ahlers, and Pesch [1] derive a pair of equations for the two-dimensional case, and Brand, Lomdahl, and Newell [7], [8] derive an amplitude equation for the case of a single traveling wave resulting from a Hopf bifurcation. Martel, Knobloch, and Vega [51], Revallo and Ševčovič [57], Riecke and Kramer [58], and van Hecke, Storm, and van Saarloos [68] analyze similar systems of equations. Bestehorn, Friedrich,

and Haken [4] derive a generalized Ginzburg-Landau and apply it to binary fluid convection.

One complication resulting from the Hopf bifurcation is the group velocity, which appears as a result of the solvability condition at second order. The calculation of appendix A, which shows that the group velocity is zero for a station bifurcation, does not hold for a Hopf bifurcation. This results in an amplitude equation at second order, which much be eliminated in order for the stability of Stokes wave solutions to be analyzed. With only one traveling wave and no Y-dependence, it is possible to write the equations in a reference frame that moves with the group velocity, eliminating it from the amplitude equation. In the three-dimensional case, the group velocity may be removed by using this change of variables and assuming a special solution form.

For reference, the nonlinear system of equations is:

$$\begin{pmatrix} \frac{\partial}{\partial t} - \mathrm{Pr}\nabla^2 & 0 & -\mathrm{Pr}\mathcal{T}\frac{\partial}{\partial z} \\ 0 & \frac{\partial}{\partial t} - \nabla^2 & -1 \\ \mathrm{Pr}\mathcal{T}\frac{\partial}{\partial z} & -\mathrm{PrRa}\nabla_h^2 & \nabla^2\frac{\partial}{\partial t} - \mathrm{Pr}\nabla^4 \end{pmatrix} \begin{pmatrix} \zeta \\ \theta \\ w \end{pmatrix} = \begin{pmatrix} -\nabla \times (\vec{v} \cdot \nabla\vec{v}) \cdot \hat{z} \\ -\vec{v} \cdot \nabla\theta \\ \nabla \times \nabla \times (\vec{v} \cdot \nabla\vec{v}) \cdot \hat{z} \end{pmatrix} \tag{3.2}$$

3.2 Linearized Problem (Order ϵ)

The linearized problem can be solved, as in the previous chapter, using the method of normal modes. The only difference is that now each time-derivative corresponds with multiplication by a frequency, $\sigma = i\omega$. For a Hopf bifurcation, the linear analysis leads to the following relation:

$$\begin{aligned} \mathrm{Ra} = {} & \frac{\omega\left(i\pi^2\mathrm{Pr}\mathcal{T}^2 + ia^6\mathrm{Pr} + 2ia^6\right)}{a^2k^2\mathrm{Pr} + ik^2\omega} \\ & + \frac{\pi^2a^2\mathrm{Pr}^2\mathcal{T}^2 + a^8\mathrm{Pr}^2 - \omega^2\left(2a^4\mathrm{Pr} + a^4\right) - ia^2\omega^3}{a^2k^2\mathrm{Pr}^2 + ik^2\omega\mathrm{Pr}} \end{aligned} \tag{3.3}$$

The imaginary part of equation 3.3 gives three solutions for ω:

$$\omega = 0 \tag{3.4}$$

which was investigated in the previous chapter, and the Hopf bifurcation frequency,

$$\omega = \pm \mathrm{Pr} \sqrt{\frac{\mathcal{T}^2 \pi^2 (1 - \mathrm{Pr}) - a^6 (1 + \mathrm{Pr})}{a^2 (\mathrm{Pr} + 1)}} \tag{3.5}$$

The positive root is taken as the value of ω throughout this chapter and ω_c is this value evaluated at the critical wave-number. This new frequency brings with it dependence of the critical values on the Prandtl number. The real part of equation 3.3 results in an equation for the neutral curve:

$$\mathrm{Ra} = \frac{2\pi^2 \mathcal{T}^2 \mathrm{Pr}(1 - \mathrm{Pr})(\pi^2 \mathcal{T}^2 \mathrm{Pr}^2 + a^6 (\mathrm{Pr} + 1)^2)}{a^2 k^2 (\mathrm{Pr} + 1)^2 (\omega + a^4 \mathrm{Pr})} \tag{3.6}$$

for nonzero Prandtl number. The critical Rayleigh number is the minimum of this curve, and corresponds to the critical wave-number k_c.

Figure 3.1 shows the neutral curves for both bifurcation types at the transition between stationary and Hopf bifurcations when $\mathrm{Pr} = 0.51$ and $\mathcal{T} = 100$. The critical Rayleigh numbers are equal while the critical wave-numbers differ. In a situation where the wave-number is selected by an outside factor, such as the size of the container, the type of bifurcation may vary.

Chandrasekhar finds that oscillatory solutions occur for a lower critical Rayleigh number than stationary solutions when $\mathcal{T} > 23.4094$ and $0 \leq \mathrm{Pr} \leq 0.67659 = \mathrm{Pr}^*$ by requiring that the limits of the critical Rayleigh numbers for the two bifurcation types converge as the Taylor number goes to infinity. This requirement leads to the equation

$$\frac{2\mathrm{Pr}^{\frac{4}{3}}}{(1 + \mathrm{Pr}^{\frac{1}{3}})} = 1 \tag{3.7}$$

whose numerical solution he finds. Chandrasekhar remarks, "there is no simple formula which gives [the Taylor number] as a function of [the Prandtl number]: it

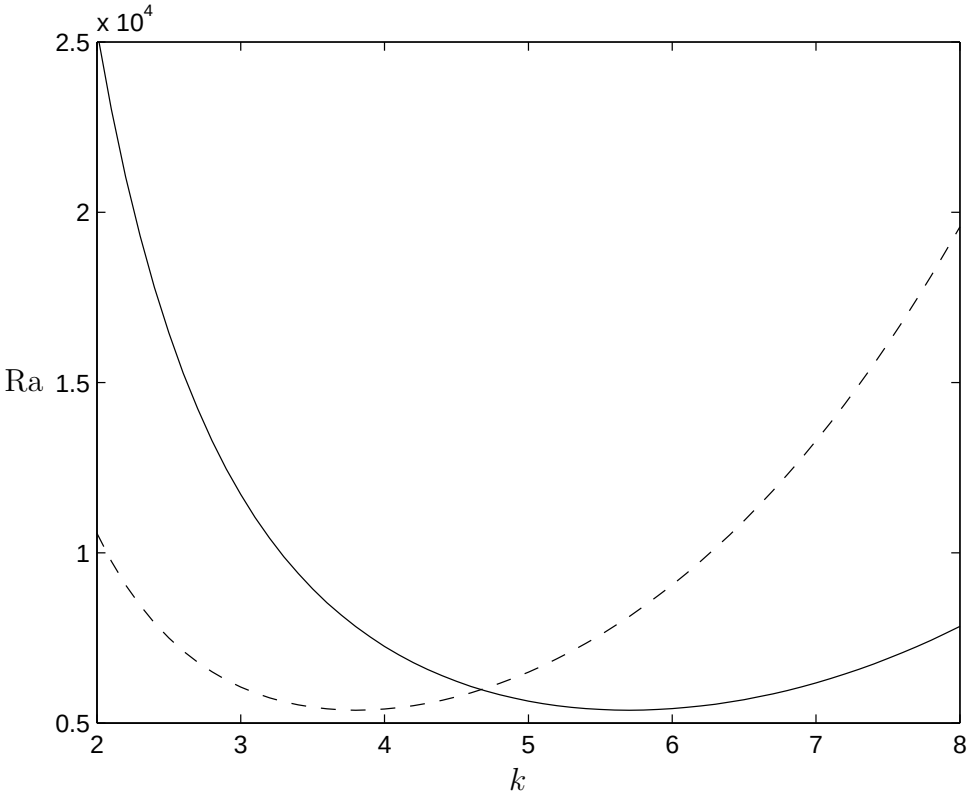

Figure 3.1: Neutral curves for $\mathrm{Pr} = 0.51$ and $\mathcal{T} = 100$. The solid line is the curve for a stationary bifurcation and the dashed line is the curve for a Hopf bifurcation.

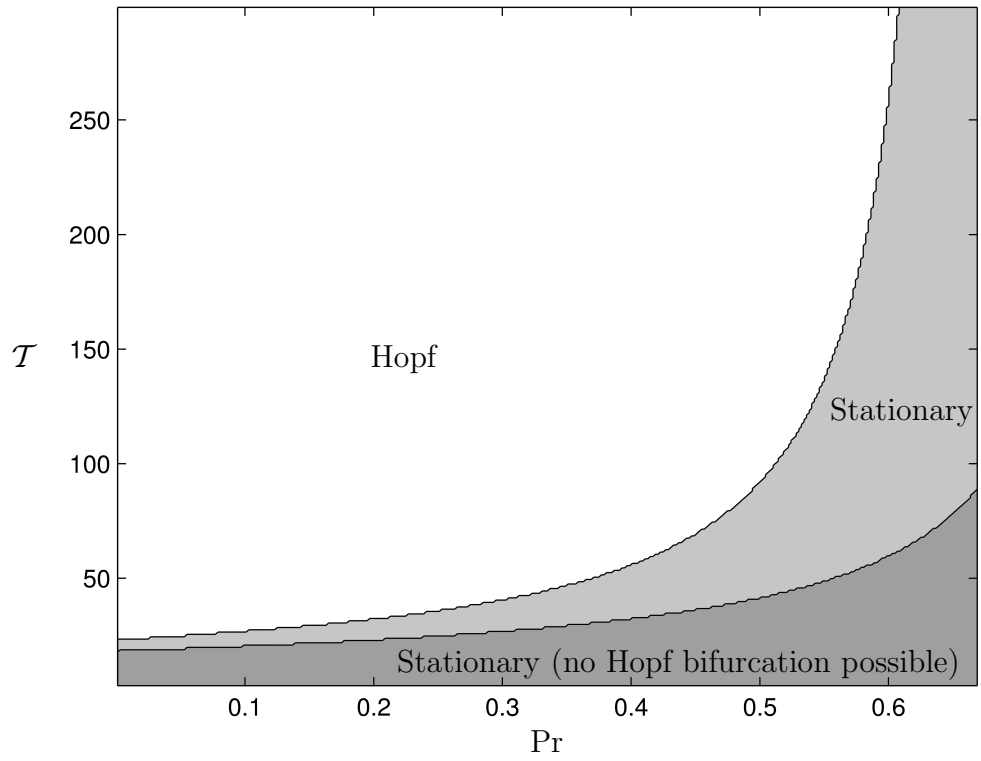

Figure 3.2: In the white region, the bifurcation with the lower critical Rayleigh number is a Hopf bifurcation; a stationary bifurcation also exists but its critical Rayleigh number is higher. In the shaded region, the stationary bifurcation has a lower critical Rayleigh number. In the lower part of the shaded region, no Hopf bifurcation exists.

is simply determined by the condition that [the two Rayleigh numbers] are equal" [11, p.118–119]. The relationship between $\mathcal{T}$ and the Prandtl number is shown in figure 3.2. In the lowest region, Hopf bifurcations are not possible because the nonzero frequency ω_c does not exist. For Prandtl numbers larger than Pr^*, a Hopf bifurcation is impossible because ω_c does not exist.

The critical values for sample parameters in the "Hopf first" region of figure 3.2, calculated using the formulae given, are shown in figures 3.3 through 3.8. Numerical results are given in appendix E. These figures show how the critical

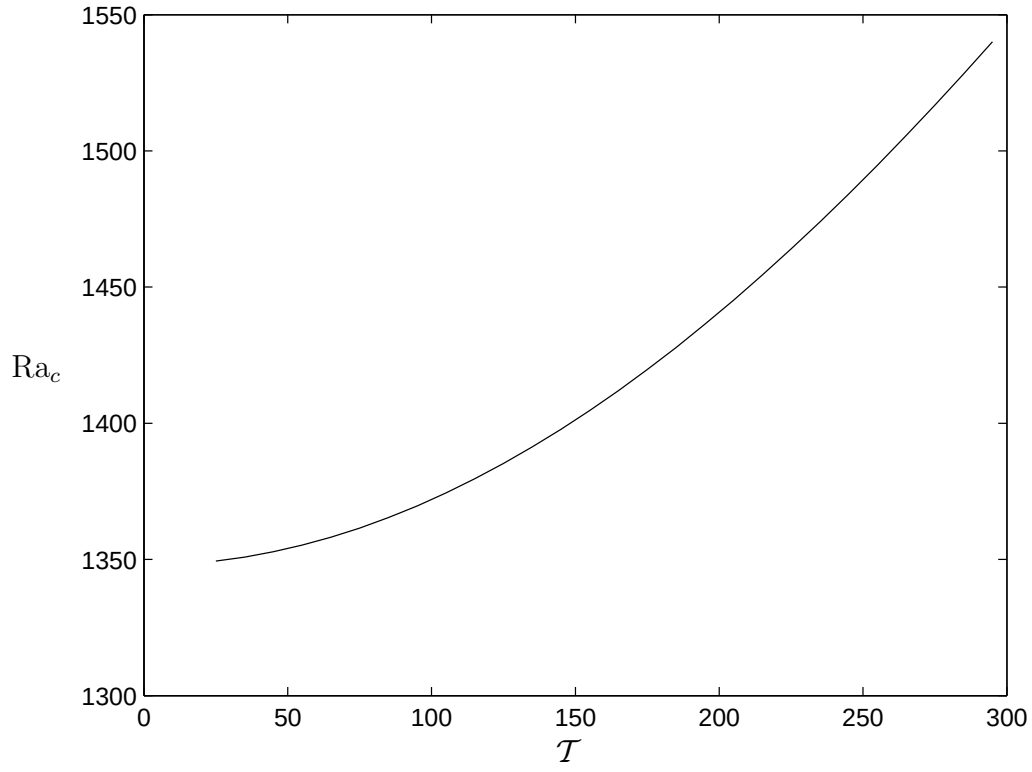

Figure 3.3: Critical Rayleigh number versus rotation rate $\mathcal{T}$, for Pr = 0.025.

Rayleigh number, wave-number, and frequency change with the rotation rate $\mathcal{T}$ for a Prandtl number of 0.025 (a reasonable value for mercury) and with the Prandtl number for a rotation rate of $\mathcal{T} = 100$. Qualitatively, the critical Rayleigh and wave numbers increase with the rotation rate and the Prandtl number. The critical frequency varies linearly with the rotation rate. When the Prandtl number is varied, the frequency's variation has a maximum near Pr = 0.4.

The solutions to the linearized problem for free boundaries are:

$$\zeta_1 = \frac{ik_c \mathrm{Pr}\mathcal{T}\pi}{a_c^2 C}\cos\pi z\left(\frac{i\omega_c + a_c^2}{i\omega_c + \mathrm{Pr}a_c^2}Ae^{i(k_c x+\omega t)} + \frac{-i\omega_c + a_c^2}{-i\omega_c + \mathrm{Pr}a_c^2}Be^{i(k_c x-\omega_c t)}\right) + c.c. \tag{3.8}$$

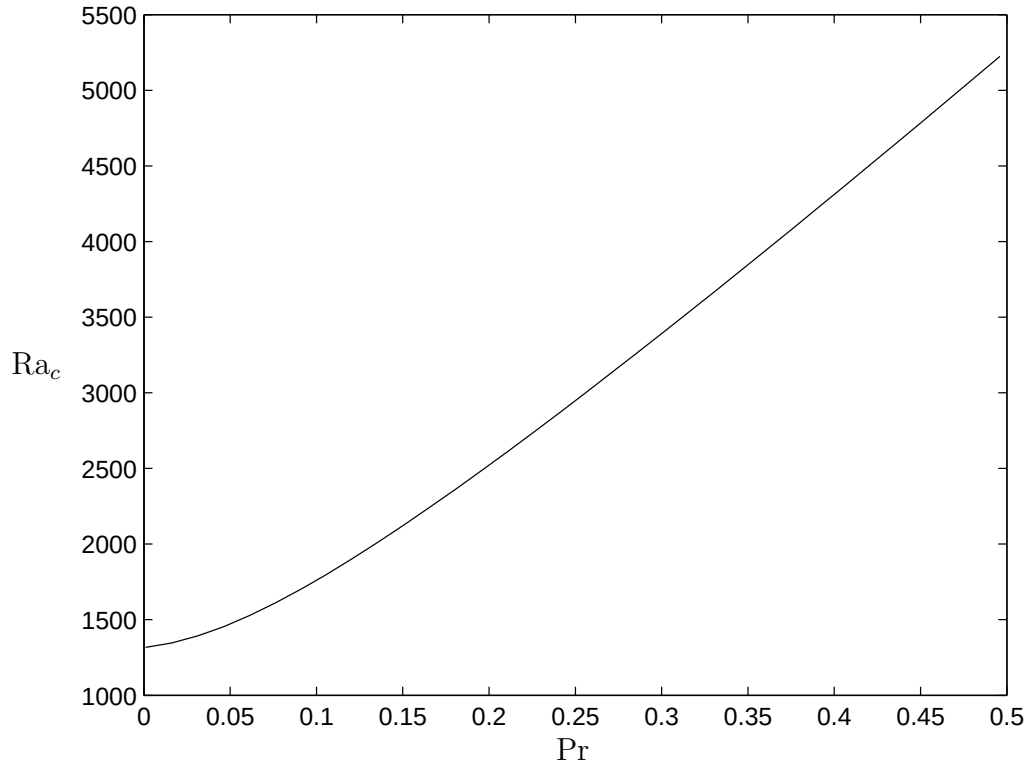

Figure 3.4: Critical Rayleigh number versus Prandtl number, for $\mathcal{T} = 100$.

$$\theta_1 = \frac{ik_c}{a_c^2 C} \sin \pi z \left(A e^{i(k_c x + \omega_c t)} + B e^{i(k_c x - \omega_c t)} \right) + c.c. \tag{3.9}$$

$$w_1 = \frac{ik_c}{a_c^2 C} \sin \pi z \left((i\omega_c + a_c^2) A e^{i(k_c x + \omega_c t)} + (-i\omega_c + a_c^2) B e^{i(k_c x - \omega_c t)} \right) + c.c. \tag{3.10}$$

$$u_1 = -\frac{\pi}{a_c^2 C} \cos \pi z \left((i\omega_c + a_c^2) A e^{i(k_c x + \omega_c t)} + (-i\omega_c + a_c^2) B e^{i(k_c x - \omega_c t)} \right) + c.c. \tag{3.11}$$

$$v_1 = \frac{\mathrm{Pr}\mathcal{T}\pi}{a_c^2 C} \cos \pi z \left(\frac{i\omega_c + a_c^2}{i\omega_c + \mathrm{Pr} a_c^2} A e^{i(k_c x + \omega_c t)} + \frac{-i\omega_c + a_c^2}{-i\omega_c + \mathrm{Pr} a_c^2} B e^{i(k_c x - \omega_c t)} \right) + c.c. \tag{3.12}$$

These solutions agree with those of the previous chapter when $\omega_c = 0$.

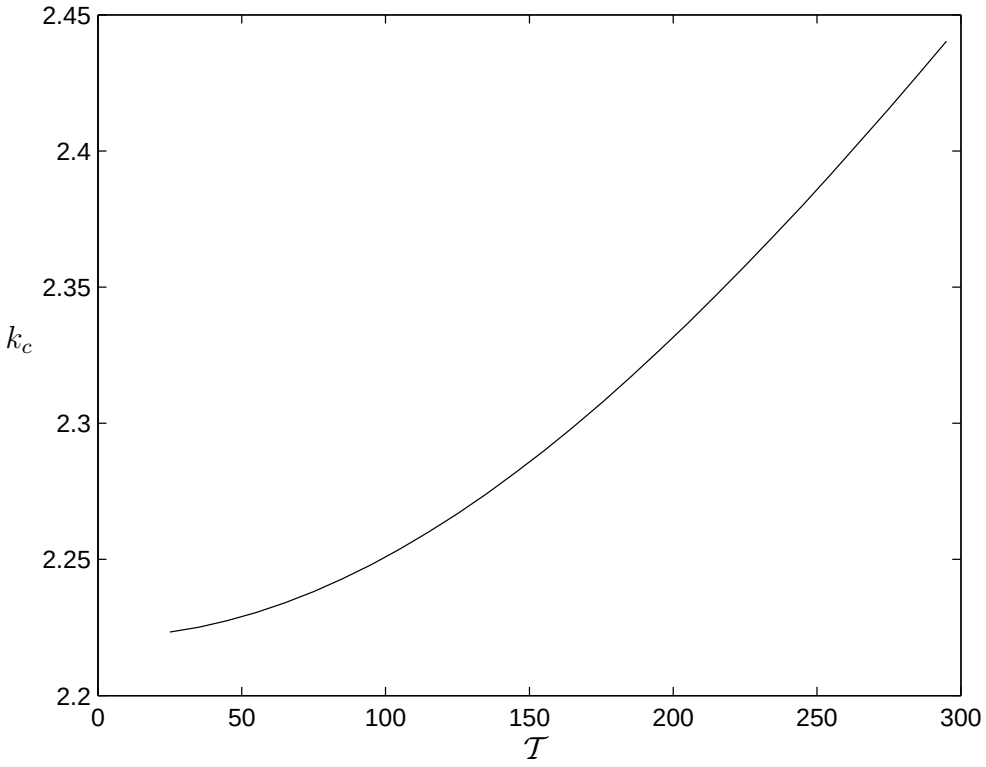

Figure 3.5: Critical wave-number versus rotation rate $\mathcal{T}$, for $\mathrm{Pr} = 0.025$.

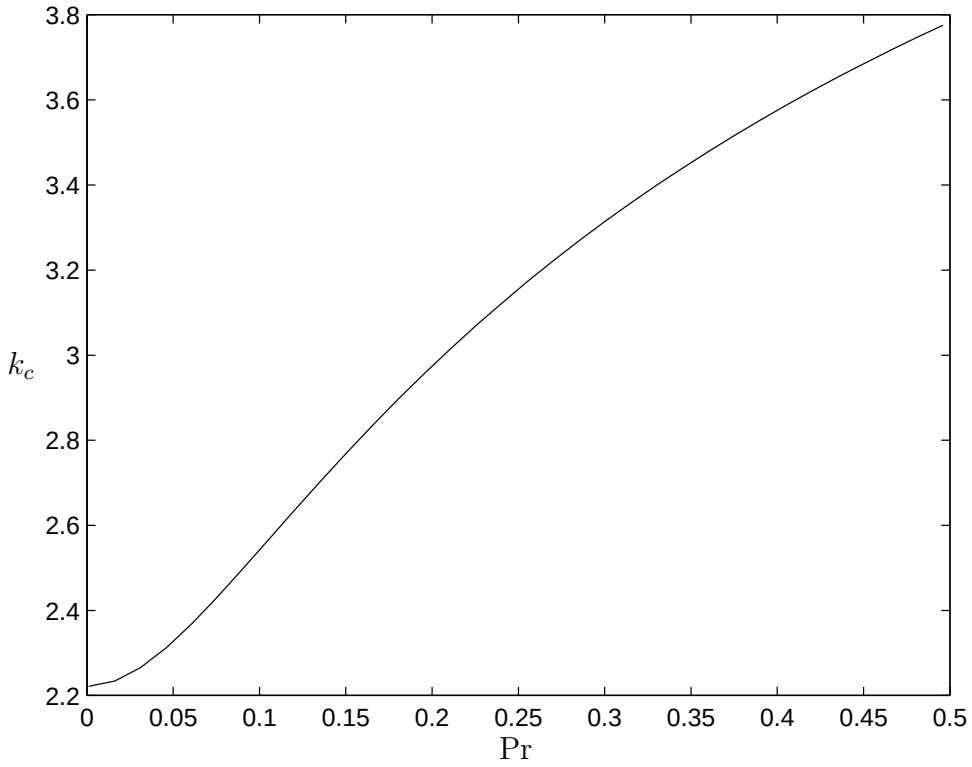

Figure 3.6: Critical wave-number versus Prandtl number, for $\mathcal{T} = 100$.

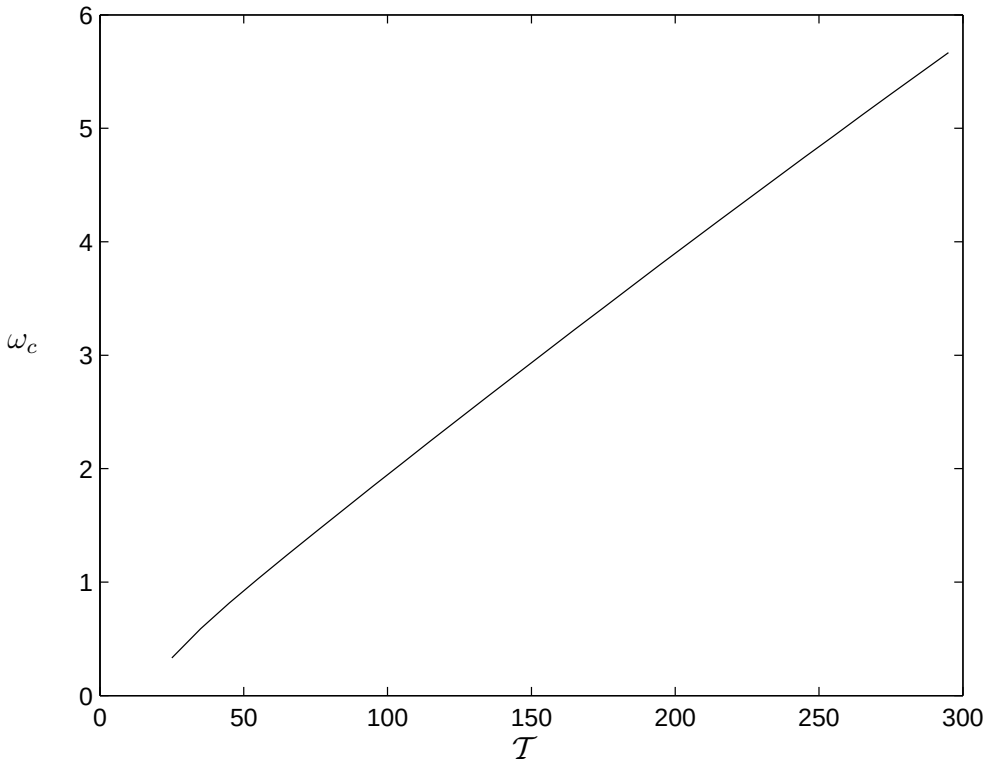

Figure 3.7: Critical frequency versus rotation rate $\mathcal{T}$, for $\mathrm{Pr} = 0.025$.

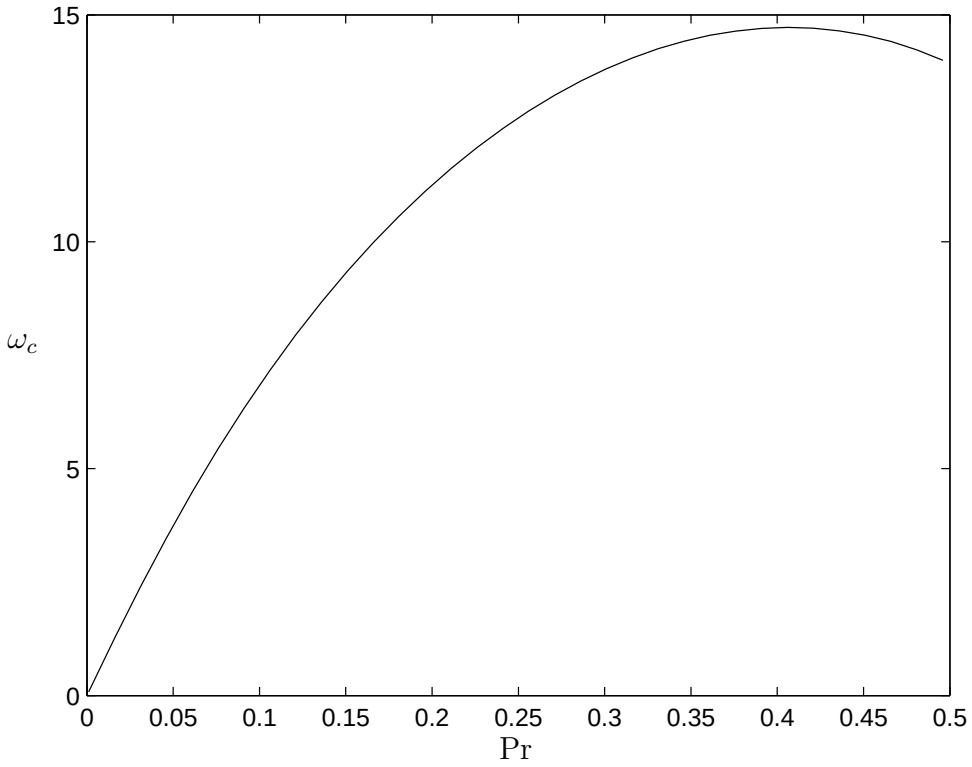

Figure 3.8: Critical frequency versus Prandtl number, for $\mathcal{T} = 100$.

3.3 Adjoint Problem

The adjoint problem is

$$\begin{pmatrix} \frac{\partial}{\partial t} - \mathrm{Pr}\nabla^2 & 0 & -\mathrm{Pr}\mathcal{T}\frac{\partial}{\partial z} \\ 0 & \frac{\partial}{\partial t} - \nabla^2 & -\mathrm{PrRa_c}\nabla_h^2 \\ \mathrm{Pr}\mathcal{T}\frac{\partial}{\partial z} & -1 & \frac{\partial \nabla^2}{\partial t} - \mathrm{Pr}\nabla^4 \end{pmatrix} \begin{pmatrix} \zeta_A \\ \theta_A \\ w_A \end{pmatrix} = \begin{pmatrix} 0 \\ 0 \\ 0 \end{pmatrix} \tag{3.13}$$

with solutions

$$\zeta_A = -\mathcal{T}\pi \cos \pi z (e^{-ik_c x + i\omega_c t} + e^{-ik_c x - i\omega_c t}) + c.c. \tag{3.14}$$

$$\theta_A = \mathrm{Ra}k_c^2 \sin \pi z \left(\frac{(\mathrm{Pr}a_c^2 + i\omega_c)}{a_c^2 + i\omega_c} e^{-ik_c x + i\omega_c t} + \frac{(\mathrm{Pr}a_c^2 - i\omega_c)}{a_c^2 - i\omega_c} e^{-ik_c x - i\omega_c t} \right) + c.c. \tag{3.15}$$

$$w_A = \sin \pi z \left(\left(\frac{-i\omega_c}{\mathrm{Pr}} - a_c^2 \right) e^{-ik_c x + i\omega_c t} + \left(\frac{i\omega_c}{\mathrm{Pr}} - a_c^2 \right) e^{-ik_c x - i\omega_c t} \right) + c.c. \tag{3.16}$$

The two parts relevant to the derivation of the final system are given here, in numerical order, so that the w_{A1} referred to later is the first term of w, and so on.

3.4 Order $\epsilon^{3/2}$

As in the previous chapter, the solutions at this order can be derived by using the continuity equation and the definition of ζ. They are:

$$u_{3/2} = -\frac{\mathcal{T}\pi}{ik_c a_c^4 C} cos\pi z \left((i\omega_c + a_c^2) \frac{\partial A}{\partial Y} e^{i(k_c x + \omega_c t)} + (-i\omega_c + a_c^2) \frac{\partial B}{\partial Y} e^{i(k_c x - \omega_c t)} \right) + c.c. \tag{3.17}$$

$$v_{3/2} = -\frac{\pi}{ik_c a_c^2 C} cos\pi z \left((i\omega_c + a_c^2) \frac{\partial A}{\partial Y} e^{i(k_c x + \omega_c t)} + (-i\omega_c + a_c^2) \frac{\partial B}{\partial Y} e^{i(k_c x - \omega_c t)} \right) + c.c. \tag{3.18}$$

All other components are zero.

3.5 Order ϵ^2

At second order, the right hand has additional terms involving the new amplitude, B. The problem is now:

$$
\begin{aligned}
L\begin{pmatrix}\zeta_2\\ \theta_2\\ w_2\end{pmatrix} &= \begin{pmatrix}0\\ -(\theta_{1a}w_{1a}^*)' - (\theta_{1a}^* w_{1a})'\\ 0\end{pmatrix}|A|^2 + \begin{pmatrix}0\\ -(\theta_{1b}w_{1b}^*)' - (\theta_{1b}^* w_{1b})'\\ 0\end{pmatrix}|B|^2 \\
&\quad + \begin{pmatrix}2(-w_{1b}\zeta_{1a}' - w_{1a}\zeta_{1b}' + w_{1a}'\zeta_{1b} + w_{1b}'\zeta_{1a})\\ -\theta_{1a}'w_{1b} - \theta_{1b}'w_{1a} + \theta_{1a}w_{1b}' + \theta_{1b}w_{1a}'\\ 2(w_{1a}'w_{1b}'' + w_{1b}'w_{1a}'' - w_{1a}w_{1b}''' - w_{1b}w_{1a}''')\end{pmatrix} ABe^{2ik_c x} \\
&+ \begin{pmatrix}0\\ -(\theta_{1a}w_{1b}^*)' - (\theta_{1b}^* w_{1a})'\\ 0\end{pmatrix} AB^* e^{2i\omega_c t} + \begin{pmatrix}0\\ -(\theta_{1a}^* w_{1b})' - (\theta_{1b}w_{1a}^*)'\\ 0\end{pmatrix} A^* B e^{-2i\omega_c t} \\
&+ \begin{pmatrix}2(-\zeta_{1b}'w_{1b} + w_{1b}'\zeta_{1b})\\ w_{1b}'\theta_{1b} - \theta_{1b}'w_{1b}\\ 2(w_{1b}'w_{1b}'' - w_{1b}w_{1b}''')\end{pmatrix} B^2 e^{2ik_c x - 2i\omega_c t} + \begin{pmatrix}2(-w_{1a}\zeta_{1a}' + \zeta_{1a}w_{1a}')\\ w_{1a}'\theta_{1a} - \theta_{1a}'w_{1a}\\ 2(w_{1a}'w_{1a}'' - w_{1a}w_{1a}''')\end{pmatrix} A^2 e^{2ik_c x + 2i\omega_c t} \\
&+ \begin{pmatrix}\mathrm{Pr}\zeta_{1a}\\ \theta_{1a}\\ \mathrm{Pr}(\mathrm{Ra}_c\theta_{1a} + 2(w_{1a}'' - k_c^2 w_{1a})) - i\omega_c w_{1a}\end{pmatrix} 2ik_c\left(\frac{\partial}{\partial X} + \frac{1}{2ik_c}\frac{\partial^2}{\partial Y^2}\right) Ae^{ik_c x + i\omega_c t} \\
&+ \begin{pmatrix}\mathrm{Pr}\zeta_{1b}\\ \theta_{1b}\\ \mathrm{Pr}(\mathrm{Ra}_c\theta_{1b} + 2(w_{1b}'' - k_c^2 w_{1b})) + i\omega_c w_{1b}\end{pmatrix} 2ik_c\left(\frac{\partial}{\partial X} + \frac{1}{2ik_c}\frac{\partial^2}{\partial Y^2}\right) Be^{ik_c x - i\omega_c t}
\end{aligned}
\tag{3.19}
$$

Additional complex conjugate terms have not been printed here because they are quite similar to these, and are not necessary for the final system. The parts of

the first-order solutions that appear on the right hand side are named according to their amplitude, so that $w_{1a} = \frac{ik_c}{a_c^2 C}(i\omega_c + a_c^2)\sin\pi z$ is the coefficient of $Ae^{ik_c x}$ in w_1. As compared to the system for rotating convection with a stationary bifurcation, there are additional exponential terms, and the change in the frequency as well as in the wave-vector must be taken into account in the linear operator. The k_c and ω_c-dependence of the left-hand-side operator varies with the right hand side's dependence on these variables.

The last two parts of this system are proportional to $e^{ik_c x}$ and may result in secular terms. This means that the solvability condition must be checked here, and the results of appendix A do not hold. Each right hand side may be split into two parts, one perpendicular to the adjoint eigenvector, which may be handled as in the previous chapter, and the other parallel, which results in an amplitude equation at second order with a timescale, τ, of order ϵ. These equations are

$$\alpha_1 \frac{\partial A}{\partial \tau} = \nu_1 \left(\frac{\partial}{\partial X} + \frac{1}{2ik_c}\frac{\partial^2}{\partial Y^2} \right) A \tag{3.20}$$

$$\alpha_2 \frac{\partial B}{\partial \tau} = \nu_2 \left(\frac{\partial}{\partial X} + \frac{1}{2ik_c}\frac{\partial^2}{\partial Y^2} \right) B \tag{3.21}$$

where $\tau = \epsilon t$ and the coefficients are given by

$$\alpha_1 = \int_0^1 (ik_c v_{1a}\zeta_{A1} + w''_{1a}w_{A1} - k_c^2 w_{1a}w_{A1} + \theta_{1a}\theta_{A1})dz \tag{3.22}$$

$$\alpha_2 = \int_0^1 (ik_c v_{1b}\zeta_{A2} + w''_{1b}w_{A2} - k_c^2 w_{1b}w_{A2} + \theta_{1b}\theta_{A2})dz = -\alpha_1^* \tag{3.23}$$

$$\nu_1 = \int_0^1 -2k_c^2 \mathrm{Pr} v_{1a}\zeta_{A1} + 2ik_c\theta_{1a}\theta_{A1} + (\mathrm{Pr}(2ik_c\mathrm{Ra}_c\theta_{1a} + 4ik_c(w''_{1a} - k_c^2 w_{1a})) + 2k_c\omega_c w_{1a})w_{A1}dz \tag{3.24}$$

$$\nu_2 = \int_0^1 -2k_c^2 \mathrm{Pr} v_{1b}\zeta_{A2} + 2ik_c\theta_{1b}\theta_{A2} + (\mathrm{Pr}(2ik_c\mathrm{Ra}_c\theta_{1b} + 4ik_c(w''_{1b} - k_c^2 w_{1b})) - 2k_c\omega_c w_{1b})w_{A2}dz = \nu_1^* \tag{3.25}$$

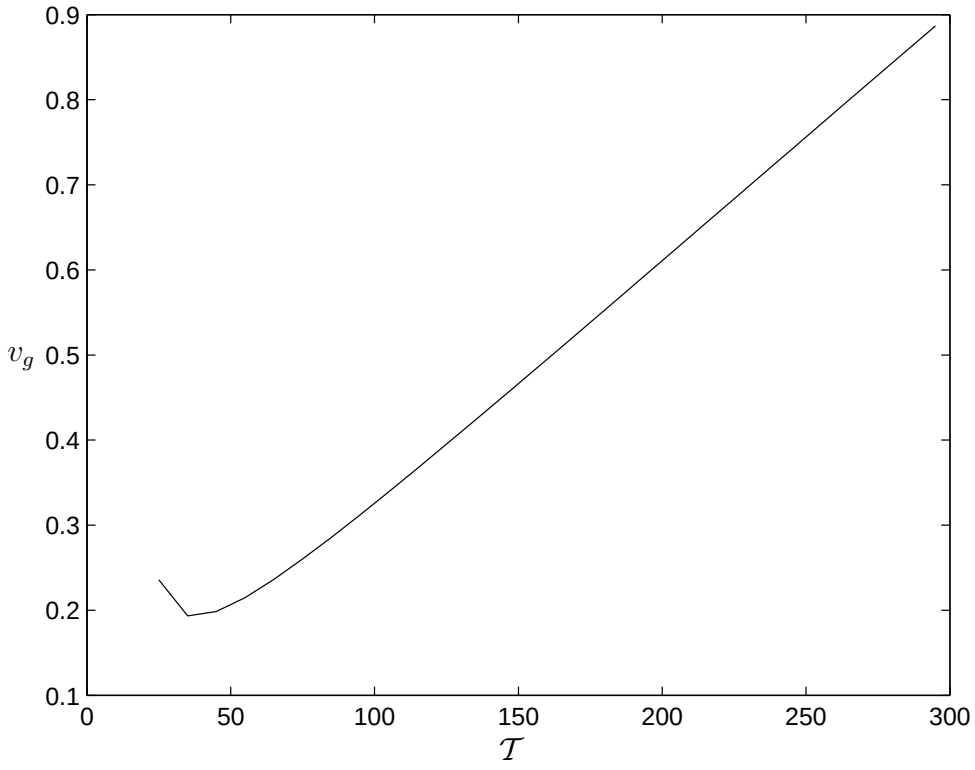

Figure 3.9: Group velocity versus rotation rate, for Pr = 0.025.

Typical values of the group velocity $v_g = \frac{\nu_1}{\alpha_1}$ are given in appendix E and figures 3.10 and 3.9. As shown in appendix A, ν_1 is zero when the bifurcation is stationary. In agreement with the results of Brand, Lomdahl, and Newell [8] [7], $v_g = -\frac{\partial \omega_c}{\partial k}\big|_{k_c}$.

Equations 3.20 and 3.21 may be incorporated into the final system of amplitude equations, which appears at third order, following the example of Brand, Lomdahl, and Newell [8], [7] and Bajaj, Ahlers, and Pesch [1]. A more general alternative to this method, described by Knobloch and de Luca [41], involves integral conditions.

If only one traveling wave is to be considered, it is possible to use a change of variables and special solution form to eliminate the group velocity. Using

$$X' = X - v_g \tau \tag{3.26}$$

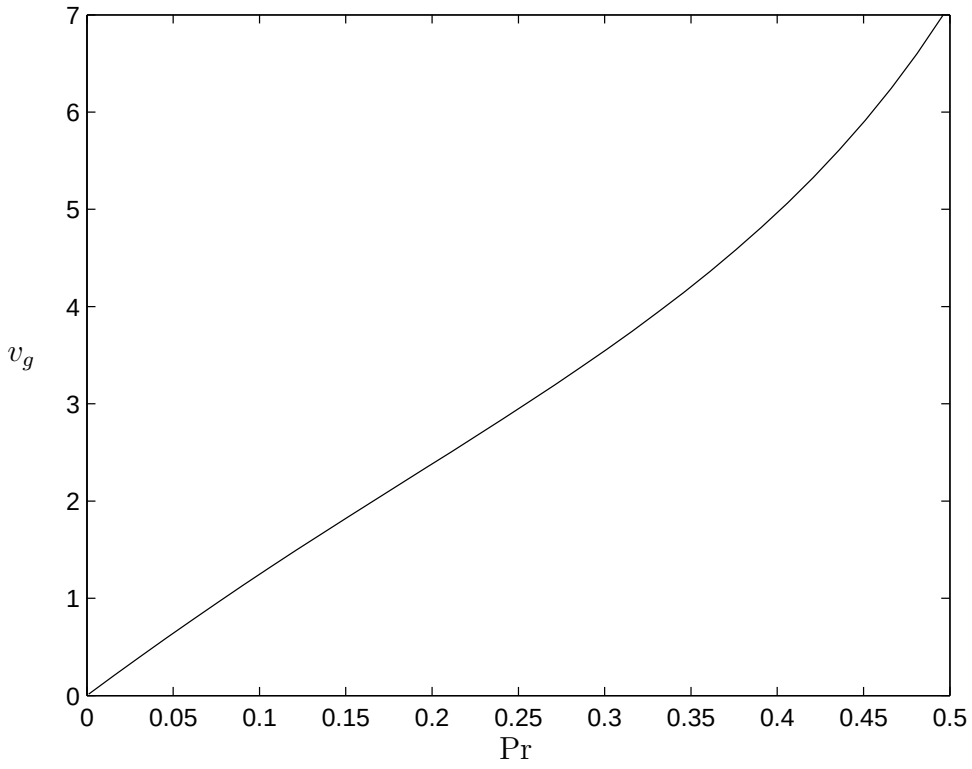

Figure 3.10: Group velocity versus Prandtl number, for $\mathcal{T} = 100$.

equation 3.20 becomes

$$\frac{\partial A}{\partial \tau} = i\frac{v_g}{2k_c}\frac{\partial^2 A}{\partial Y^2} \tag{3.27}$$

which has the special solution

$$\bar{A} = \hat{A}(X', Y, T)e^{i(Q_y Y - \frac{Q_y^2 k_c v_g}{2}\tau)} \tag{3.28}$$

where Q_y is real and $T = \epsilon^2 t$. This solves equation 3.20 when

$$\hat{A} = \hat{A}_1(X', T) + \hat{A}_2(X', T)e^{-2iQ_y Y} \tag{3.29}$$

Since Q_y is arbitrary, one of these two terms may be set to zero, leaving

$$\bar{A} = \hat{A}_1(X', T)e^{i(Q_y Y - \frac{Q_y^2 k_c v_g}{2}\tau)} \tag{3.30}$$

with similar results for B. For solutions of this form, the solvability condition at this order is satisfied. This will restrict the solutions whose stability may be analyzed in section 3.9. When Q_y is selected, the solution is a plane wave moving with a multiple of the group velocity and the third-order amplitude equation will be defined in terms of X and T only. It is not possible to use one change of variables to satisfy equations 3.20 and 3.21 simultaneously because these two equations have different signs on the group velocity; one of A and B takes this form while the other must be zero.

The solutions to the other parts of 3.19 are:

$$\begin{aligned}\zeta_2 &= \zeta_{2aa}A^2 e^{2ik_c x + 2i\omega_c t} + \zeta_{2bb}B^2 e^{2ik_c x - 2i\omega_c t} + \zeta_{2ab}ABe^{2ik_c x} \\ &+ \zeta_{2da}\left(\frac{\partial}{\partial X} + \frac{1}{2ik_c}\frac{\partial^2}{\partial Y^2}\right)Ae^{ik_c x + i\omega_c t} + \zeta_{2db}\left(\frac{\partial}{\partial X} + \frac{1}{2ik_c}\frac{\partial^2}{\partial Y^2}\right)Be^{ik_c x - i\omega_c t}\end{aligned} \tag{3.31}$$

with coefficients

$$\zeta_{2aa} = \frac{k_c^2}{a_c^4 C^2}\frac{\mathrm{Pr}\mathcal{T}\pi^2(\omega_c^2 - 2ia_c^2\omega_c - a_c^4)}{2a_c^2 k_c^2 \mathrm{Pr}^2 + 2ik_c^2\omega_c \mathrm{Pr} + ia_c^2\omega_c \mathrm{Pr} - \omega_c^2} \tag{3.32}$$

$$\zeta_{2bb} = \frac{k_c^2}{a_c^4 C^2} \frac{\mathrm{Pr}\mathcal{T}\pi^2(\omega_c^2 + 2ia_c^2\omega_c - a_c^4)}{2a_c^2 k_c^2 \mathrm{Pr}^2 - 2ik_c^2\omega_c \mathrm{Pr} - ia_c^2\omega_c \mathrm{Pr} - \omega_c^2} \tag{3.33}$$

$$\zeta_{2ab} = -\frac{\pi^2(\omega_c^2 + a_c^4)\mathrm{Pr}\mathcal{T}}{a_c^2 C^2 (a_c^2 \mathrm{Pr} - i\omega_c)(a_c^2 \mathrm{Pr} + i\omega_c)} \tag{3.34}$$

$$\zeta_{2da} = \frac{2ik_c \mathrm{Pr}\zeta_{1a}(z)}{i\omega_c + \mathrm{Pr}a_c^2} \tag{3.35}$$

$$\zeta_{2db} = \frac{2ik_c \mathrm{Pr}\zeta_{1b}(z)}{-i\omega_c + \mathrm{Pr}a_c^2} \tag{3.36}$$

$$\begin{aligned} \theta_2 &= \theta_{2aa^*}|A|^2 + \theta_{2bb^*}|B|^2 + \theta_{2ab^*}AB^* e^{2i\omega_c t} + \theta_{2a^*b}A^* B e^{-2i\omega_c t} \\ &+ \theta_{2da}\left(\frac{\partial}{\partial X} + \frac{1}{2ik_c}\frac{\partial^2}{\partial Y^2}\right) A e^{ik_c x + i\omega_c t} + \theta_{2db}\left(\frac{\partial}{\partial X} + \frac{1}{2ik_c}\frac{\partial^2}{\partial Y^2}\right) B e^{ik_c x - i\omega_c t} \end{aligned} \tag{3.37}$$

with coefficients

$$\theta_{2aa^*} = \theta_{2bb^*} = -\frac{k_c^2}{2\pi a_c^2 C^2} \sin 2\pi z \tag{3.38}$$

$$\theta_{2ab^*} = -\left(\frac{i\omega_c + a_c^2}{i\omega_c + 2\pi^2}\right) \frac{\pi k_c^2}{a_c^4 C^2} \sin 2\pi z \tag{3.39}$$

$$\theta_{2a^*b} = -\left(\frac{i\omega_c - a_c^2}{i\omega_c - 2\pi^2}\right) \frac{\pi k_c^2}{a_c^4 C^2} \sin 2\pi z \tag{3.40}$$

$$\theta_{2da} = \frac{2ik_c^2}{a_c^2 C(\omega_c - ia_c^2)} \sin \pi z \tag{3.41}$$

$$\theta_{2db} = -\frac{2ik_c^2}{a_c^2 C(\omega_c + ia_c^2)} \sin \pi z \tag{3.42}$$

At this order, the vertical velocity w_2 is zero. The horizontal velocity components are given by the continuity equation and the definition of ζ:

$$u_2 = U(X, Y, T) - \int \left(\frac{\partial v_{3/2}}{\partial Y} + \frac{\partial w_2}{\partial z} + \frac{\partial u_1}{\partial X}\right) dx \tag{3.43}$$

and

$$v_2 = \int \left(\zeta_2 + \frac{\partial u_{3/2}}{\partial Y} - \frac{\partial v_1}{\partial X}\right) dx \tag{3.44}$$

where $U(X, Y, T)$ is the mean drift, as in the previous chapter. The parts relevant to amplitude equation derivation are:

$$v_{2ab} = \frac{\zeta_{2ab}}{2ik_c} \tag{3.45}$$

$$v_{2aa} = \frac{\zeta_{2aa}}{2ik_c} \tag{3.46}$$

$$v_{2bb} = \frac{\zeta_{2bb}}{2ik_c} \tag{3.47}$$

3.6 Order $\epsilon^{5/2}$

Since the solutions at order $\epsilon^{5/2}$ do not contribute to the final amplitude equation, they are not computed here. They are expected to be similar to the solutions derived in the previous chapter.

3.7 Order ϵ^3

At third order, the system is

$$L\begin{pmatrix}\zeta_3\\ \theta_3\\ w_3\end{pmatrix} = \begin{pmatrix}(-\nabla\times(\vec{v}\cdot\nabla\vec{v})\cdot\hat{z} + \mathrm{Pr}\nabla^2\zeta)_3 - \frac{\partial\zeta_1}{\partial T}\\ (-\vec{v}\cdot\nabla\theta + \nabla^2\theta)_3 - \frac{\partial\theta_1}{\partial T}\\ (\nabla\times\nabla\times(\vec{v}\cdot\nabla\vec{v})\cdot\hat{z} + \mathrm{Pr}\nabla^4 w + \mathrm{PrRa}_c\nabla_h^2\theta)_3 - \frac{\partial\nabla^2 w_1}{\partial T} + \mathrm{Pr}R_2\nabla_h^2\theta_1\end{pmatrix} \tag{3.48}$$

The subscript 3 refers to the order ϵ^3 parts of this that do not involve the third-order solutions, such as $\frac{\partial}{\partial X}$ and $\frac{\partial}{\partial Y}$ terms. When the solvability condition is applied, the following system of equations results:

$$\begin{aligned}&\alpha_1\left(\epsilon\frac{\partial}{\partial T} + \frac{\partial}{\partial\tau}\right)A - \nu_1\left(\frac{\partial}{\partial X} + \frac{1}{2ik_c}\frac{\partial^2}{\partial Y^2}\right)A\\ &= \epsilon\sigma_1 A - \epsilon\lambda_1|A|^2A - \epsilon\lambda_2|B|^2A + \epsilon\delta_1\left(\frac{\partial}{\partial X} + \frac{1}{2ik_c}\frac{\partial^2}{\partial Y^2}\right)^2 A + \epsilon\frac{\nu_1}{2ik_c}\frac{\partial^2 A}{\partial X^2} - i\epsilon\eta_1 AU\end{aligned} \tag{3.49}$$

$$\alpha_2\left(\epsilon\frac{\partial}{\partial T}+\frac{\partial}{\partial\tau}\right)B-\nu_2\left(\frac{\partial}{\partial X}+\frac{1}{2ik_c}\frac{\partial^2}{\partial Y^2}\right)A$$
$$=\epsilon\sigma_2 B-\epsilon\lambda_3|A|^2B-\epsilon\lambda_4|B|^2B+\epsilon\delta_2\left(\frac{\partial}{\partial X}+\frac{1}{2ik_c}\frac{\partial^2}{\partial Y^2}\right)^2B+\epsilon\frac{\nu_2}{2ik_c}\frac{\partial^2 B}{\partial X^2}-i\epsilon\eta_2 BU \tag{3.50}$$

with coefficients

$$\sigma_1=\int_0^1(-k_c^2\theta_{1a}w_{A1}\mathrm{Pr}R_2)dz \tag{3.51}$$

$$\sigma_2=\int_0^1(-k_c^2\theta_{1b}w_{A2}\mathrm{Pr}R_2)dz \tag{3.52}$$

$$\lambda_1=-\int_0^1(2k_c^2u_{1a}^*v_{2aa}\zeta_{A1}-\theta'_{2aa^*}\theta_{A1}w_{1a})dz \tag{3.53}$$

$$\lambda_2=-\int_0^1(2k_c^2u_{1b}^*v_{2ab}\zeta_{A1}-\theta'_{2ab^*}\theta_{A1}w_{1b}-\theta'_{2bb^*}\theta_{A1}w_{1a})dz \tag{3.54}$$

$$\lambda_3=-\int_0^1(2k_c^2u_{1a}^*v_{2ab}\zeta_{A2}-\theta'_{2a^*b}\theta_{A2}w_{1a}-\theta'_{2aa^*}\theta_{A2}w_{1b})dz \tag{3.55}$$

$$\lambda_4=-\int_0^1(2k_c^2u_{1b}^*v_{2bb}\zeta_{A2}-\theta'_{2bb^*}\theta_{A2}w_{1b})dz \tag{3.56}$$

$$\delta_1=-4k_c^2\int_0^1\left(\mathrm{Pr}\left(w_{1a}-\frac{i\mathrm{Ra}_c\theta_{2da}}{2k_c}\right)w_{A1}-\frac{i\theta_{2da}\theta_{A1}}{2k_c}-\frac{i\mathrm{Pr}\zeta_{2da}\zeta_{A1}}{2k_c}\right)dz \tag{3.57}$$

$$\delta_2=-4k_c^2\int_0^1\left(\mathrm{Pr}\left(w_{1b}-\frac{i\mathrm{Ra}_c\theta_{2db}}{2k_c}\right)w_{A2}-\frac{i\theta_{2db}\theta_{A2}}{2k_c}-\frac{i\mathrm{Pr}\zeta_{2db}\zeta_{A2}}{2k_c}\right)dz \tag{3.58}$$

$$\eta_1=\int_0^1(k_c^2v_{1a}\zeta_{A1}-ik_c\theta_{1a}\theta_{A1}+(ik_c^3w_{1a}-k_c^2u'_{1a})w_{A1})dz \tag{3.59}$$

$$\eta_2=\int_0^1(k_c^2v_{1b}\zeta_{A2}-ik_c\theta_{1b}\theta_{A2}+(ik_c^3w_{1b}-k_c^2u'_{1b})w_{A2})dz \tag{3.60}$$

$\alpha_{1,2}$ and $\nu_{1,2}$ are given in equations 3.22 through 3.25. Substituting the linear (equations 3.8–3.12) and adjoint (equations 3.14–3.16) solutions shows that $\alpha_1=-\alpha_2^*$. Similar results hold for the other coefficients (each term is equal to the negative complex conjugate of its corresponding term in the other equation, except that $\eta_1=\eta_2$ and $\nu_1=\nu_2^*$). When each equation is divided through by its α, the coefficients of the B equation are, with few exceptions, the complex conjugates of the coefficients of the A equation, giving the system:

$$\left(\epsilon\frac{\partial}{\partial T}+\frac{\partial}{\partial \tau}\right)A-v_g\left(\frac{\partial}{\partial X}+\frac{1}{2ik_c}\frac{\partial^2}{\partial Y^2}\right)A$$
$$=\epsilon\sigma A-\epsilon\lambda_a|A|^2A-\epsilon\lambda_b|B|^2A+\epsilon\delta\left(\frac{\partial}{\partial X}+\frac{1}{2ik_c}\frac{\partial^2}{\partial Y^2}\right)^2A+\epsilon\frac{v_g}{2ik_c}\frac{\partial^2 A}{\partial X^2}-i\epsilon k_cAU \tag{3.61}$$

$$\left(\epsilon\frac{\partial}{\partial T}+\frac{\partial}{\partial \tau}\right)B+v_g\left(\frac{\partial}{\partial X}+\frac{1}{2ik_c}\frac{\partial^2}{\partial Y^2}\right)B$$
$$=\epsilon\sigma^*B-\epsilon\lambda_b^*|A|^2B-\epsilon\lambda_a^*|B|^2B+\epsilon\delta^*\left(\frac{\partial}{\partial X}+\frac{1}{2ik_c}\frac{\partial^2}{\partial Y^2}\right)^2B+\epsilon\frac{v_g}{2ik_c}\frac{\partial^2 B}{\partial X^2}-i\epsilon k_cBU \tag{3.62}$$

Sample numerical values of the coefficients are given in appendix E, and graphs are shown in figures 3.11 through 3.16. R_2 is taken to be equal to Ra_c.

In figures 3.11 and 3.12, the imaginary part of the growth rate is seen to change much more than the real part, but it remains negative. The real part does not vary much with rotation rate, but does vary significantly with Prandtl number. The two Landau coefficients, λ_a and λ_b, as depicted in figures 3.13 and 3.14, have large real and imaginary parts for low rotation rates and Prandtl numbers, and decrease as both physical parameters increase. Figure 3.15 shows that δ is fairly constant with respect to the rotation rate after an initial increase. As the Prandtl number increases, the real part of δ increases while the imaginary part decreases (figure 3.16).

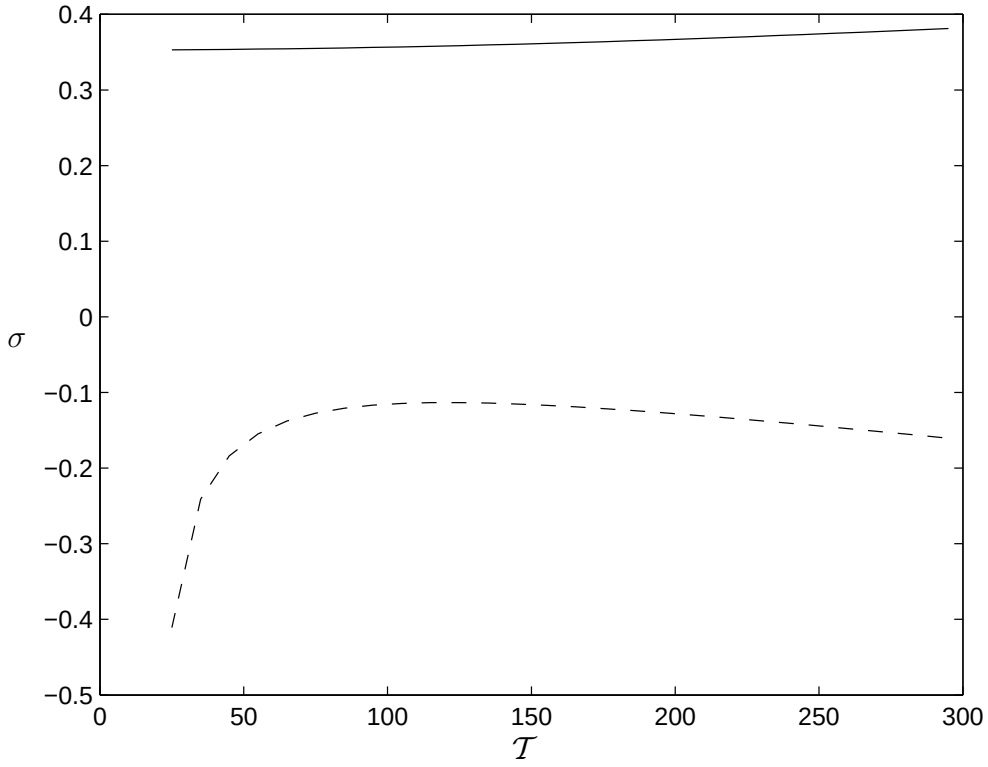

Figure 3.11: The growth rate σ versus rotation rate $\mathcal{T}$, for Pr = 0.025: the solid line represents the real part and the broken line the imaginary part.

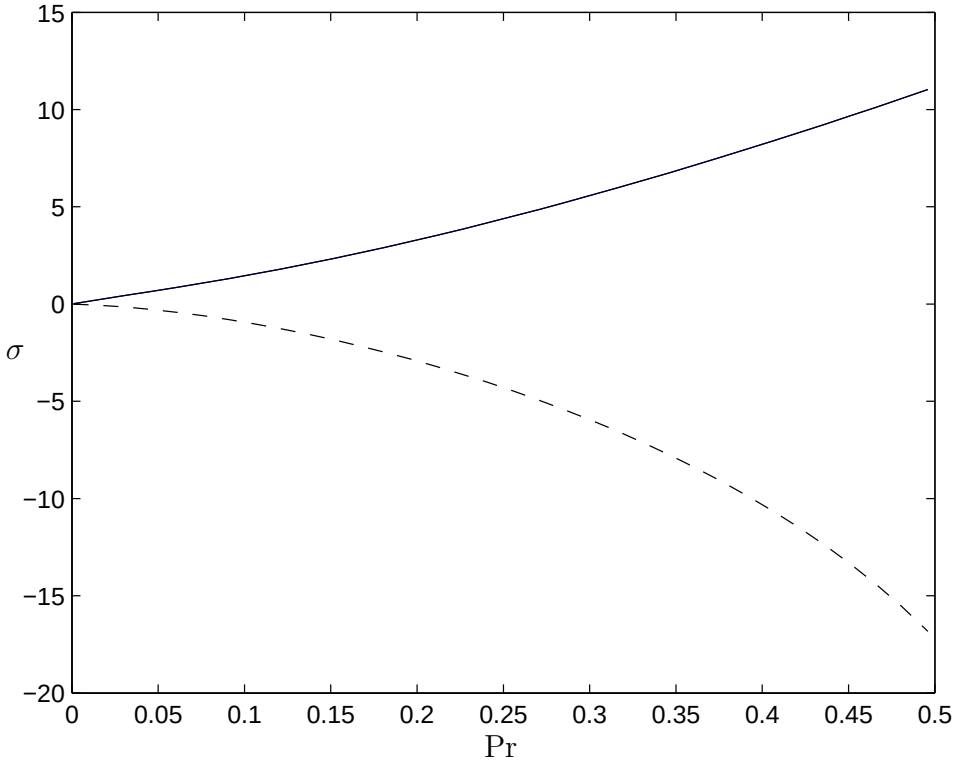

Figure 3.12: The growth rate σ versus Prandtl number, for $\mathcal{T} = 100$: the solid line represents the real part and the broken line the imaginary part.

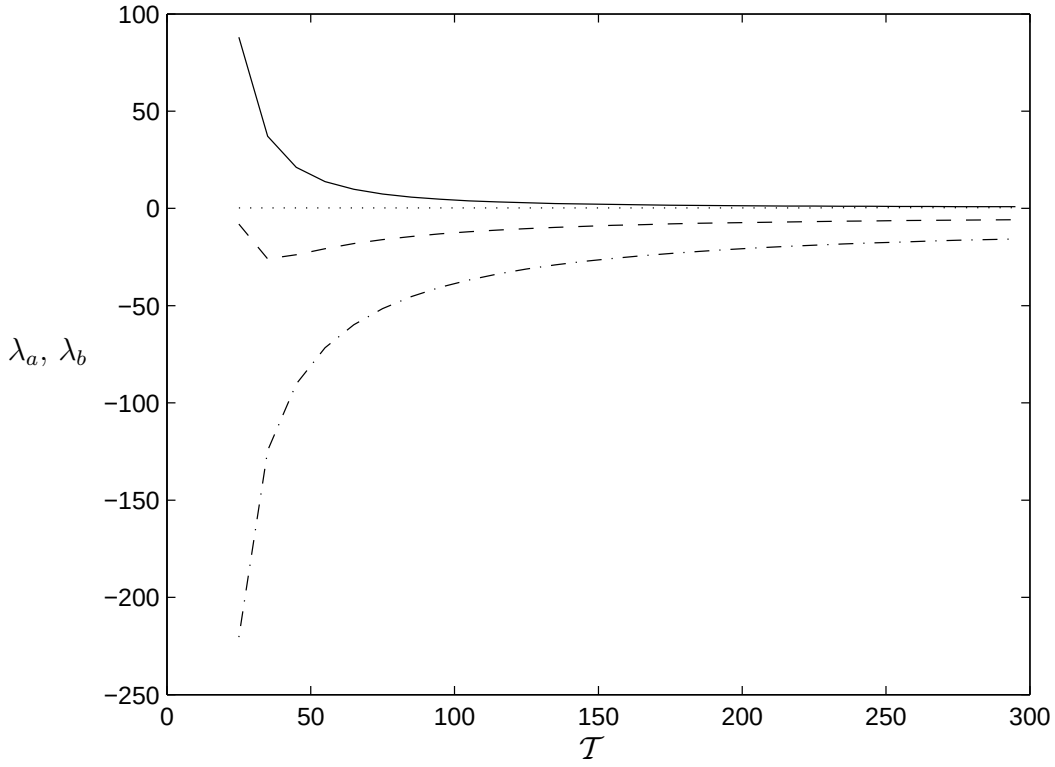

Figure 3.13: The coefficients λ_a and λ_b versus rotation rate $\mathcal{T}$, for $\mathrm{Pr} = 0.025$: the solid line represents the real part of λ_a and the broken line the imaginary part; the dotted line represents the real part of λ_b and the dash-dotted line the imaginary part.

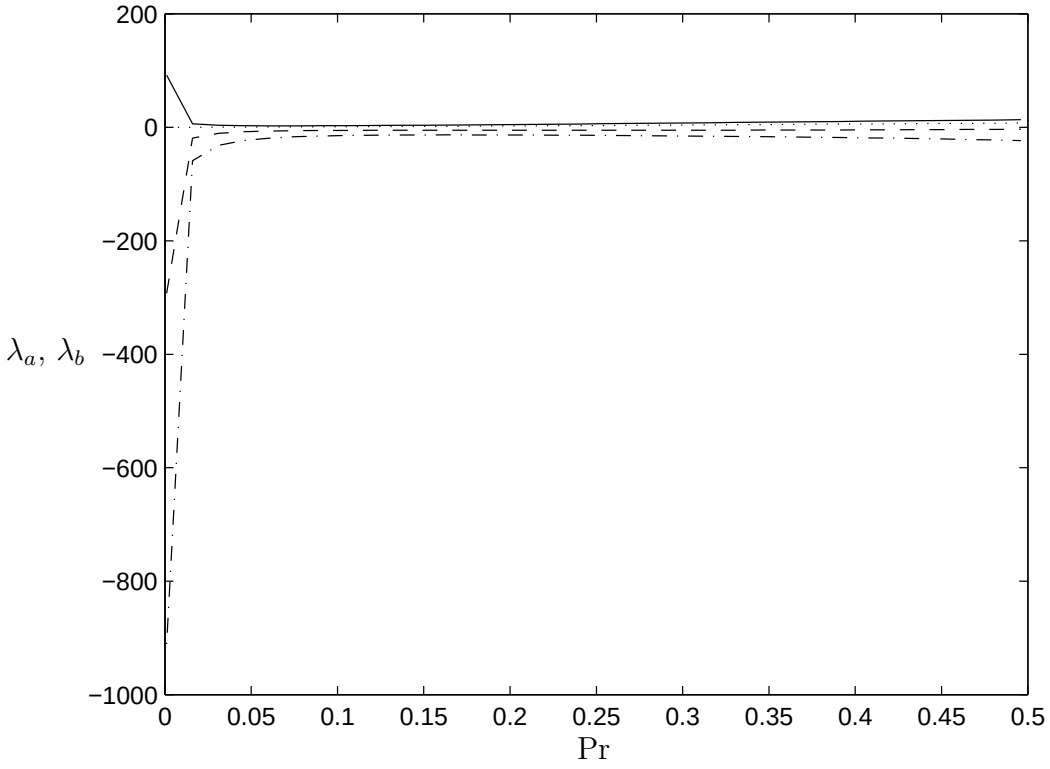

Figure 3.14: The coefficients λ_a and λ_b versus Prandtl number, for $\mathcal{T} = 100$: the solid line represents the real part of λ_a and the broken line the imaginary part; the dotted line represents the real part of λ_b and the dash-dotted line the imaginary part.

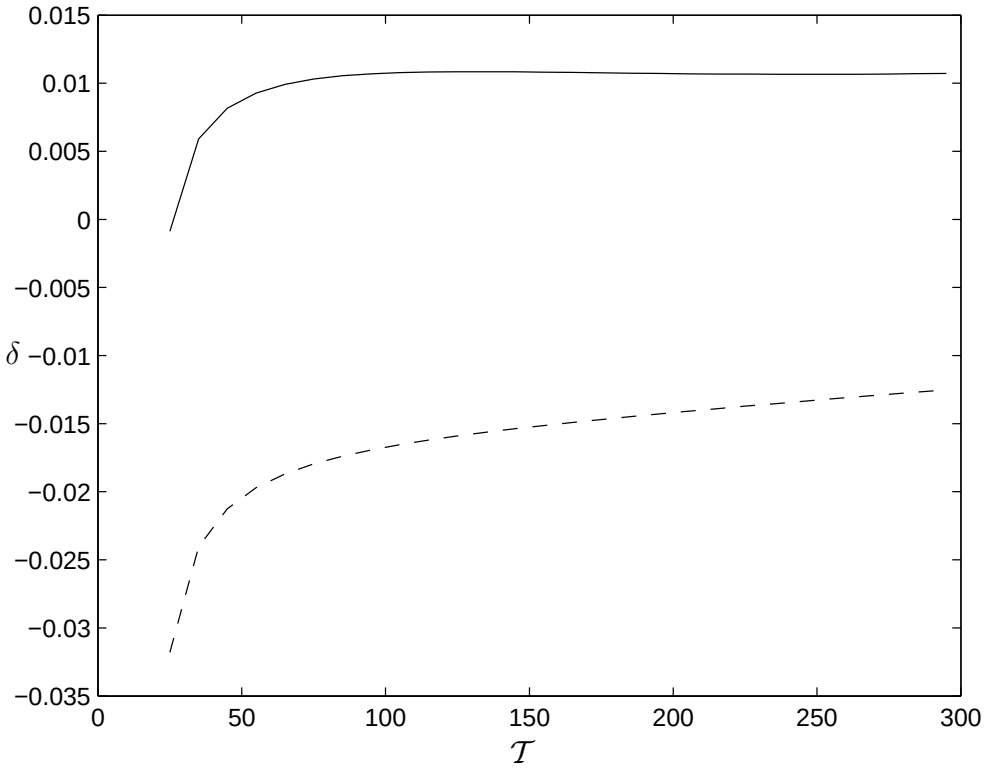

Figure 3.15: The coefficient δ versus rotation rate $\mathcal{T}$, for $\mathrm{Pr} = 0.025$: the solid line represents the real part and the broken line the imaginary part.

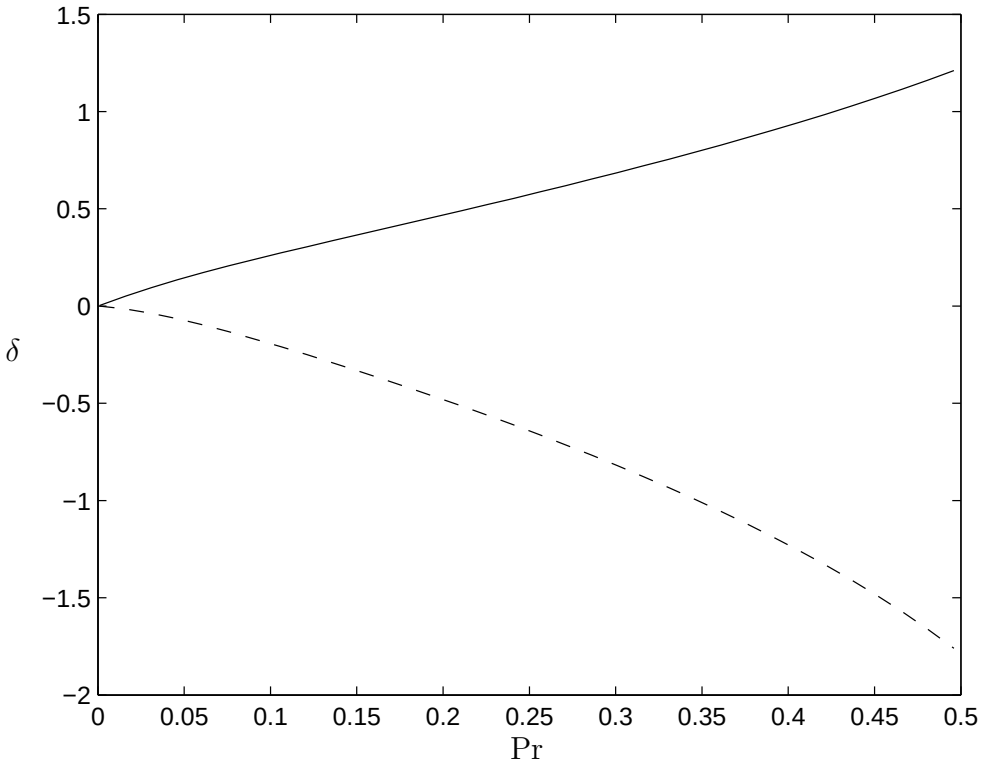

Figure 3.16: The coefficient δ versus Prandtl number, for $\mathcal{T} = 100$: the solid line represents the real part and the broken line the imaginary part.

3.8 Order $\epsilon^{7/2}$

As in the previous chapter, a third equation appears at order $\epsilon^{7/2}$. This equation, derived using the method in appendix B, is:

$$\mathrm{Pr}\frac{\partial^3 U}{\partial Y^3} = \frac{\partial}{\partial Y}\left(A^*\left(\Gamma_{ax}\frac{\partial}{\partial X} + \Gamma_{ay}\frac{\partial^2}{\partial Y^2}\right)A\right) + \frac{\partial}{\partial Y}\left(B^*\left(\Gamma_{bx}\frac{\partial}{\partial X} + \Gamma_{by}\frac{\partial^2}{\partial Y^2}\right)B\right) + c.c. \quad (3.63)$$

with coefficients:

$$\Gamma_{ax} = \frac{\pi^2(\omega_c^2 + a_c^4)\left(2a_c^2\mathrm{Pr}^2\mathcal{T}^2 - i\omega_c\mathrm{Pr}\mathcal{T}^2 - 2a_c^6\mathrm{Pr}^2 - 2a_c^2\omega_c^2\right)}{2a_c^6C^2(a_c^2\mathrm{Pr} - i\omega_c)(a_c^2\mathrm{Pr} + i\omega_c)} \quad (3.64)$$

$$\Gamma_{bx} = \frac{\pi^2(\omega_c^2 + a_c^4)\left(2a_c^2\mathrm{Pr}^2\mathcal{T}^2 + i\omega_c\mathrm{Pr}\mathcal{T}^2 - 2a_c^6\mathrm{Pr}^2 - 2a_c^2\omega_c^2\right)}{2a_c^6C^2(a_c^2\mathrm{Pr} - i\omega_c)(a_c^2\mathrm{Pr} + i\omega_c)} \quad (3.65)$$

$$\Gamma_{ay} = -\frac{i\pi^2(\omega_c^2 + a_c^4)(\mathrm{Pr}\mathcal{T}^2 - a_c^4\mathrm{Pr} + ia_c^2\omega_c)}{2a_c^6k_cC^2(a_c^2\mathrm{Pr} - i\omega_c)} \quad (3.66)$$

$$\Gamma_{by} = -\frac{i\pi^2(\omega_c^2 + a_c^4)(\mathrm{Pr}\mathcal{T}^2 - a_c^4\mathrm{Pr} - ia_c^2\omega_c)}{2a_c^6k_cC^2(a_c^2\mathrm{Pr} + i\omega_c)} \quad (3.67)$$

These coefficients simplify to those given in section 2.9 when $\omega_c = 0$.

3.9 Stability of Stokes Wave Solutions

The system of equations 3.61 and 3.62 admits solutions in the form of Stokes waves, $F_{\{a,b\}}e^{i(\omega_{s\{a,b\}}T + \vec{Q}_{\{a,b\}}\cdot\vec{X})}$. The stability of these general solutions can not be analyzed because of the solvability condition at second order: the full system of equations is no longer asymptotic (ϵ can not be eliminated). In this section, the the stability of a single traveling Stokes wave of the form 3.30 is analyzed. The perturbation f may only depend on X and T. Throughout this section U and B are assumed to be zero for the reasons given in sections 2.10 and 3.5, and the bifurcation is assumed to fall into the "Hopf first" region of figure 3.2.

The stability of Stokes wave solutions to similar systems has been examined in the past. Knobloch [40] examines the stability of traveling and standing wave solutions to a pair of coupled Landau equations. Matkowsky and Volpert [52] derive stability criteria for a pair of coupled one-dimensional Ginzburg-Landau equations. The stability of the system given here may not be analyzed for both traveling waves or for the composite solution, because it is not possible to eliminate the group velocity of both waves simultaneously.

First the change of variables 3.26 is applied to remove the group velocity. This changes X to the X' given in equation 3.26, but has no other effects. The prime is simply dropped. A is assumed to be equal to $\bar{A}$, as given in equation 3.28. This solution is a wave traveling in a chosen direction with a multiple of the group velocity; Q_y must be fixed at this point. Then, the equations are rescaled using the following new variables in order to simplify the coefficients:

$$T' = \sigma_r T \qquad Y' = \sqrt{2k_c}\left(\frac{\sigma_r}{\delta}\right)^{\frac{1}{4}} Y \qquad X' = X\sqrt{\frac{\sigma_r}{\delta}} \tag{3.68}$$

$$A' = \hat{A} e^{-\frac{i\sigma_i}{\sigma_r}T}\sqrt{\frac{\lambda_{ar}}{\sigma_r}} \tag{3.69}$$

The subscript r refers to the real part. Since the wave-number Q_y, which is fixed to satisfy 3.20, is arbitrary, this change of variables need not alter it. Substituting these expressions into this equation 3.61 and the complex conjugate of equation 3.62 and then dropping primes yields the new equation:

$$\frac{\partial A}{\partial T} = A - (1-ib)|A|^2\hat{A}\left(\frac{\partial}{\partial X} + iQ_y^2\right)^2 A - g\frac{\partial^2 A}{\partial X^2} \tag{3.70}$$

with coefficients

$$b = -\frac{\lambda_{ai}}{\lambda_{ar}} \qquad g = g_r + ig_i = \frac{iv_g}{2k_c\delta} \tag{3.71}$$

The next step is to find Stokes wave solutions of the form

$$A = Fe^{i(\omega_s T + \vec{Q}\cdot\vec{X})} \tag{3.72}$$

where F is real. Substitution yields the trivial solution $F = 0$ as well as the traveling wave solution

$$F^2 = 1 - K^2 + g_r Q_x^2 \qquad\qquad \omega_s = bF^2 + g_i Q_x^2 \tag{3.73}$$

where $K = Q_x + Q_y^2$. For these solutions to exist, F must be nonnegative. In the remainder of this section, stability criteria for solution 3.73 are derived. This is the same as the stability analysis of section 2.10 except for the addition of the term with constant g and the frequency ω_s. Perturbing A by substituting

$$A = (F + f)e^{i(\omega_s T + \vec{Q}\cdot\vec{X})} \tag{3.74}$$

into the equation 3.70 and linearizing in f yields the new system

$$\frac{\partial f}{\partial T} = cf - (1 - ib)F^2 f^* + Df \tag{3.75}$$

with

$$c = 1 - i\omega_s - K^2 + 2(ib - 1)F^2 + gQ_x^2 \tag{3.76}$$

The derivative terms become

$$D = 2iK\frac{\partial}{\partial X} + \frac{\partial^2}{\partial X^2} - 2igQ_x\frac{\partial}{\partial X} - g\frac{\partial^2}{\partial X^2} \tag{3.77}$$

The perturbation f is only allowed to vary in time and the X-direction because the wave-number Q_y must be fixed in order to satisfy equation 3.20 and keep equation 3.70 asymptotic. The general dispersion relation is derived by substituting solutions of the form $f = u + iv$ and separating into real and imaginary parts, then substituting

$$u = \hat{u}e^{\Omega T + i\kappa_x X} \qquad\qquad v = \hat{v}e^{\Omega T + i\kappa_x X} \tag{3.78}$$

for u and v yields a system of two algebraic equations in two unknowns:

$$\begin{pmatrix} C_0 - 2F^2 - \Omega & -C_1 \\ C_1 + 2bF^2 & C_0 - \Omega \end{pmatrix} \begin{pmatrix} \hat{u}_a \\ \hat{v}_a \end{pmatrix} = \vec{0} \tag{3.79}$$

where the C_i are constants which depend on the other constants in the problem, as well as the perturbation wave-vector. The constants are:

$$C_0 = 2ig_i\kappa_x Q_x + (g_r - 1)\kappa_x^2 \tag{3.80}$$

$$C_1 = 2i\kappa_x Q_y^2 + 2i(1 - g_r)\kappa_x Q_x + g_i\kappa_x^2 \tag{3.81}$$

The eigenvalues Ω of this matrix determine the stability of the system. The characteristic equation is

$$\Omega^2 - 2\beta\Omega + \gamma = 0 \tag{3.82}$$

with

$$\beta = C_0 - F^2 \tag{3.83}$$

$$\gamma = C_1^2 + C_0^2 - 2F^2 C_0 \tag{3.84}$$

The maximum real part of the growth rate $\Omega = \beta \pm \sqrt{\beta^2 - \gamma}$ determines whether a perturbation grows or decays. The general stability of the system can be derived as follows. First, note that the values of Ω are 0 and $-2F^2 < 0$ when $\kappa_x = 0$. The modes to either side of 0 are unstable when $\Omega_r(\kappa_x = 0)$ is concave up, i.e. when $\frac{\partial^2 \Omega_r}{\partial \kappa_x^2}\big|_{\kappa_x=0} > 0$. These regions correspond to the "Unstable" sections of figure 3.17, which is for $\mathrm{Pr} = 0.025$ and $\mathcal{T} = 100$, with $g = -0.29 + 0.83i$. The results are similar to those given in section 2.10; the size of the unstable region may change as g is changed, but its shape is similar. The eigenvalue with the largest real part for $|\kappa_x| < 2$ is $\Omega_{max} = 1.29 \pm 0.83i$ at $\kappa_x = -1$. This value occurs for $\vec{Q} = (-1, 0)$ (positive imaginary part) and $\vec{Q} = (1, 0)$ (negative imaginary part).

The next question is whether, given $\frac{\partial^2 \Omega_r}{\partial \kappa_x^2}\big|_{\kappa_x=0} < 0$, there is a value of κ_x such that $\frac{\partial^2 \Omega_r}{\partial \kappa_x^2} > 0$. This would mean that at some point, the concavity of $\Omega_r(\kappa_x)$

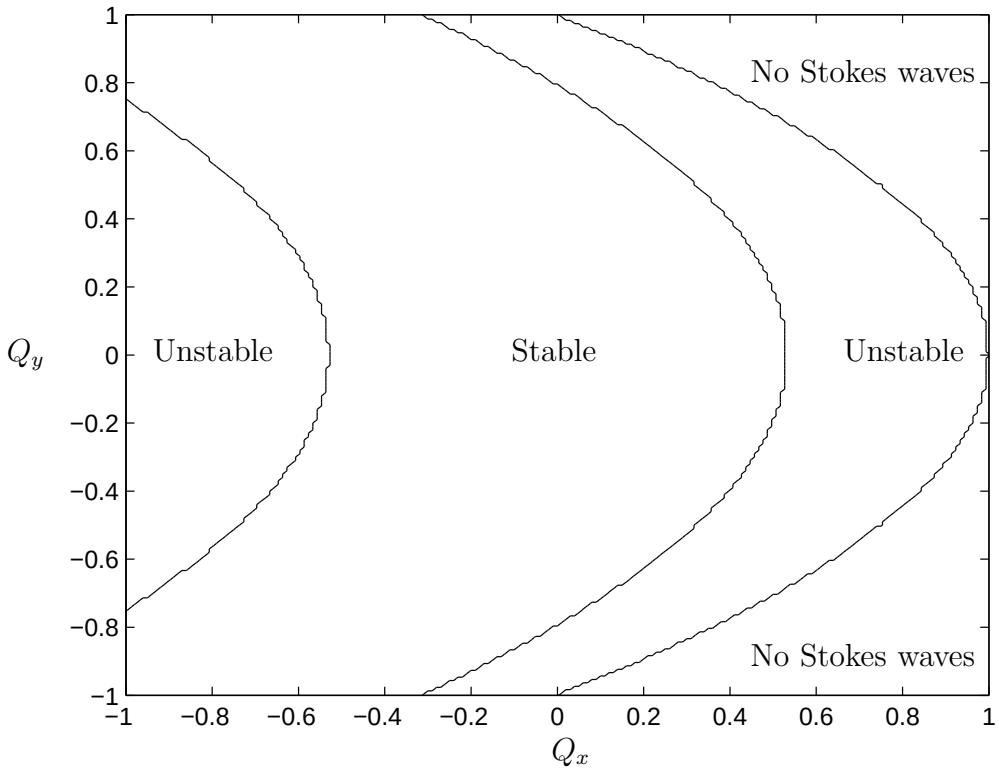

Figure 3.17: Stability of Stokes waves for κ_x near zero. In the unstable regions, at least one such perturbation grows. In the stable region, Stokes waves are (neutrally) stable for all such perturbations. The regions labeled "No Stokes waves" are where $F^2 < 0$.

becomes upwards and an unstable mode is possible. Numerically minimizing $\left|\frac{\partial^2 \Omega_r}{\partial \kappa_x^2}\right|$ using Matlab's `fminsearch` function with $Q_x = 0$ reports a minimum is at $\kappa_x = 0$ for all values tried, suggesting that the answer is no. In the limit of large κ_x, $\Omega \to (g_r \pm g_i - 1)\kappa_x^2$, whose second derivative is a constant. Therefore Stokes wave solutions are expected to be either unstable to a mode near zero, or stable for all modes.

3.10 Conclusion

The subject of this chapter has been the derivation of a system of amplitude equations for rotating convection with a Hopf bifurcation and stress-free boundaries. Several interesting results were uncovered as a result of this investigation.

At second order, a timescale of order ϵ and a group velocity appeared due to the solvability condition. The group velocity could not be eliminated using a simple change of variables because of the Y-dependence of the system. Since X and Y scale differently with ϵ, a special form of the solution for A must be assumed in order to satisfy the second-order equation and move on to higher order. This form is not unreasonable; it simply restricts the solution to a Stokes wave (as far as its Y-dependence goes) moving in a chosen direction. The choice of direction is arbitrary, resulting in infinitely many amplitude equations at third order, each with a different constant standing for the Y-derivative. The result is more general than dropping variation in Y, but not completely general. It was also necessary to assume that B is zero, because the group velocity can only be eliminated from one amplitude equation at a time. These restrictions allow a stability analysis of Stokes wave solutions to the amplitude equations at third order to be carried out.

At third order, a pair of coupled equations similar to the complex Ginzburg-Landau equation appears. An equation for the mean drift was derived at order $\epsilon^{7/2}$ to complete the system. All three of the equations simplify, as expected, to the corresponding amplitude equations for rotating convection with a stationary bifurcation.

In addition, the stability of Stokes wave solutions to the two coupled amplitude equations (neglecting the mean drift U) was analyzed and stability criteria were derived for perturbations with spatial modulation in the X-direction. Unstable solutions exist and their location in the $\vec{Q}$-plane is shown.

The next steps are to simulate the full system of equations, and to use the results of these simulations to reconstruct the physical velocity field. This will result in a full description of the flow that could be compared, both qualitatively and quantitatively, with experimental results. In particular, this system of equations provides a full description of the nonlinear flow effects for low-Prandtl number fluids, such as mercury, when the Rayleigh number is slightly above critical.

CHAPTER 4

A LINEARIZED MODEL OF LANGMUIR CIRCULATIONS WITH THERMAL EFFECTS

4.1 Introduction

Irving Langmuir[1] first observed the circulations which bear his name on 7 August, 1927, while traveling from New York to England. His 1938 paper [44] stands out as the first scientific description of these circulations and includes details of a number of experiments he performed at Lake George over the years between his voyage and publication. The Langmuir family owned a vacation home on the shore of Lake George and visited it frequently [70, p.95–97]. However, Langmuir was not the first to observe such streaks on surface waters; several nineteenth-century English authors referred to them [47].

Langmuir circulations take the form of convection rolls, but are driven by the wind. The simplest explanation of the mechanics behind these rolls starts with the wind blowing across the surface of the water, causing surface waves. Nonlinear effects generate the mass drift discovered by Stokes [64]. Then a small perturbation in the surface velocity field results in vertical vorticity. The Stokes drift velocity due to the surface waves causes this new vorticity vector to stretch and develop a horizontal component. Horizontal vorticity means that the fluid has an azimuthal velocity component, which leads to rolls. This, in turn, strengthens the perturbation velocity because the high-momentum fluid is pulled inwards.

A number of aspects of Langmuir circulations have been investigated and reported in the literature. My work on this subject is a direct extension of the work of Thomas Haeusser [30], who examines the effect of the Coriolis force on the for-

[1]Langmuir (1881–1957) was an American chemist who won the Nobel Prize in 1932 for his work on surface chemistry, and is the author of over 250 scientific papers [70].

mation of Langmuir circulations, and Leibovich and Tandon [48], who examine the changes in windrow angles that result from density variations in the absence of Coriolis acceleration.

The goal of this chapter is to show how temperature changes in the mixed layer affect the formation of Langmuir circulations when rotational effects are important, as in the oceans. In most lakes and other smaller bodies of water, the effects of rotation can usually be safely ignored. Temperature variations are not necessary for the formation of Langmuir circulations, but they can lead to convective instability on their own. Large thermally stable temperature gradients can have a significant effect on the stability of the water in the presence of surface waves. Stable temperature gradients, equivalent to a negative Rayleigh number, are the norm in the ocean's surface waters. As expected, a stable temperature gradient makes it more difficult for Langmuir circulations to form. The effects of varying the latitude and wind direction for a given negative Rayleigh number are also investigated. These variations do not have a significant effect on the critical Reynolds number.

One important application of this research is the possibility of using infrared photographs to determine properties of the oceanic mixed layer. Once the effects of temperature variations on Langmuir circulation patterns are fully understood, it may be possible to infer the subsurface temperature field from the temperature of surface water, as depicted in infrared photographs.

4.2 Governing Equations

The governing equations for this system are the same as those for rotating convection, with the addition of an apparent force encapsulating the rectified effects of surface gravity waves. The latter are presumed given, and their effects on the mean

motions are represented by the Craik-Leibovich theory [20]. First, continuity:

$$\nabla \cdot \vec{u} = 0 \tag{4.1}$$

The continuity equation includes the Boussinesq approximation, which says small changes in density are negligible in the inertia term, but important in the buoyancy term, where they are retained. Changes in fluid properties are also neglected.

The left hand side of the momentum equation,

$$\frac{D\vec{u}}{Dt} = -\nabla P + \nu\nabla^2\vec{u} + \vec{U}_s \times (2\vec{\Omega} + \nabla \times \vec{u}) + \beta g\theta\hat{z} - 2\vec{\Omega} \times \vec{u} \tag{4.2}$$

is the material derivative. The terms on the right hand side are the pressure gradient force, dissipation due to viscosity, Langmuir or vortex force (representing the wave-current interaction), buoyancy, and the Coriolis force due to the earth's rotation. ν is the kinematic viscosity, β is the coefficient of thermal expansion ($-\frac{1}{\rho}\frac{\partial\rho}{\partial T}$ for a fluid with density ρ), g represents gravity, and $\vec{\Omega}$ is the angular velocity vector. The pressure P in this equation is a modified pressure that includes the usual pressure, the centrifugal force $\vec{\Omega} \times (\vec{\Omega} \times \vec{r})$ (where $\vec{r}$ is the position vector), and contributions from the Stokes drift.

The Stokes drift, $\vec{U}_s$, modeled as an additional velocity term, is assumed to be a function of depth only and oriented along $\hat{x}$: $\vec{U}_s = U_s(z)\hat{x}$. The velocity vector, when expanded in powers of a small parameter $\epsilon = \sqrt{\frac{\mathrm{Re}-\mathrm{Re}_c}{\mathrm{Re}_c}}$, becomes $\vec{u} = \vec{U} + \epsilon\vec{u}_1 + \epsilon^2\vec{u}_2 + ...$ $\vec{U}$ is the basic state of the flow, which is derived later in this section.

The energy equation,

$$\frac{D\theta}{Dt} + w\frac{\partial\bar{T}}{\partial z} = \kappa\nabla^2\theta \tag{4.3}$$

governs the evolution of the temperature. The perturbation temperature is θ and $\bar{T}(z)$ is the temperature distribution in the absence of horizontal variations, with

$T = \bar{T}(z) + \theta$ and $\bar{T} = (T_{bottom} - T_{top})z/d$. The thermal diffusivity is κ (heat conductivity χ over heat capacity per unit volume C) and d is the layer depth.

The system of equations 4.1, 4.2, and 4.3, is nondimensionalized following Haeusser [30]: the friction velocity, $u_* = \sqrt{\tau/\rho}$, where τ is the shear stress exerted on the surface of the water by the wind, is the reference for velocity, the temperature difference $\Delta T = T_{top} - T_{bottom}$ is the scale for temperature, and the layer depth d is the length scale. Taking small perturbations around the basic state $\vec{U}(z)$ results in the dimensionless perturbation equations:

$$\frac{\partial \vec{u}}{\partial t} + \vec{u} \cdot \nabla \vec{u} = -\nabla P + \frac{1}{\mathrm{Re}} \nabla^2 \vec{u} + \vec{U}_s \times (\nabla \times \vec{u}) + \mathcal{G}\theta \hat{z} - 2\vec{\Omega} \times (\vec{u} + \vec{U}_s) \tag{4.4}$$

$$\frac{\partial \theta}{\partial t} + (\vec{u} + \vec{U}_s) \cdot \nabla \theta = \frac{\nabla^2 \theta}{\mathrm{PrRe}} + w \tag{4.5}$$

$$\nabla \cdot \vec{u} = 0 \tag{4.6}$$

In these equations, w is the $\hat{z}$ component of the velocity and $\vec{\Omega}$ is a dimensionless rotation vector. The dimensionless groups are the Reynolds number based on the friction velocity, $\mathrm{Re} = u_* d/\nu$, the Prandtl number $\mathrm{Pr} = \frac{\nu}{\kappa}$, and $\mathcal{G}$, a measure of temperature change: $\mathcal{G} = \beta g \Delta T d/u_*^2 = \mathrm{Ra}/\mathrm{PrRe}^2$. $\mathcal{G}$ is related to the Rayleigh number, Ra, of convection, which is the parameter I will set when determining the critical Reynolds number. The Rayleigh number is defined by $\mathrm{Ra} = \frac{\beta g \Delta T d^3}{\kappa \nu}$, with a typical mixed layer temperature difference of up to $\Delta T = -0.8K$ [38] due to surface heating and depth $d \simeq 11\mathrm{m}$. The coefficient of thermal expansion for water is $\beta = 0.207 \times 10^{-3}$ per Kelvin at $T = 20°\mathrm{C}$ [26], $g = 9.81\mathrm{m/s}^2$ is the acceleration of gravity, and the viscosity is assumed to be a turbulent viscosity $\nu_T = 100\mathrm{cm}^2/\mathrm{s}$ and the friction velocity is typically $u_* = 1\mathrm{cm/s}$ [30]. The Prandtl number is one. This leads to typical Rayleigh numbers between zero and $-20,000$, corresponding to stable stratification.

The rotation vector $\vec{\Omega}$ is

$$\vec{\Omega} = \frac{\mathrm{sgn}\psi}{\mathrm{ReEk}} \left(\cot\psi \sin\phi,\ \cot\psi \cos\phi, 1\right) \tag{4.7}$$

The Ekman number $\mathrm{Ek} = \nu/(d^2\Omega_E|\sin\psi|)$ is based on the Earth's angular velocity Ω_E. ψ is the latitude and the wind's surface stress is exerted in a direction ϕ north of east.

The boundary conditions associated with this system are a rigid bottom boundary with no slip

$$\vec{u}(z = -1) = 0 \tag{4.8}$$

constant shear stress on the top boundary

$$\frac{\partial u}{\partial z}|_{z=0} = \mathrm{Re} \tag{4.9}$$

$$\frac{\partial v}{\partial z}|_{z=0} = 0 \tag{4.10}$$

and no vertical velocity on the top boundary

$$w(z = 0) = 0 \tag{4.11}$$

following Langmuir's early suggestion of a free upper surface and rigid bottom boundary [44, p.123]. The constant stress condition is satisfied by the basic flow and the derivatives of the horizontal perturbation velocities are zero on the top boundary. The temperature perturbation is zero on both boundaries,

$$\theta(-1) = \theta(0) = 0 \tag{4.12}$$

The system of equations 4.4–4.6 and boundary conditions 4.8–4.12 is, like Haeusser's system [30] invariant under the transformation

$$(\psi, \phi, y, v) \rightarrow (-\psi, -\phi, -y, -v) \tag{4.13}$$

when no other variables are changed. This is equivalent to symmetry across the x axis for infinite Ekman number (when the problem does not depend on either

angle). Because of this symmetry, it is unnecessary to perform calculations for the southern hemisphere. They can be obtained from the northern hemisphere results by means of the symmetry transformation.

To find the basic state $\vec{U} = U(z)\hat{x} + V(z)\hat{y}$, it is necessary to solve the horizontal components of the momentum equation (4.4):

$$V'' = 2\Omega_z \mathrm{Re}(U + U_s) \tag{4.14}$$

$$U'' = -2\Omega_z \mathrm{Re} V \tag{4.15}$$

with boundary conditions $U(-1) = V(-1) = V'(0) = 0$, $U'(0) = \mathrm{Re}$. The solution is the basic state $\vec{U}$:

$$U + iV = C_s \sinh(\beta(1+z)) + C_c \cosh(\beta(1+z)) + C_e e^{z/l} \tag{4.16}$$

with $\beta = (1+i)\mathrm{Ek}^{-1/2}$ and $\theta = 0$ on [-1 0]. The coefficients are:

$$C_e = \frac{2il^2 U_s(0)}{\mathrm{Ek} - 2il^2} \tag{4.17}$$

$$C_c = -e^{-1/l} C_e \tag{4.18}$$

$$C_s = \frac{\mathrm{Re} - C_e/l - \beta C_c \sinh\beta}{\beta \cosh\beta} \tag{4.19}$$

Huang [35] calls this the "wave-modified Ekman solution": it is the flow that occurs when the Coriolis and friction forces balance. Without the shear stress on the surface force (zero Stokes drift), the basic flow becomes plane Couette flow, $U + iV = \mathrm{Re}(1+z)$. The Stokes drift is $\vec{U}_s = U_s(0)e^{z/l}\hat{x}$, where l is a dimensionless depth parameter. When the Coriolis force is zero, the basic flow assumes the form derived by Ekman [25],

$$U + iV = \frac{\mathrm{Re}}{\beta \cosh\beta} \sinh(\beta(1+z)) \tag{4.20}$$

A hodograph of the basic flow is shown in figure 4.1.

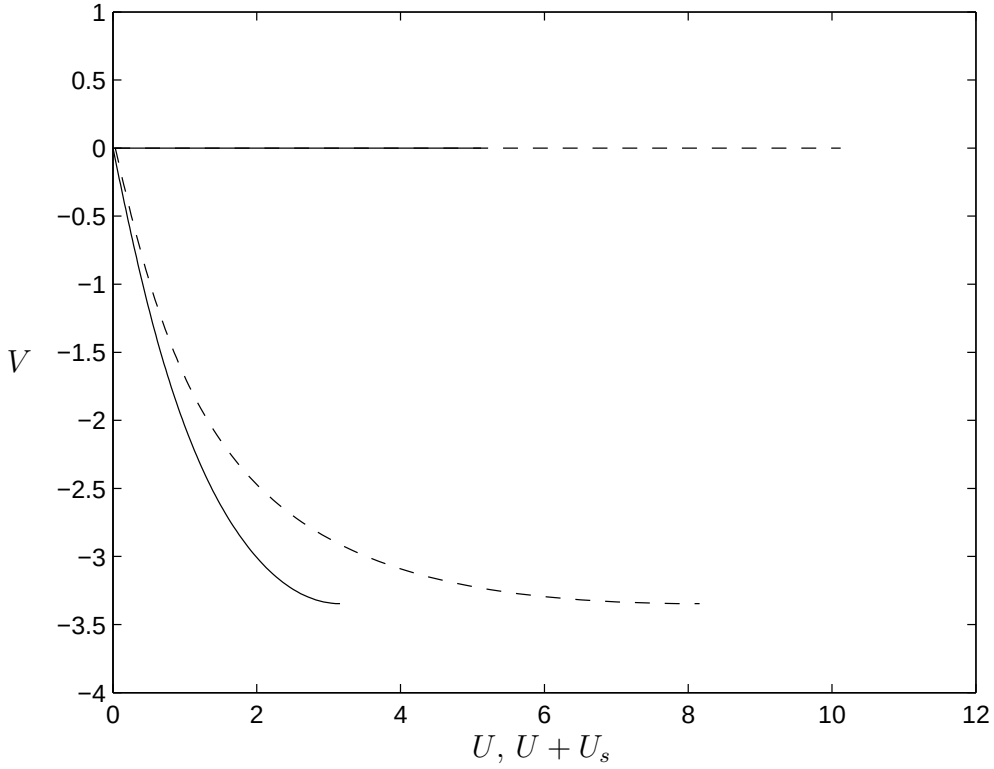

Figure 4.1: The basic flow. The horizontal axis is U (solid line) or $U + U_s$ (dashed line), and the vertical axis is V. The straight line is for Re = 5.12, Ek = ∞ and the curved line is for Re = 5.74, Ek = 1. Both cases assume a latitude of 90^o, a wind direction of 0^o, and a Rayleigh number of zero.

Taking the vertical vorticity equation, the energy equation, and the vertical component of the curl of the vorticity equation gives the final system of equations:

$$\begin{pmatrix} -(\nabla \times (\vec{v} \cdot \nabla \vec{v})) \cdot \hat{z} \\ -\vec{v} \cdot \nabla \theta \\ (\nabla \times \nabla \times (\vec{v} \cdot \nabla \vec{v})) \cdot \hat{z} \end{pmatrix} = \begin{pmatrix} \frac{\partial}{\partial t} & 0 & 0 \\ 0 & \frac{\partial}{\partial t} & 0 \\ 0 & 0 & \frac{\nabla^2 \partial}{\partial t} \end{pmatrix} \begin{pmatrix} \zeta \\ \theta \\ w \end{pmatrix}$$
$$+ \begin{pmatrix} -\frac{\nabla^2}{\mathrm{Re}} + (\vec{U} + \vec{U}_s) \cdot \vec{\nabla} & 0 & -2\vec{\Omega} \cdot \vec{\nabla} + V' \frac{\partial}{\partial x} - U' \frac{\partial}{\partial y} \\ 0 & -\frac{\nabla^2}{\mathrm{PrRe}} + (\vec{U} + \vec{U}_s) \cdot \nabla & -1 \\ -U_s' \frac{\partial}{\partial y} + 2\vec{\Omega} \cdot \vec{\nabla} & -\mathcal{G} \nabla_h^2 & \aleph \end{pmatrix} \begin{pmatrix} \zeta \\ \theta \\ w \end{pmatrix} \tag{4.21}$$

with

$$\aleph = -\vec{U}'' \cdot \vec{\nabla} + (\vec{U} + \vec{U}_s) \cdot \nabla \nabla^2 - \frac{1}{\mathrm{Re}} \nabla^4 \tag{4.22}$$

and $\vec{u} = \vec{U} + \vec{v}$: here $\vec{v}$ does not include the drift terms. These equations are in agreement with Haeusser's [30] when $\mathcal{G} = 0$ and $\theta = 0$.

4.3 Linearized System and Results

The linearized system can be set up utilizing the method of normal modes. This involves setting each variable equal to a function of z times an exponential:

$$w = w_1(z) e^{i(\vec{k} \cdot \vec{x} + \omega t)} \tag{4.23}$$

$$\theta = \theta_1(z) e^{i(\vec{k} \cdot \vec{x} + \omega t)} \tag{4.24}$$

$$\zeta = \zeta_1(z) e^{i(\vec{k} \cdot \vec{x} + \omega t)} \tag{4.25}$$

The boundary conditions 4.8–4.12 become $w_1 = w_1' = \zeta_1 = \theta_1 = 0$ on $z = -1$ and $w_1 = \theta_1 = \zeta_1' = w_1'' = 0$ on $z = 0$. The numerical methods used to solve the linear problem are described in appendix C.

Sample eigenfunctions for the linear problem are shown in figures 4.2 through 4.7. Critical values for $U_s(0) = 11.6$ are given in appendix F. This value was derived from the Pierson-Moskowitz spectrum by Leibovich and Yang [46]. It may also be roughly obtained from the model of Kenyon [39], who shows that the dimensional Stokes drift constant, $U_s'(0)$, is equal to AW, where W is the wind speed 19.5 meters above the surface and $A = 0.0358$ is a constant derived from the Pierson-Moskowitz spectrum for fully-developed seas [55]. Since Langmuir circulations form when the wind speed is greater than about three meters per second [47], I choose $W = 3.25$m/s. Nondimensionalizing the result by the friction velocity $u_* = 1$cm/s leads to $U_s(0) = \frac{0.0358 \times 3.25}{0.01} \simeq 11.6$.

As expected, these results agree with Haeusser's [30] for his parameters, and the critical Reynolds number decreases with increasingly negative Rayleigh number. Figures 4.8 through 4.12 depict various linear results for an Ekman number of 1, with $U_s(0) = 11.6$.

Figure 4.8 shows the variation of the critical Reynolds number with the Rayleigh number. The critical Reynolds number starts out near 4.5, then increases (rapidly at first, then gradually leveling out) as the Rayleigh number becomes more negative. The curve seems to be approaching a linear asymptote. If this is the case, then there is no Rayleigh number large enough to completely suppress Langmuir circulations for the wind speed investigated. As Li and Garrett [49] find, surface heating is never strong enough to stop Langmuir circulations from forming for reasonable physical parameters.

Figure 4.9 shows how the frequency of the travelling waves changes with the Rayleigh number. This frequency starts out near 3.5 for a Rayleigh number of zero, but as the Rayleigh number becomes more negative, it decreases, reaching a minimum value of 3.28 for a Rayleigh number of -2500. It then increases for all

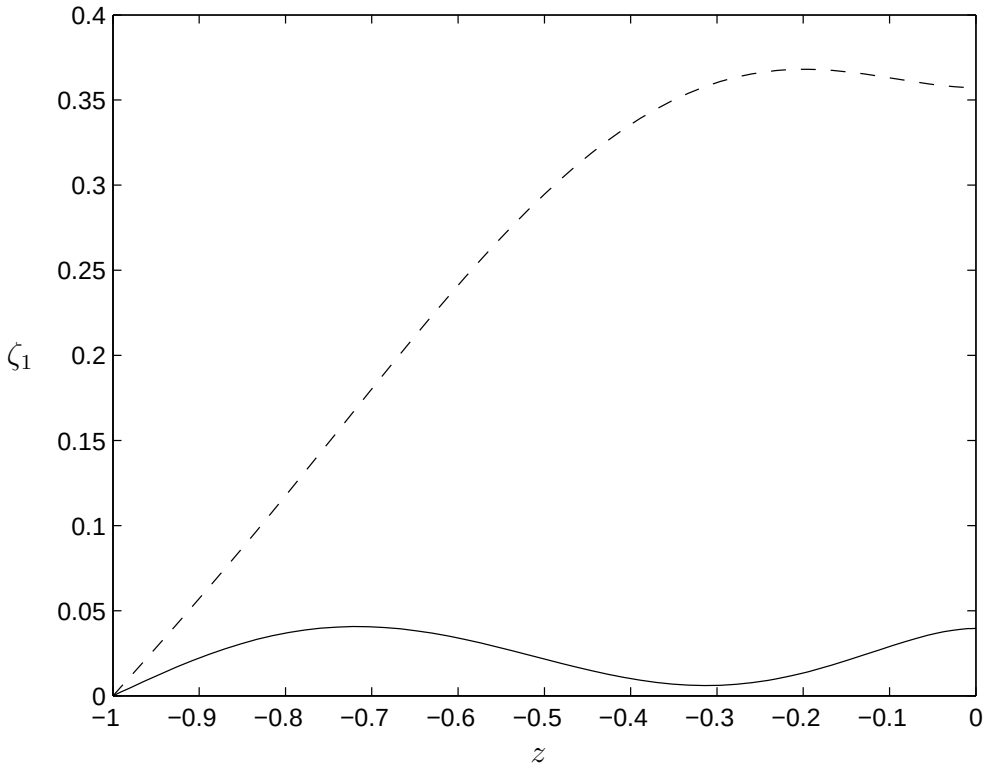

Figure 4.2: Solutions to the linearized problem with Ra = 0, $U_s(0) = 5$, Ek = 1, $\psi = 90°$, $\phi = 0°$ (Haeusser's case II): ζ_1. The solid line is the real part and the broken line is the imaginary part.

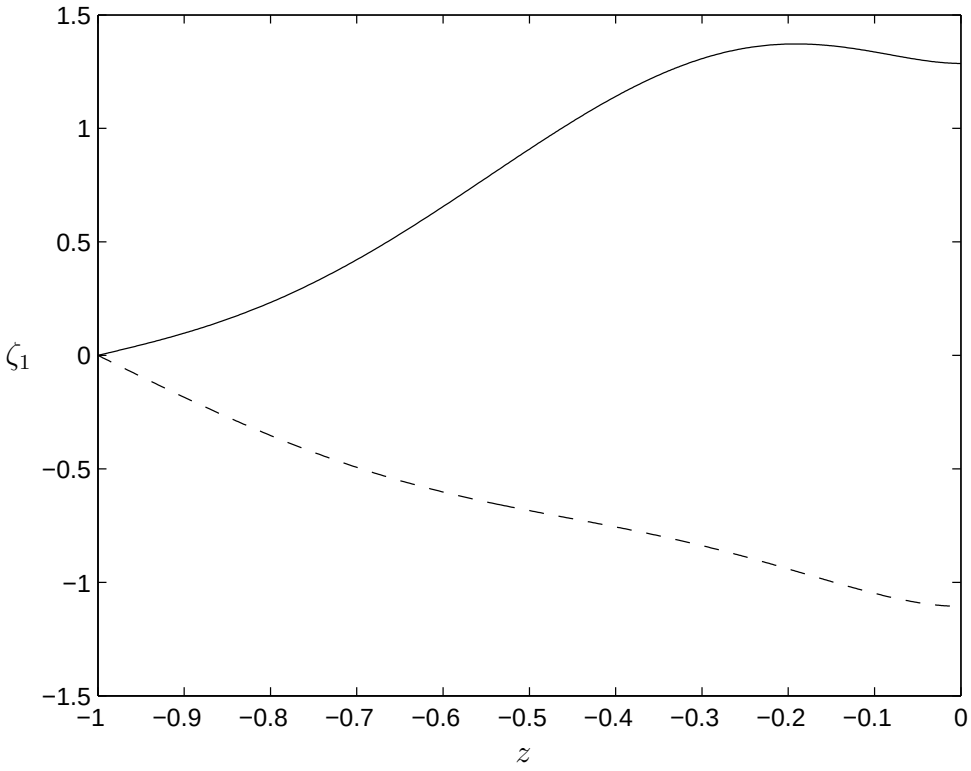

Figure 4.3: Solutions to the linearized problem with Ra $= -8000$, $U_s(0) = 11.6$, Ek $= 1$, $\psi = 90°$, $\phi = 0°$: ζ_1. The solid line is the real part and the broken line is the imaginary part.

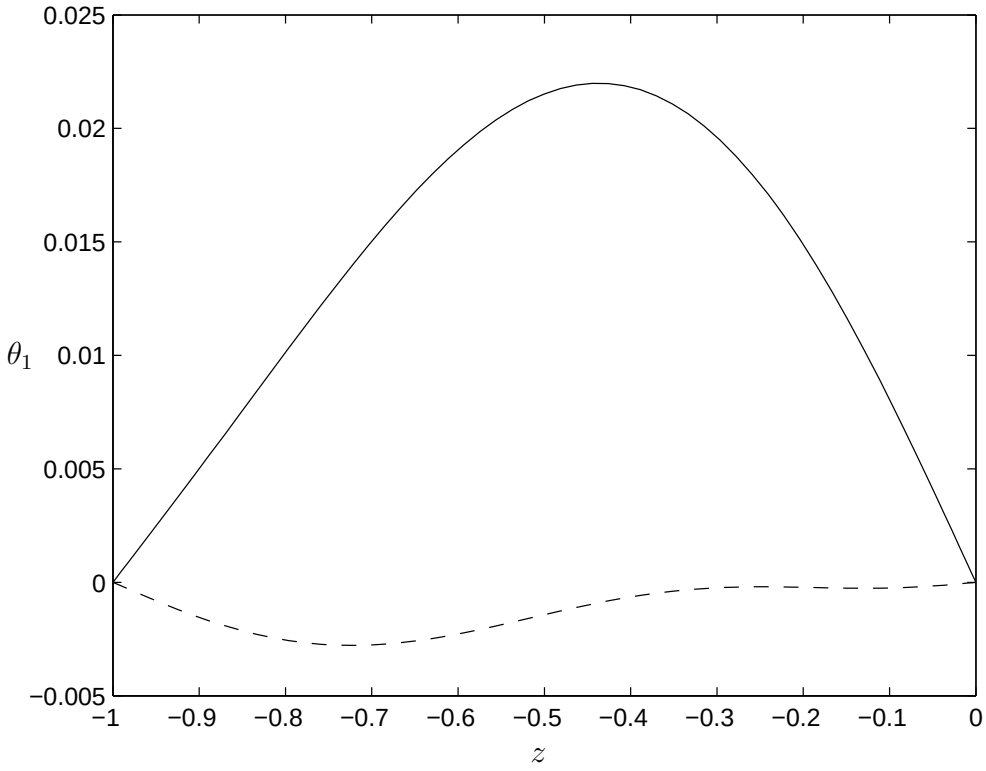

Figure 4.4: Solutions to the linearized problem with Ra = 0, $U_s(0) = 5$, Ek = 1, $\psi = 90°$, $\phi = 0°$ (Haeusser's case II): θ_1. The solid line is the real part and the broken line is the imaginary part.

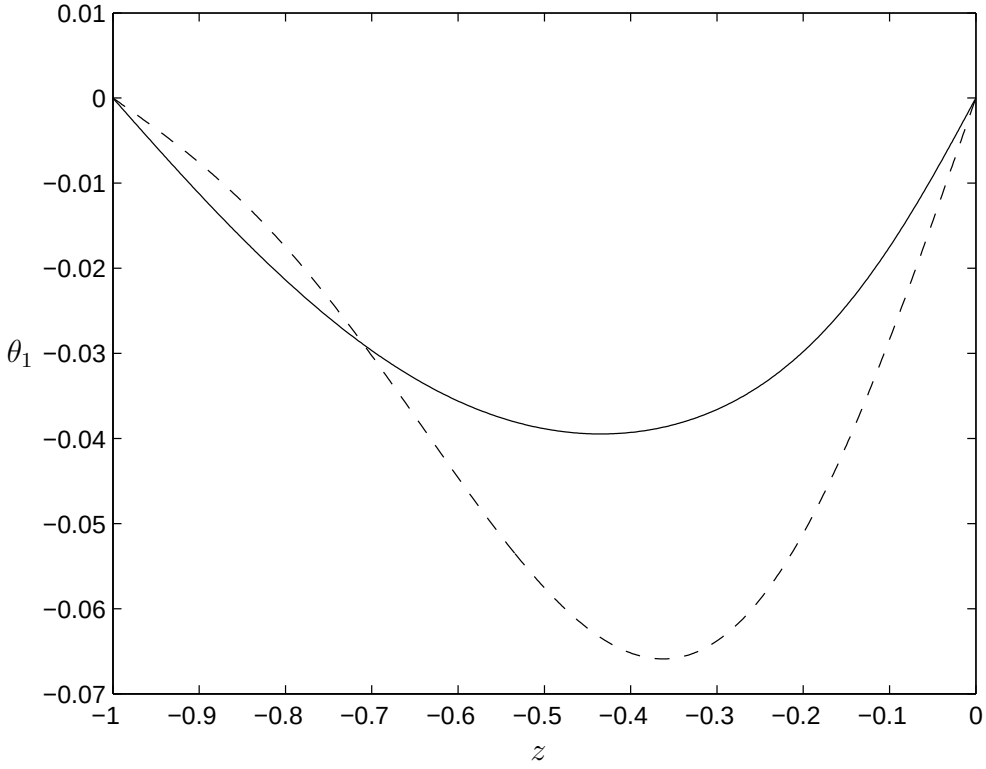

Figure 4.5: Solutions to the linearized problem with Ra $= -8000$, $U_s(0) = 11.6$, Ek $= 1$, $\psi = 90°$, $\phi = 0°$: θ_1. The solid line is the real part and the broken line is the imaginary part.

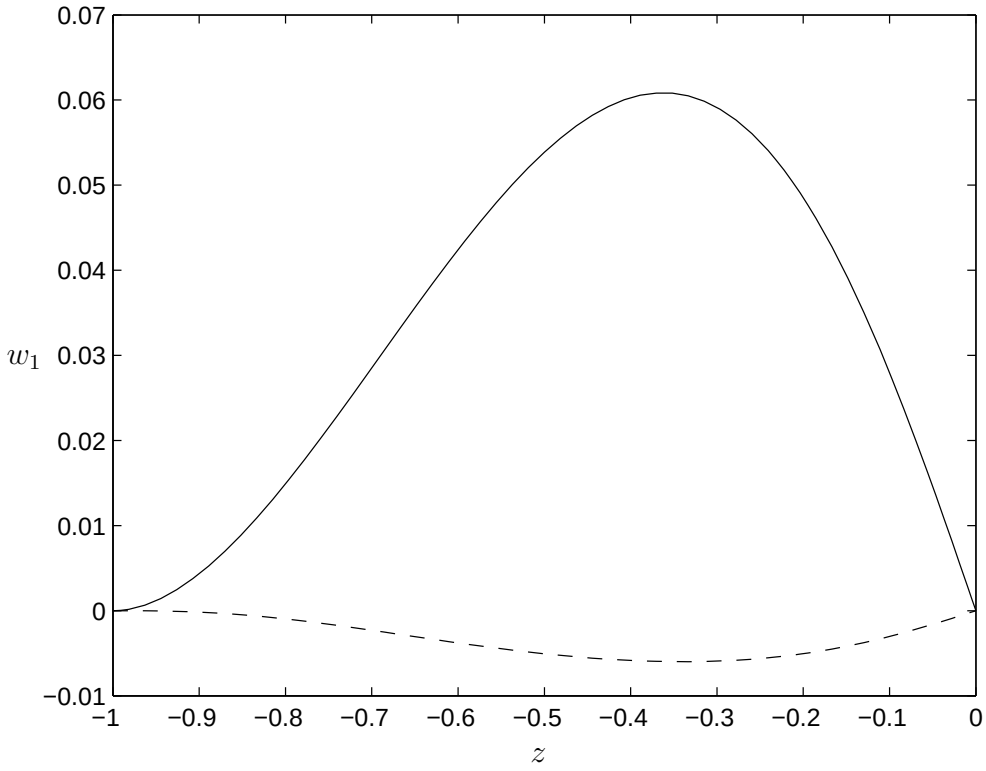

Figure 4.6: Solutions to the linearized problem with Ra = 0, $U_s(0) = 5$, Ek = 1, $\psi = 90°$, $\phi = 0°$ (Haeusser's case II): w_1. The solid line is the real part and the broken line is the imaginary part.

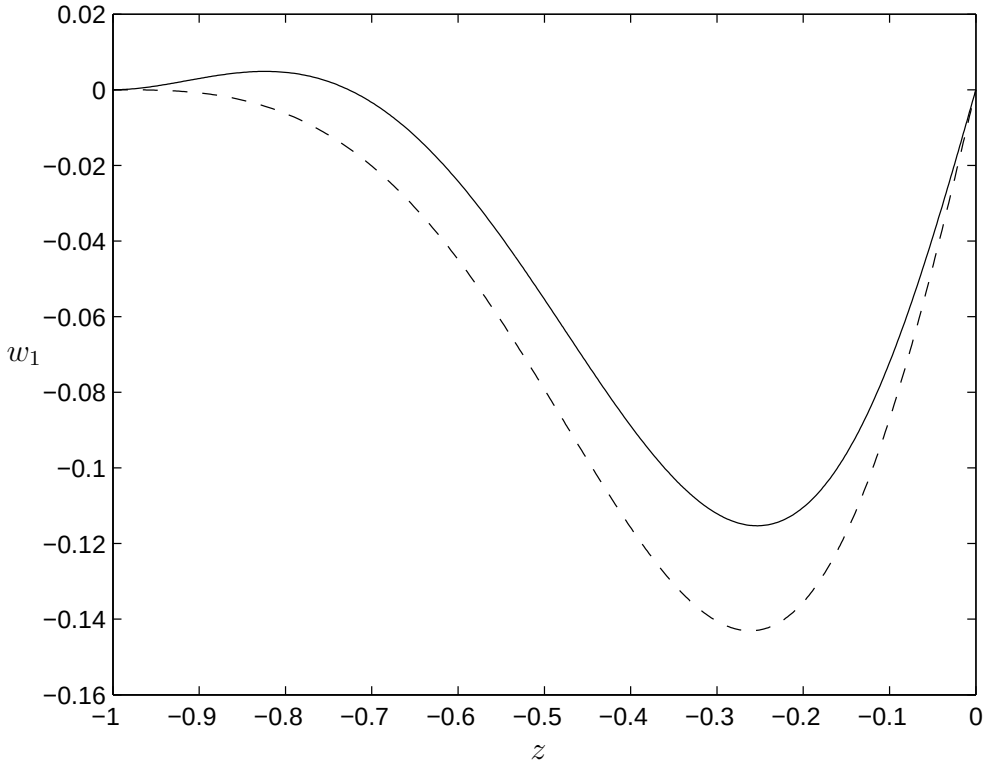

Figure 4.7: Solutions to the linearized problem with Ra $= -8000$, $U_s(0) = 11.6$, Ek $= 1$, $\psi = 90°$, $\phi = 0°$: w_1. The solid line is the real part and the broken line is the imaginary part.

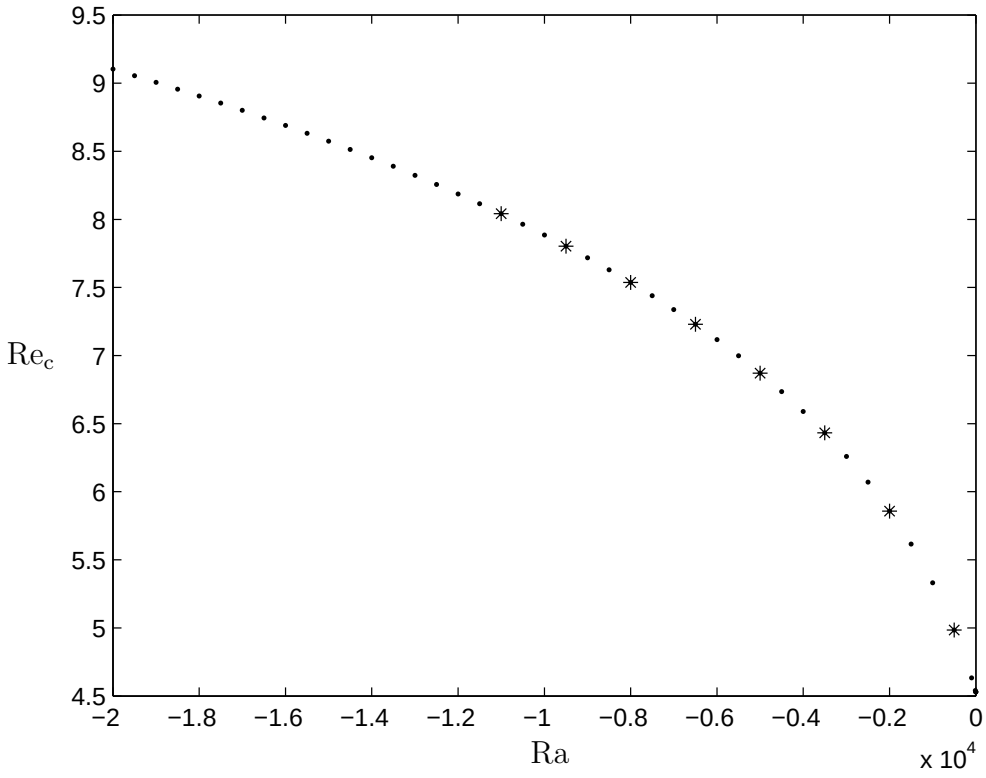

Figure 4.8: Critical Reynolds number versus Rayleigh number, for $U_s(0) = 11.6$. Dots were computed with a tolerance of 10^{-4}, stars with 10^{-8}.

subsequent Rayleigh numbers investigated.

In figures 4.10 and 4.11, the variation of the wave-number's magnitude and of each wave-number component are shown. These figures show that the direction of the rolls' orientation and the spacing between the rolls change with Rayleigh number. However, the changes are not very large. The angle of the most unstable rolls with respect to the wind, $\alpha_c = \arctan \frac{k_x}{k_y}$, starts out at about 19° for Rayleigh number zero, but decreases to 15° as the magnitude of the Rayleigh number increases. Positive values of α_c indicate that the rolls are deflected to the right of the wind.

Together, figures 4.9, 4.10, and 4.11 show the critical frequency, as well as the wave-number's magnitude and direction as functions of the Rayleigh number. Since this scenario results in a Hopf bifurcation, the final pattern oscillates in time, in the form of a travelling wave. The wave-vector $\vec{k}$ is perpendicular to the axes of the rolls that form above the critical Reynolds number, and the frequency ω shows how quickly the travelling waves propagate. The rolls travel with a phase velocity (shown in figure 4.12) of $-(\omega_c/|\vec{k}_c|)\hat{k}_c$, where $\hat{k}_c$ is a unit vector in the direction of the wave-vector $\vec{k}_c$.

Figures 4.13 through 4.20 assume a Rayleigh number of -8000, an Ekman number of 1, depth l of 0.2, and drift parameter $U_s(0) = 11.6$. These figures show the variation of the critical values with wind direction and latitude.

Changes in wind angle (figures 4.13 through 4.16) result in only slight changes in roll angle, which is always between 15.7° and 16°. Haeusser found a similar range of roll angles for mid-latitudes, though his were between about 18.5° and 19.7° for 40° latitude. This, combined with the previous angle data, suggests that temperature variations cause the most unstable rolls to change their direction, but that the rolls still try to maximize the interactions of the surface waves and

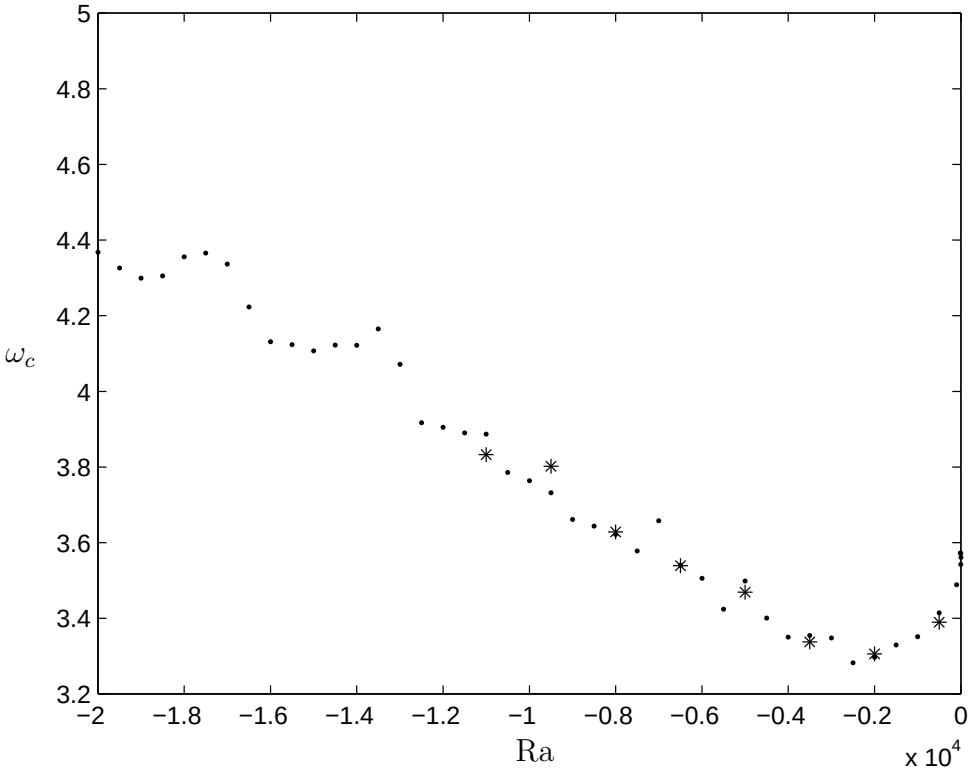

Figure 4.9: Frequency versus Rayleigh number, for $U_s(0) = 11.6$. Dots were computed with a tolerance of 10^{-4}, stars with 10^{-8}.

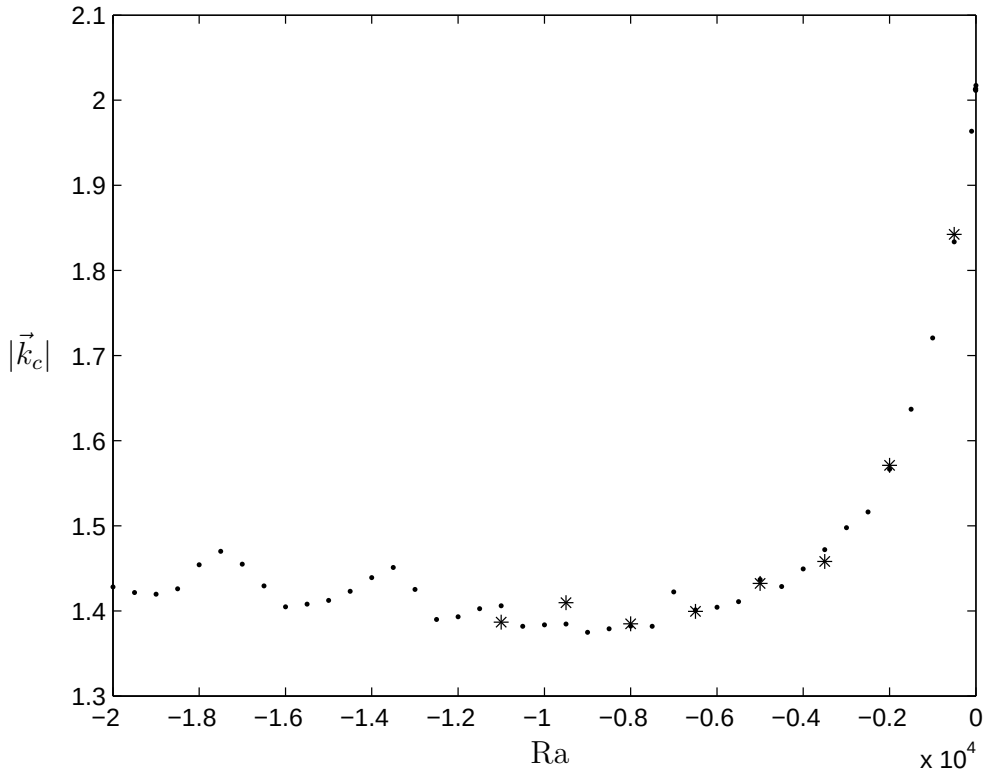

Figure 4.10: Wave-Number magnitude $|\vec{k}_c|$ versus Rayleigh number, for $U_s(0) = 11.6$. Dots were computed with a tolerance of 10^{-4}, stars with 10^{-8}.

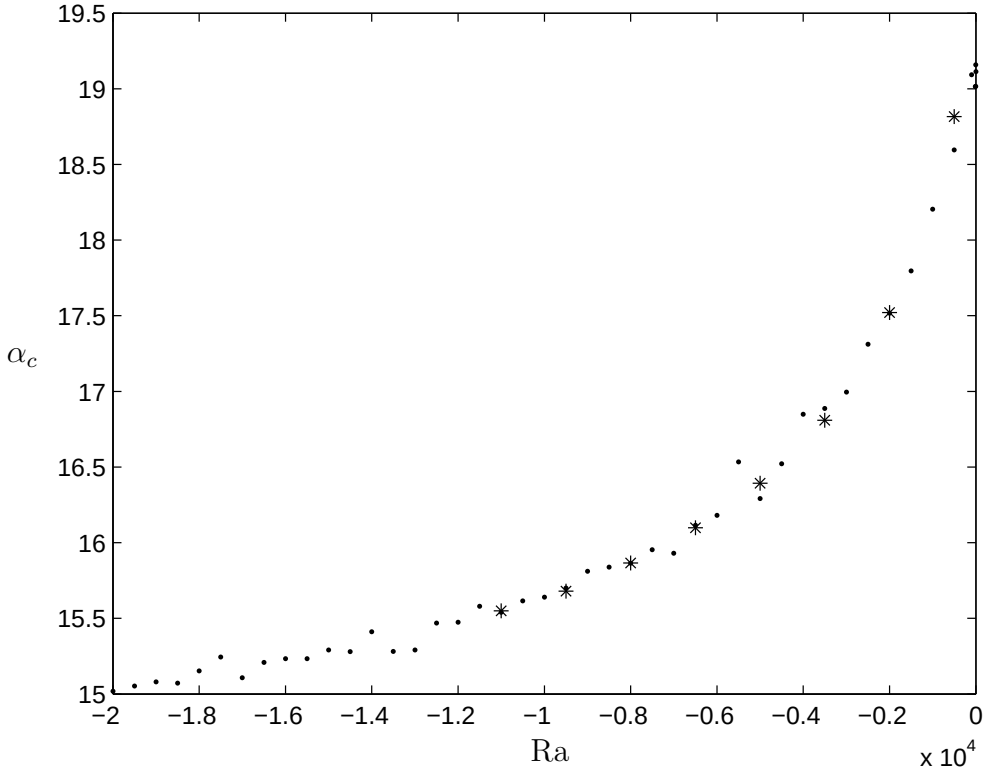

Figure 4.11: Roll angle α_c (degrees) versus Rayleigh number, for $U_s(0) = 11.6$. Dots were computed with a tolerance of 10^{-4}, stars with 10^{-8}.

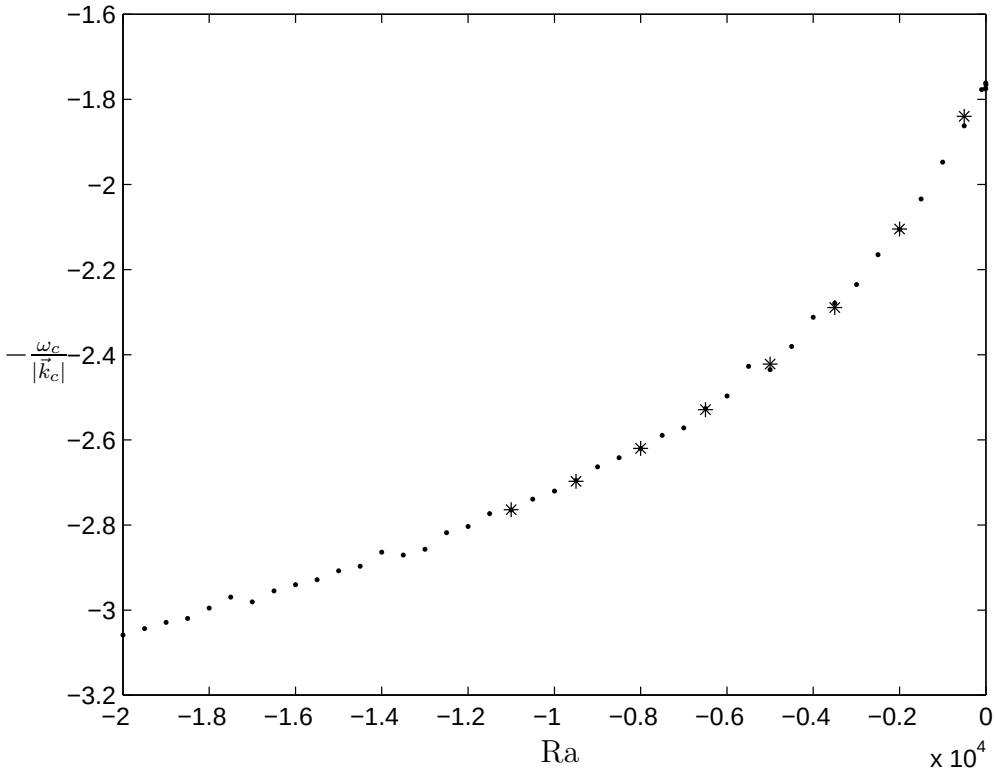

Figure 4.12: Phase velocity $-\frac{\omega_c}{|\vec{k}_c|}$ versus Rayleigh number, for $U_s(0) = 11.6$. Dots were computed with a tolerance of 10^{-4}, stars with 10^{-8}.

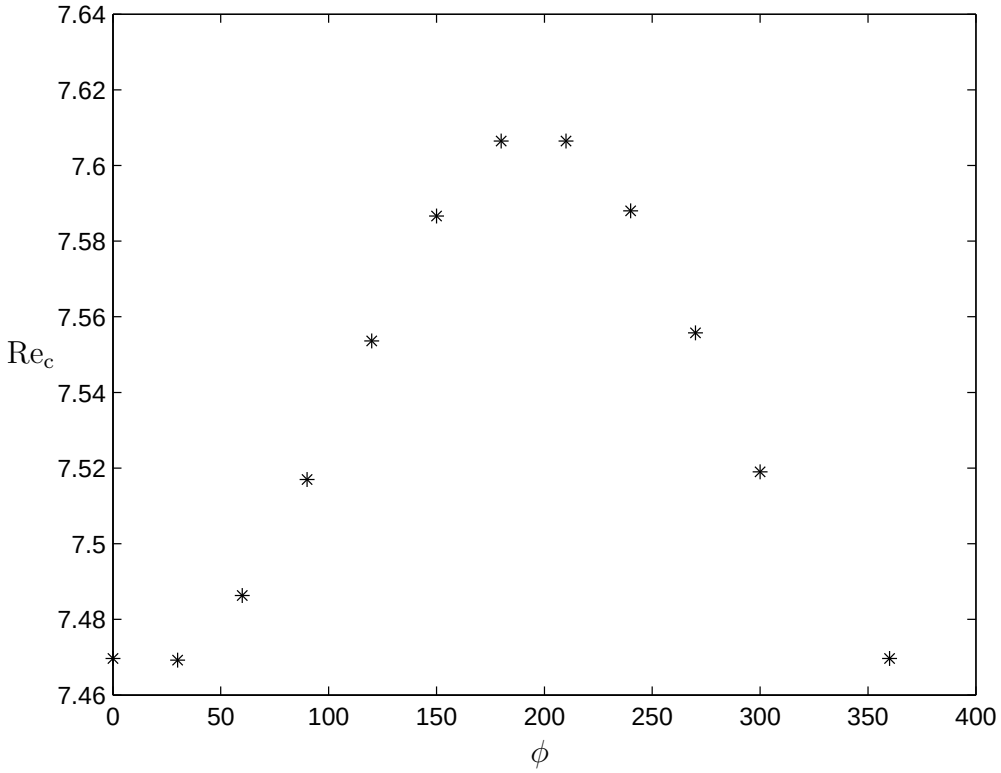

Figure 4.13: Critical Reynolds number versus wind angle, ϕ, for $\psi = 45°$, Ra $= -8000$, with $U_s(0) = 11.6$.

currents. Haeusser points out that "For Ek $\neq \infty$, α_c is about midway between the Stokes drift direction and the direction of strongest shear, so that the wave-current interaction is maximized" [30]. Gnanadesikan and Weller [29] investigated the interaction of surface waves and currents in more detail, but do not consider thermal effects.

Latitude variations (figures 4.17 to 4.20) do not cause the critical Reynolds number to vary as much as might be expected. As the approximated tangent-plane moves through the latitudes, the magnitude of the z component of the angular velocity of the tangent plane reference frame changes, until, at the equator, it is parallel to the tangent plane. Because of this, the physics of the flow is somewhat different, and there may be problems with numerical accuracy. The symmetry requirement 4.13 guarantees that the critical values will be smooth. Numerical results are shown in figures 4.17–4.20.

Rotation has a stabilizing effect in convection. Because of this, it is expected that a larger $\hat{z}$ component, as on the north pole, would result in a higher critical Reynolds number, which would then decrease nearer the equator. In fact, the critical Reynolds number remains constant until about thirty degrees from either side of the equator, then decreases rapidly. The wave-number magnitude, roll angle, and frequency are fairly constant for middle to high latitudes.

4.4 Towards a Weakly Nonlinear Model

A multiple-scales analysis of this model is expected to lead to a set of coupled amplitude equations, along the lines of those derived in the previous chapter (though without the different X and Y dependence, as here Y is proportional to ϵ rather than $\sqrt{\epsilon}$). Since there is a Hopf bifurcation, the solution is a pair of waves traveling in opposite directions, giving two complex amplitudes, $A(T)$ and $B(T)$. Amplitude

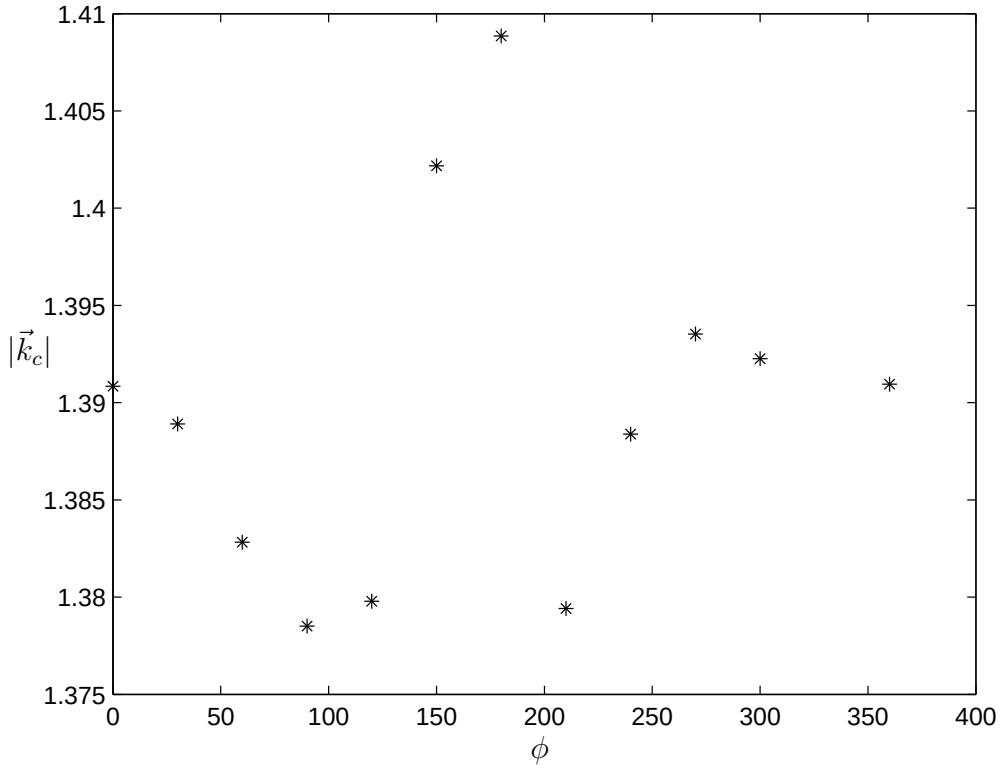

Figure 4.14: Critical wave number versus wind angle, ϕ, for $\psi = 45°$, Ra $= -8000$, and $U_s(0) = 11.6$.

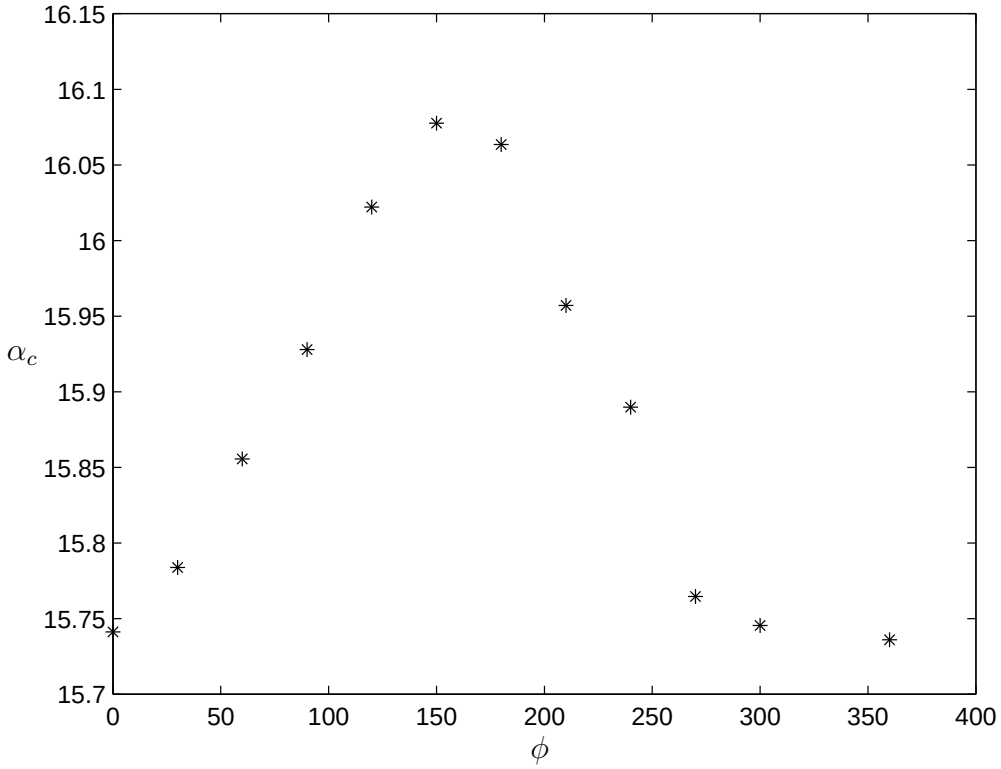

Figure 4.15: Critical angle α_c versus wind angle, ϕ, for $\psi = 45°$, Ra=-8000, with $U_s(0) = 11.6$.

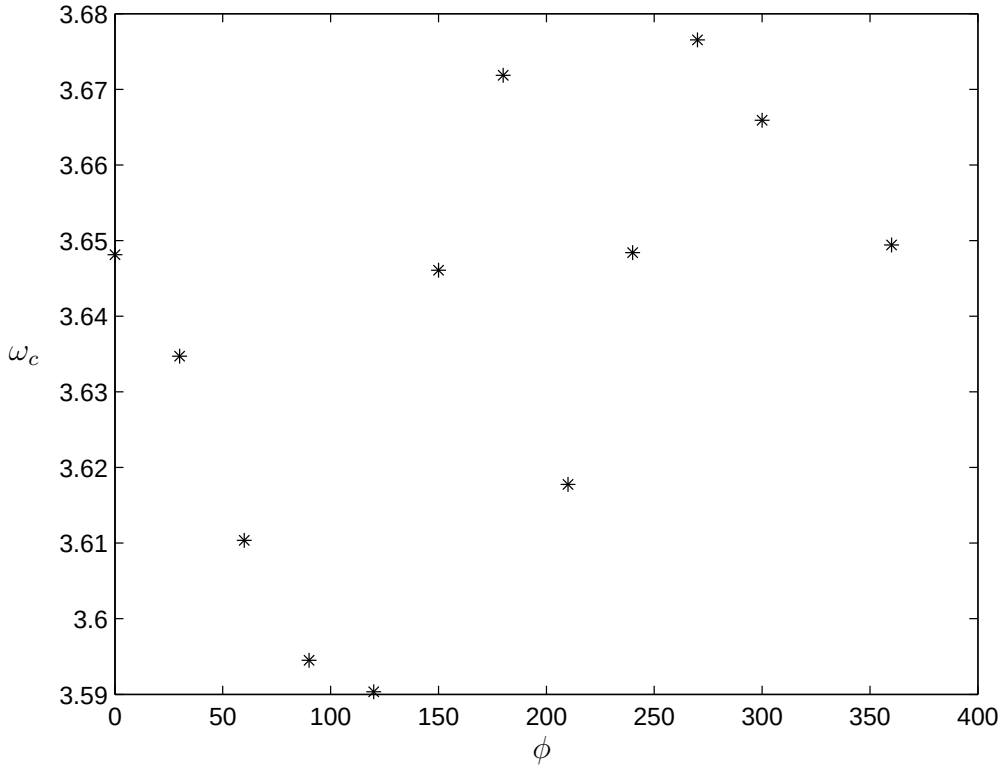

Figure 4.16: Critical frequency ω_c versus wind angle, ϕ, for $\psi = 45°$, Ra $= -8000$, with $U_s(0) = 11.6$.

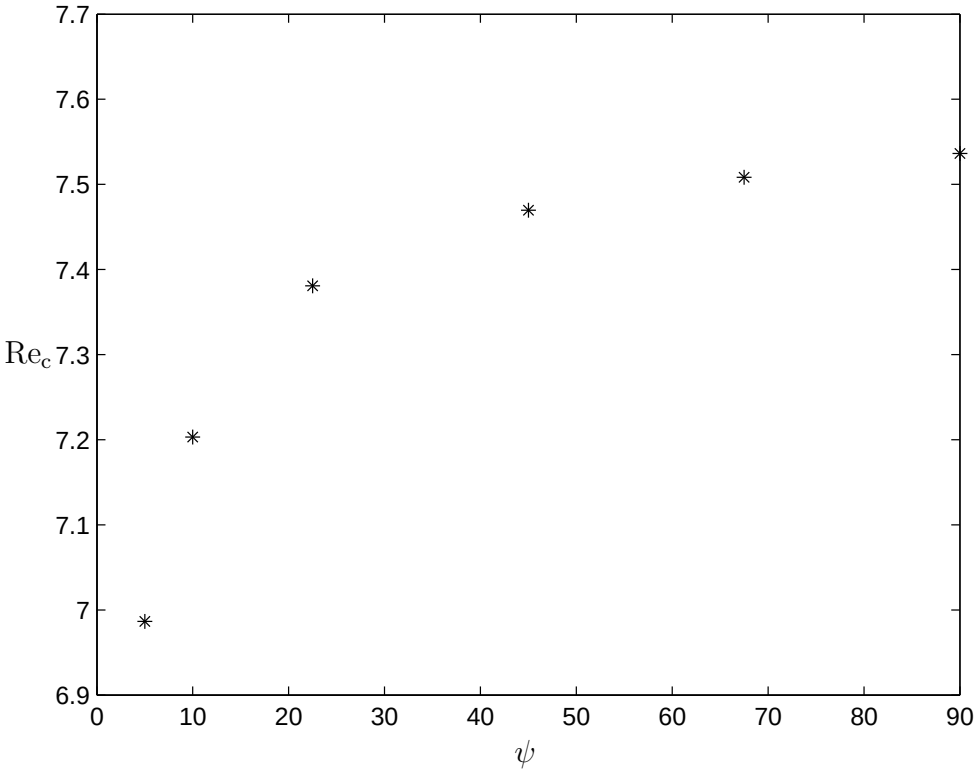

Figure 4.17: Critical Reynolds number versus latitude, ψ, for Ra $= -8000$, with $U_s(0) = 11.6$.

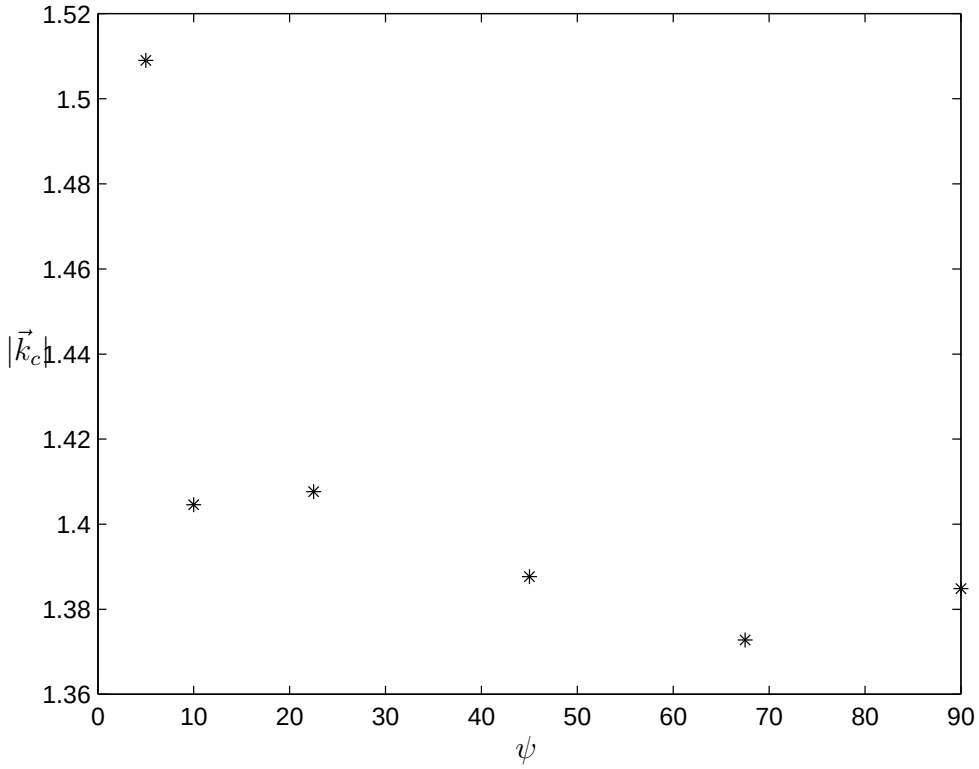

Figure 4.18: Wave-Number magnitude ($|\vec{k}_c|$) versus latitude, ψ, for Ra $= -8000$, with $U_s(0) = 11.6$.

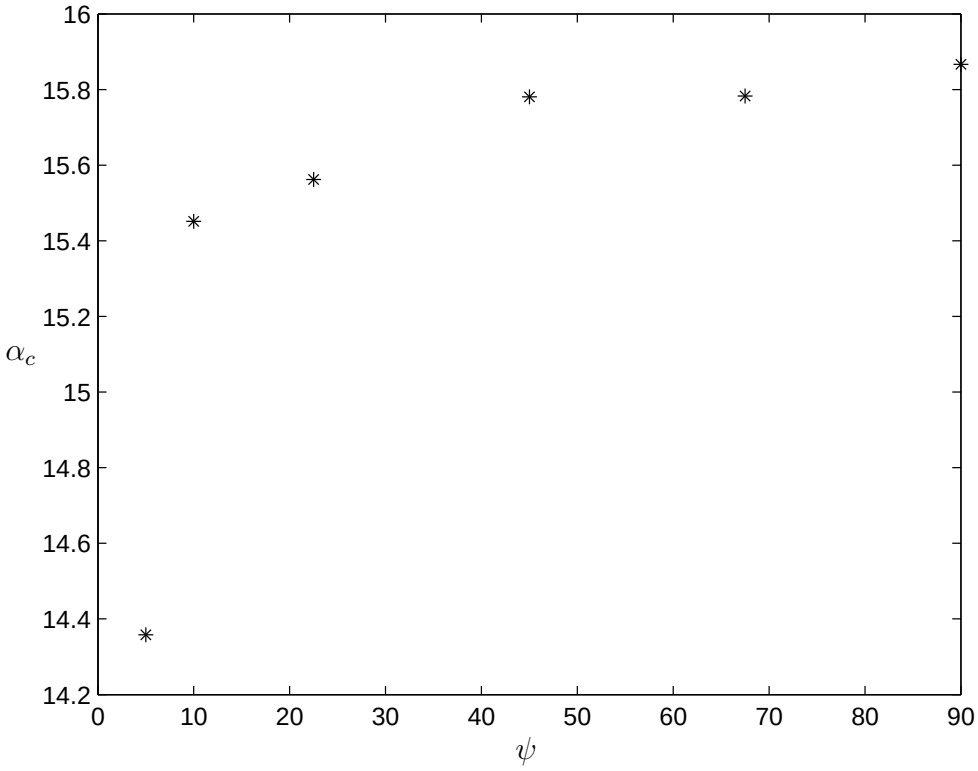

Figure 4.19: Critical angle versus latitude, ψ, for Ra $= -8000$, with $U_s(0) = 11.6$.

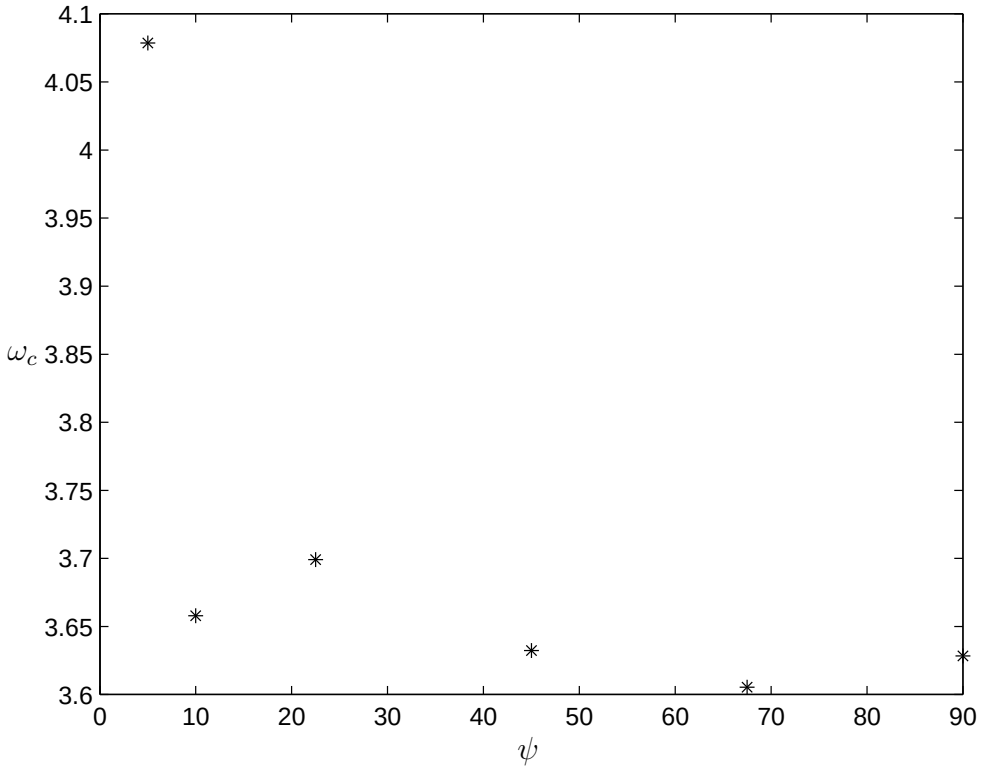

Figure 4.20: Frequency versus latitude, ψ, for Ra $= -8000$, with $U_s(0) = 11.6$.

equations for similar problems have been derived by Knobloch [40], Knobloch and de Luca [41] and Cox, Leibovich, Moroz, and Tandon [18], [19], and in chapter three of this dissertation.

The slow timescale T is equal to $\epsilon^2 t$. The first-order solutions are then rewritten as:

$$w_1 = w_{1a}(z)Ae^{i(\vec{k}_{ac}\cdot\vec{x}+\omega t)} + w_{1b}Be^{i(\vec{k}_{bc}\cdot\vec{x}-\omega t)} + c.c. \tag{4.26}$$

$$\theta_1 = \theta_{1a}(z)Ae^{i(\vec{k}_{ac}\cdot\vec{x}+\omega t)} + \theta_{1b}Be^{i(\vec{k}_{bc}\cdot\vec{x}-\omega t)} + c.c. \tag{4.27}$$

$$\zeta_1 = \theta_{1a}(z)Ae^{i(\vec{k}_{ac}\cdot\vec{x}+\omega t)} + \zeta_{1b}Be^{i(\vec{k}_{bc}\cdot\vec{x}-\omega t)} + c.c. \tag{4.28}$$

The A-solutions were presented this chapter. The parts corresponding to the new amplitude B are also solutions to the linear problem, but are associated with a different eigenvalue, $-i\omega$, and have different values. In a paper examining Langmuir circulations with a Hopf bifurcation, Cox et al. [18] utilized the O(2) symmetry of their problem to show that the B-solutions are the complex conjugates (or negative complex conjugate, in the case of their stream function ψ) of the A-solutions. This simplifies the problem greatly, and results in a system of amplitude equations, one of which is the complex conjugate of the other. Similar symmetry relations also hold for rotating convection (chapter three) and double-diffusive convection ([40] and [41]). This symmetry is broken by the presence of two components of the basic flow, U and V, and the resulting Landau equations could have entirely different coefficients. Because of this, the left and right travelling waves are not related, and the growth rate for a wave-number vector $\vec{k}$ need not be the same as that for its negative.

4.5 Conclusion

The model of Langmuir circulation presented in this chapter is related to the model of rotating convection presented in chapters two and three, but uses a different nondimensionalization and incorporates the additional effect of wind shear. A linear analysis of the system of governing equations reveals some of the characteristics of the flow's stability. Critical Rayleigh numbers, generally between 4 and 10 for the parameters studied, suggest that physically realistic temperature stratification is never enough to completely inhibit the formation of Langmuir circulations for the wind speed investigated. Still, a higher degree of stable temperature stratification results in a higher critical Reynolds number. The magnitude of the wave-number is between 1.4 and 1.5 for Rayleigh numbers less than about -2000. Its angle varies between 15 and 19 degrees. Wind angle and latitude were found to have small effects on the critical values.

The next step in analyzing this model is to perform a perturbation analysis and derive the amplitude equations. Adding nonlinear effects to the analysis will allow an investigation of some of the patterns which form. As shown in the previous section, this analysis is quite complex due to the lack of symmetry in the problem. Following their derivation, the amplitude equations may be simulated and the results used to reconstruct the physical field.

CHAPTER 5

LANGMUIR CIRCULATION PATTERNS

5.1 Introductory Theory

In this chapter, I present a qualitative and conceptual approach to the issue of pattern formation due to Langmuir circulations with thermal effects, rather than following the direct computational approach Haeusser [30] takes. The amplitude is assumed to be governed by a Landau equation,

$$\frac{\partial A}{\partial T} = \sigma A - \lambda |A|^2 A \tag{5.1}$$

which allows its magnitude to be computed in a simplified way. When the motion is at a steady state ($\frac{\partial A}{\partial T} = 0$, with $A \neq 0$) taking the real part and solving for $|A|^2$ yields

$$|A|^2 = \frac{\sigma_r}{\lambda_r} = \frac{c_\sigma \epsilon}{\lambda_r} \tag{5.2}$$

with the growth rate σ_r rewritten as $c_\sigma \epsilon$, where $\epsilon = \sqrt{\frac{\mathrm{Re}-\mathrm{Re}_c}{\mathrm{Re}_c}}$.

The Landau coefficient, λ, for the system with thermal effects is expected to be similar to the value computed by Haeusser, because I have shown that temperature variations (i.e., varying the Rayleigh number) produce only small changes in the critical values. Furthermore, Haeusser showed that varying the Stokes drift resulted in little change in the Landau coefficient within the range of interest [30, p.76]. Therefore I simply use Haeusser's value of $\lambda = 1.31(1+i)$, computed for $U_s(0) = 5$, although I have used $U_s(0) = 11.6$. The complex growth rate, σ, is computed according to the methods outlined in appendix C.2. At $\mathrm{Re} = 1.5\mathrm{Re}_c$ and $\mathrm{Ra} = -8000$, the complex growth rate is found to be $1.20 + 0.70i$.

When the system is supercritical, a band of wave-numbers centered around the critical wave-number $\vec{k}_c$ contribute to the flow. When several wave-numbers in

Table 5.1: Approximate values used in the modal analysis. The physical parameters are Pr = 1, Ek = 1, Ra = −8000, $l = 0.2$, $U_s(0) = 11.6$, $\psi = 90°$ (latitude), and $\phi = 0°$ (wind direction).

Re	k_x	k_y	ω_j	ϵ_j	$\lvert A_j \rvert$	$\hat{w}_j(-1/2)$	$\hat{\theta}_j(-1/2)$
7.64	0.28	1.33	4.37	0.69	0.66	0.00-0.07i	-0.01-0.04i
7.54	0.36	1.23	3.29	0.71	0.68	-0.06-0.11i	-0.04-0.08i
7.56	0.36	1.43	4.22	0.71	0.67	-0.03-0.06i	-0.03-0.04i
7.62	0.44	1.25	2.84	0.70	0.67	-0.19-0.03i	-0.12-0.06i
7.56	0.44	1.41	3.56	0.70	0.67	-0.08-0.05i	-0.05-0.04i

this band are superimposed, the result is a system that is periodic in neither space nor time. The Landau coefficient determines the amplitude and weakly modified frequency of each mode in the band. Each excited mode is at an angle to the critical mode, and its critical frequency differ slightly from that of the critical mode. Ignoring their mutual interactions, several modes can be superimposed to create a perturbation of the equilibrated most unstable mode by all the others in the collection. I choose five values of $\vec{k}$ which lie on a circle of wave-numbers centered on the critical wave-number $k_c = (0.38, 1.33)$ and compute the resulting A_j and ϵ_j for each mode. These values are shown in table 5.1. The values in the table are approximate and the patterns are sensitive to small changes in these values.

Equation 5.3 can be set up for each mode considered, giving the various amplitudes

$$|A_j|^2 = \frac{\sigma_{rj}}{\lambda_r} = \frac{c_\sigma \epsilon_j}{\lambda_r} \tag{5.3}$$

where $\epsilon_j = \sqrt{\frac{\mathrm{Re}-\mathrm{Re}_j}{\mathrm{Re}_j}}$ and $(\vec{k}_j, \mathrm{Re}_j)$ is on the neutral. This is not numerically accurate, but the resulting pattern looks similar to a spatially modulated system

and is of interest because it displays some qualitative features of the Langmuir circulation patterns.

Superimposing these modes and reconstructing the physical field yields the perturbation velocity and temperature distributions

$$w(\vec{x},t) = \sum_{j=1}^{5} |A_j| \hat{w}_j(z) e^{i\vec{k}_j \cdot \vec{x} + i\omega_j t} \tag{5.4}$$

$$\theta(\vec{x},t) = \sum_{j=1}^{5} |A_j| \hat{\theta}_j(z) e^{i\vec{k}_j \cdot \vec{x} + i\omega_j t} \tag{5.5}$$

where $\hat{w}$ and $\hat{\theta}$ are the solutions to the linearized problem, as discussed in the previous chapter, for the given wave-vector and its associated Reynolds number.

5.2 Results and Conclusions

Figures 5.1 through 5.3 show the sign of the resulting physical fields (the real parts of the temperature perturbation) for three different times. Positive values are in black and negative values are in white. Zeros are shown in red. The rolls are slanted to the right of the surface stress, as expected. Haeusser's rolls are also deflected to the right [30], the result of the Coriolis force, as discussed in the previous chapter. Values of the real (solid line) and imaginary (broken line) parts of the temperature perturbation at $t = 1000$ at selected locations are shown in figures 5.4 and 5.5.

Two interesting features of the temperature field are defects and Y-junctions. As suggested by Haeusser [30, p.84], these two may be related. Defects are localized points at which the magnitude of the amplitude $|A|$ is zero. As a result of this, a roll either appears or disappears. Haeusser assigned each defect a positive or negative charge based on the sign of A's phase change. Each of his simulations has a net charge of zero, an outcome of his assumption that the initial-value problem is

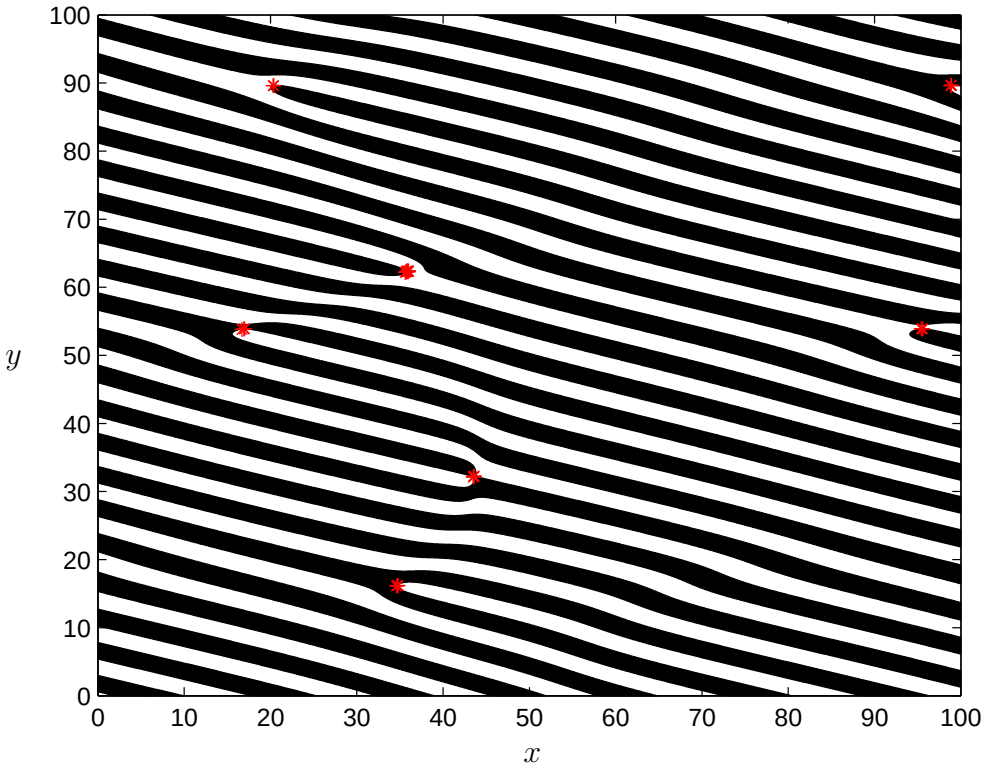

Figure 5.1: Contour plot of Real(θ) at $z = -1/2$ and $t = 0$. The minimum value is -0.26 and the maximum is 0.26, corresponding to dimensional temperature perturbations of between -0.17°C and 0.17°C when ΔT is 0.8°C.

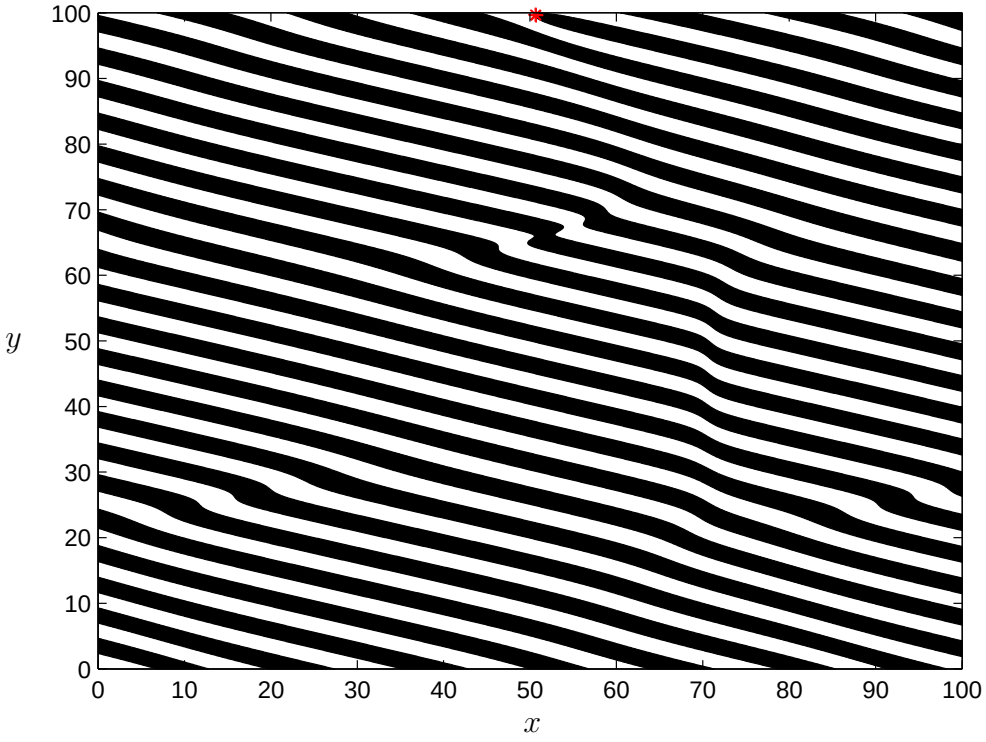

Figure 5.2: Contour plot of Real(θ) at $z = -1/2$ and $t = 500$. The minimum value is -0.23 and the maximum is 0.23, corresponding to dimensional temperature perturbations of between -0.18°C and 0.18°C when ΔT is 0.8°C.

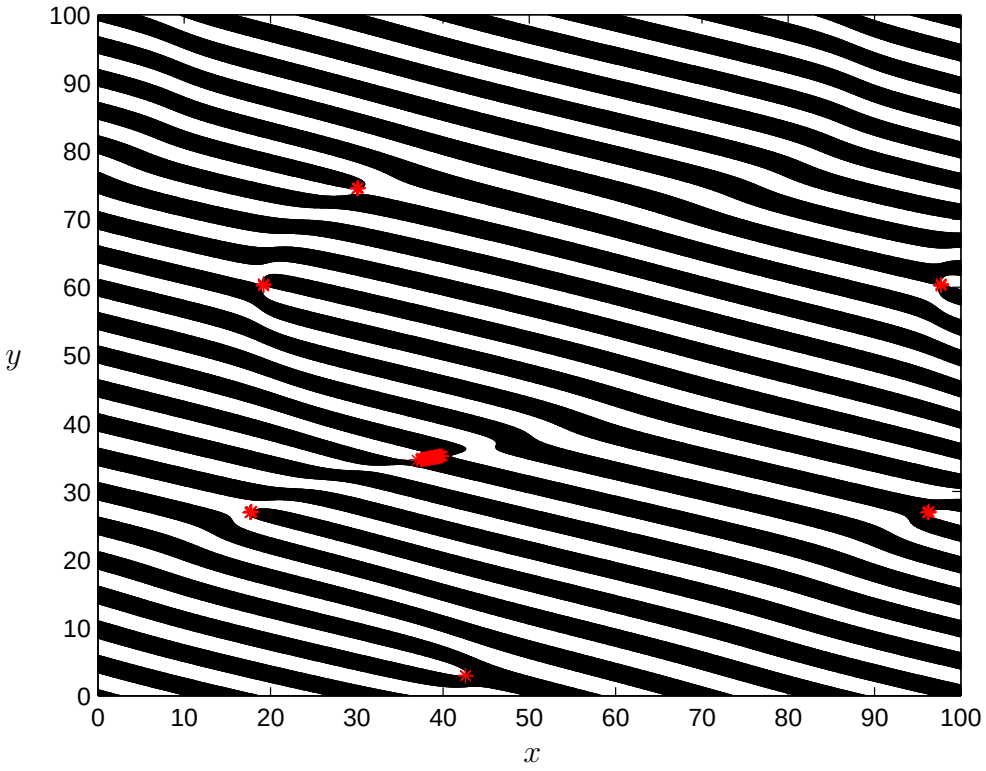

Figure 5.3: Contour plot of Real(θ) at $z = -1/2$ and $t = 1000$. The minimum value is -0.25 and the maximum is 0.25, corresponding to dimensional temperature perturbations of between -0.20°C and 0.20°C when ΔT is 0.8°C.

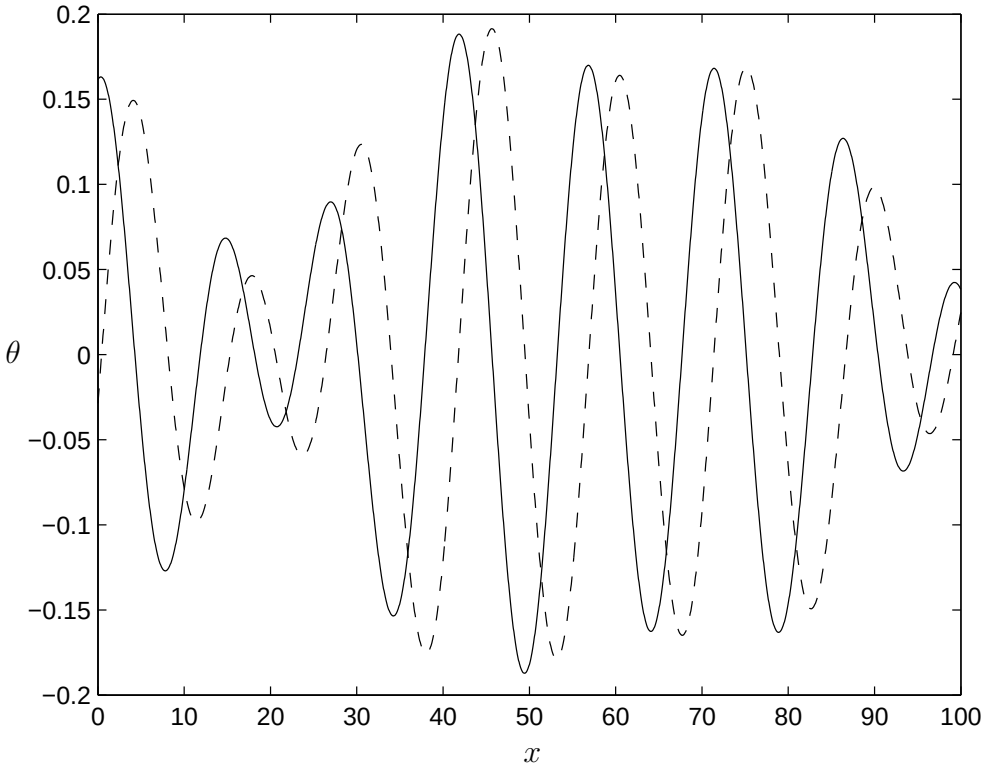

Figure 5.4: The dimensionless temperature perturbation $\theta(x, 50)$ at $t = 1000$: real part (solid line) and imaginary part (broken line).

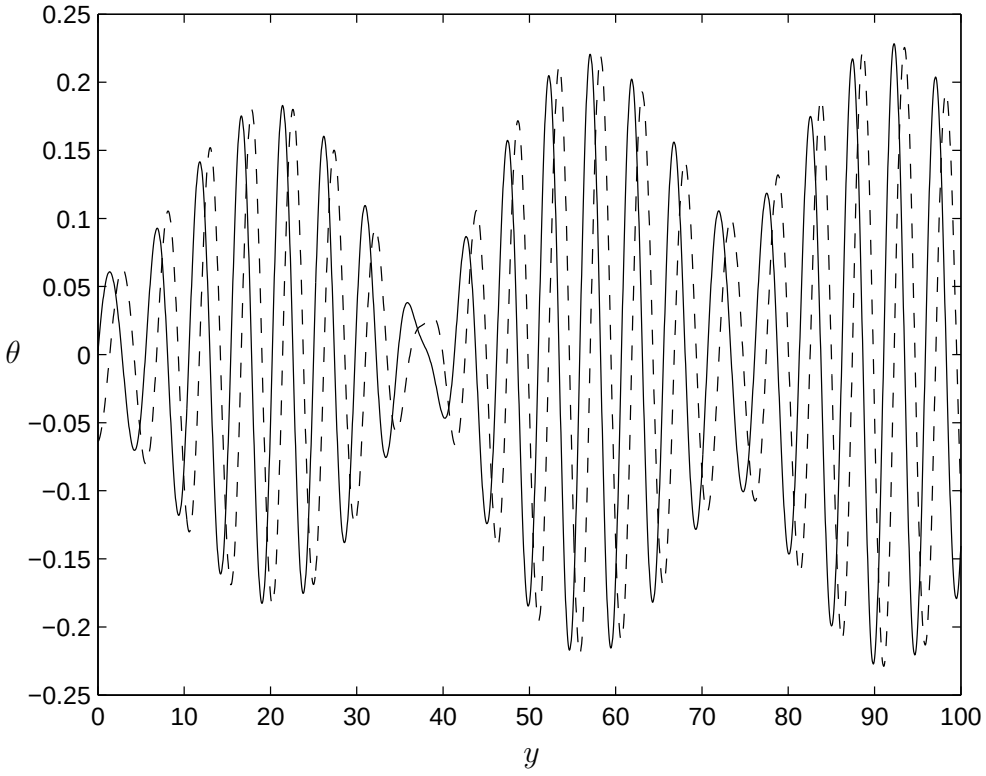

Figure 5.5: The dimensionless temperature perturbation $\theta(50, y)$ at $t = 1000$: real part (solid line) and imaginary part (broken line).

spatially periodic. Since the results presented in this chapter do not come from an initial value problem, the net charge need not, and does not, vanish. Since I have not computed the spatial dependence of A, I can not look at defects in exactly the same way as Haeusser did. Instead, I search for places where magnitude of the physical field is zero. These places are marked with red dots in the figures.

Y-junctions, places where the surface pattern looks like a Y because two rolls join and a third ends, were observed in the field by Farmer and Li [28]. Haeusser hypothesizes; this that each defect corresponds to a Y-junction, with the defect charge determining the junction's direction. However, Y-junctions appear more frequently with a downwind orientation, a result not explained by Haeusser's theory. Bhaskaran and Leibovich [5] find that Lagrangian effects cause Y-junctions to form at negative defects, but not positive defects, in a field with zero net defect charge, accounting for the preference observed by Farmer and Li.

The connection between Y-junctions and defects is something that could use further investigation. While these two features often coincide (Haeusser writes, "In the physical field, the defects manifest themselves as places at which a roll ends," i.e., Y-junctions [30, p.82].) Bhaskaran and Leibovich show that, while every Y-junction forms at a defect, not all defects result in Y-junctions. In my analysis, Y-junctions form at places where the temperature perturbation is zero, which could be caused by a defect, $|A| = 0$, or by having $\hat{\theta}(z) = 0$. It would be particularly interesting to investigate the relationship between these two features with a model that does not require a net defect charge of zero.

CHAPTER 6

DISCUSSION AND CONCLUSIONS

This dissertation has been concerned with two related problems: rotating convection and Langmuir circulation. These problems are physically similar in that both appear as stripes on the surface of a body of water, which are signs of counter-rotating vortices underneath. The physical similarity of these two phenomena means that they can e modelled using similar sets of governing equations, although the driving mechanisms differ: thermal convection is driven by surface cooling, while Langmuir circulation is driven by the wind.

Rotating thermal convection is a classical physics problem that can be modelled simply, yet has many applications and frequently appears in the natural world, particularly in atmospheric dynamics. The earth's movement supplies the rotation, and buoyancy differences in the atmosphere or ocean can result in convection. While buoyancy is usually due to thermal expansion, other density differences could be responsible. Because of its broad applicability, convection, both ordinary and rotating, has seen a great deal of interest in the years since Bénard's first experiments in 1898, done as a part of his doctoral work in France [69]. Chandrasekhar's classic book [11] contains a thorough treatment of the linearized problems for both ordinary and rotating convection, and lays the groundwork for future research. Despite the large amount of work done on rotating convection, the system is not yet fully understood. Experiments have revealed instabilities that haven't yet been explained theoretically. Theoretical analyses show features that have not been observed experimentally. The study of the effects of sidewalls, the main cause of discrepancies between theory and experiment, is still in progress.

Landau first proposed using an amplitude equation because "the very essence of this phenomenon [turbulence] is still lacking sufficient clearness...the problem

may appear in a new light if the process of initiation of turbulence is examined thoroughally" [43]. Amplitude equations are of interest because they yield information about the patterns that form in a system slightly above critical, allowing some of the difficult questions arising from experimental results — how to explain particular patterns — to be approached theoretically. These equations arise from a solvability condition, which means that satisfying them is necessary for the physical system to be accurately represented

Two different types of boundary conditions, rigid and stress-free, were treated for systems that undergo a stationary bifurcation, and free boundaries were treated analytically for the Hopf bifurcation case. Although free boundaries are not physically realistic, they are helpful in that they allow the problem to be solved analytically. This provided a way to check the results of the numerical analysis as well as analytic results.

I used the method of multiple scales to derive the amplitude equations, presenting results at each order. The amplitude equations for the general case are:

$$\left(\epsilon\frac{\partial}{\partial T}+\frac{\partial}{\partial \tau}\right)A - v_g\left(\frac{\partial}{\partial X}+\frac{1}{2ik_c}\frac{\partial^2}{\partial Y^2}\right)A$$
$$=\epsilon\sigma A-\epsilon\lambda_a|A|^2A-\epsilon\lambda_b|B|^2A+\epsilon\delta\left(\frac{\partial}{\partial X}+\frac{1}{2ik_c}\frac{\partial^2}{\partial Y^2}\right)^2A+\epsilon\frac{v_g}{2ik_c}\frac{\partial^2 A}{\partial X^2}-i\epsilon k_cAU \tag{6.1}$$

$$\left(\epsilon\frac{\partial}{\partial T}+\frac{\partial}{\partial \tau}\right)B + v_g\left(\frac{\partial}{\partial X}+\frac{1}{2ik_c}\frac{\partial^2}{\partial Y^2}\right)B$$
$$=\epsilon\sigma^* B-\epsilon\lambda_b^*|A|^2B-\epsilon\lambda_a^*|B|^2B+\epsilon\delta^*\left(\frac{\partial}{\partial X}+\frac{1}{2ik_c}\frac{\partial^2}{\partial Y^2}\right)^2B+\epsilon\frac{v_g}{2ik_c}\frac{\partial^2 B}{\partial X^2}-i\epsilon k_cBU \tag{6.2}$$

$$\mathrm{Pr}\frac{\partial^3 U}{\partial Y^3}=\frac{\partial}{\partial Y}\left(A^*\left(\Gamma_{ax}\frac{\partial}{\partial X}+\Gamma_{ay}\frac{\partial^2}{\partial Y^2}\right)A\right)$$
$$+\frac{\partial}{\partial Y}\left(B^*\left(\Gamma_{bx}\frac{\partial}{\partial X}+\Gamma_{by}\frac{\partial^2}{\partial Y^2}\right)B\right)+c.c. \tag{6.3}$$

In the case of a stationary bifurcation, the amplitude equations simplify. The amplitude of the second travelling wave, B, drops out because when $\omega = 0$, the two waves are equivalent. Numerical values of the coefficients are shown in Appendices D (rigid boundaries, stationary bifurcation) and E (free boundaries, Hopf bifurcation). Analytic coefficients for the case of a stationary bifurcation with free boundaries are given in section 2.8.1.

In the case of a Hopf bifurcation, there is an additional complication because the group velocity, which arises as a part of the solvability condition at second order, is nonzero. This leads to an amplitude equation at second order which must be satisfied for the perturbation expansion to remain asymptotic. The X-dependence of this equation may be removed using a change of variables, but the Y-dependence can not. As a result, the allowable solutions are restricted to traveling waves with a fixed but arbitrary wave-number in the Y-direction.

Reconstructing the velocity field from the perturbation expansion results and simulations of the amplitude equations ought to give results which are quantitatively as well as qualitatively correct. Knowing the coefficients which are relevant to rotating convection may also help those studying the Ginzburg-Landau equation by allowing them to access a physical system that corresponds to their theoretical interests. For example, van Hecke and van Saarloos [32] starts with a pair of coupled Ginzburg-Landau equations, then shows that rotating convection is an example of a system which can be used to perform experiments for a new parameter regime. Their interest is primarily in the equations, not in rotating convection, but experimental rotating convection allows them to understand the equations better.

The simplest nontrivial solution to the amplitude equations is a type of wave derived by Stokes [64] and bearing his name. When the amplitudes A and B are Stokes waves, the physical field is modulated over the slow spatial and temporal

scales. A stability analysis of these solutions to the amplitude equations was carried out, with the mean drift U set to zero (Sections 2.10 and 3.9). This resulted in criteria for their stability. The stability of a wave depends on its wave-number $\vec{Q}$ as well as the perturbation wave-number $\vec{\kappa}$. The Prandtl number was found to be important in determining the stability of the traveling and standing wave solutions in systems that undergo Hopf bifurcations.

The mean drift, which was assumed to be zero in the stability analysis, is actually quite important and theoretically difficult to handle. This horizontal mean drift is allowed because the horizontal velocities are defined in terms of fast derivatives, and therefore a constant can be added to them. It is necessary to describe the vertical vorticity produced by the curvature of the rolls. The x-component, U, occurs at second order and appears in the amplitude equations. The y-component, V, is higher-order and does not contribute to the final equation system.

In the experiments of Hu, Ecke, and Ahlers [33], [34], the mean drift is found to be connected to instability. In the first set of experiments, [33], the authors observe a new instability in which focus patterns nucleate new rolls, which appear as waves travelling outwards. They believe that this new instability is caused by the mean drift, which is in turn caused by the combined effects of roll curvature and defects. If the combination of roll curvature and wave number does not balance the mean drift, they find that the wave number moves into the unstable range. In further experiments [34], the authors find that the mean drift, while difficult to measure, is very important in determining the pattern dynamics.

The system of amplitude equations derived in this dissertation should be usable as a basis for future investigation into pattern formation in rotating convection. Still, the mean drift remains problematic, especially in the case of rigid boundaries,

where its dependence on depth could influence the patterns formed in convection. Scheel [60] uses the full set of governing equations for rotating convection with rigid boundaries to incorporate the mean flow from the beginning. Both experiments and theory in this area would be excellent additions to the study of rotating convection.

Another way to extend this work is to simulate the system of amplitude equations. Simulations of this particular system are difficult to perform; I tried using Comsol Multiphysics. Once they have been done, the results of these simulations will allow the velocity vector and temperature field to be reconstructed, providing quantitative information about the patterns formed and the state of the mixed layer. This information could then be compared to experimental results and used to better understand environmental systems.

Convection is an important physical process in its own right because of its industrial applications (i.e., the Czochralsky crystal growing process [37]) and appearance in many natural systems. Its simplicity also allows it to serve as a model pattern-forming system. Rotating convection has many of the features desired for a model of Langmuir circulation that incorporates thermal effects, and the mathematical model can be adjusted to account for the additional physical quantities important for Langmuir circulation.

To begin with, some generalizations are made in the model for rotating convection. Since the symmetry present in rotating convection is now broken by the wind shear, the coordinate system can no longer be aligned so that $\vec{k}$ is along the x-axis, and both components must be included. The horizontal components of the angular velocity vector $\vec{\Omega}$ are also included, making it possible to adjust the direction of the axis of rotation and compute results for a layer of water at any latitude. Only the northern hemisphere is considered, because results for the

southern hemisphere can be computed using a coordinate transformation.

The substantial changes that are necessary to transfer the mathematical model from rotating convection to Langmuir circulation are primarily in the addition of new terms. Terms representing the basic flow and Stokes drift must be added in order to describe the shear stress applied by the wind and the resulting surface waves. In the new system, it is convenient to nondimensionalize the governing equations differently. The critical parameter is changed from the Rayleigh number to the Reynolds number, because the Rayleigh number is determined by environmental parameters and the factor that determines whether Langmuir circulations form is the wind speed. The Ekman number is used as a dimensionless measure of the rotation rate.

As a mixing process in the surface layer of the ocean, Langmuir circulation is responsible for transferring gases between the atmosphere and ocean. One such gas is carbon dioxide, whose presence in the atmosphere causes long-wave radiation to be trapped, resulting in the greenhouse effect. This heats up the troposphere, enhancing oceanic surface heating. It is notable that there is no naturally-occurring amount of thermal stratification large enough to prohibit the formation of Langmuir circulations in the parameter regime investigated, although stable temperature gradients do increase the critical Reynolds number somewhat. When surface heating inhibits mixing, less carbon dioxide is transferred into the ocean, leading to a positive feedback loop and potentially reducing gas transfer.

One question that comes out of this is how much gas is transferred between the atmosphere and ocean by Langmuir circulation. Presumably the strength of the circulation is important here, with stronger circulations resulting in more gas transfer. Without defining a metric for circulation strength, it is difficult to tell exactly how this works, yet the wave-number magnitude may be important. Both

the wave-number magnitude and the roll angle were found to decrease with the Rayleigh number. Without further investigation, the implication of this change for atmosphere-ocean transfer is unclear, but it is clear that surface heating plays a role in the patterns formed.

While important parts of the problem, the latitude and wind direction are unrelated to the temperature perturbation, and changing them is not expected to change the system in new ways now that thermal effects are included. The wind direction was found to play a small role in the critical values. Langmuir circulations are generally aligned at an angle to the right of the wind in the northern hemisphere, which is to be expected when the Coriolis force is included. Latitude variation was found to have small effects on the critical values in the high mid-latitudes. However, at low latitudes the vertical component of the angular velocity vector disappears, making the physics slightly different. Numerical results in this range were found to be more difficult to obtain, and this region is not treated in detail here. A detailed analysis of Langmuir circulation formation, with or without thermal effects, near the equator may reveal some interesting phenomena because of this.

In general, the results are not surprising. It is to be expected that stable stratification makes it more difficult for Langmuir circulations to form, which is exactly what the results show. One feature left unexplained is the oscillation in the critical frequency (figure 4.9) and wave-number magnitude (figure 4.10) for large negative Rayleigh numbers. These oscillations are not apparent in the results for the roll angle α_c (figure 4.11) and phase velocity (figure 4.12), suggesting that the latter may be the physically important quantities.

Extending the analysis to higher orders follows slightly different path than rotating convection did because of the lack of symmetry in this problem: the

horizontal directions do have different scales. The eigenvalue corresponding to the second wave is the complex conjugate of the first one, but its wave-vector is independent and the growth rate is different. As a result, only the traveling wave solution with the larger growth rate need be examined. Haeusser's [30] amplitude equation derivation for the problem without thermal effects considers one of the two traveling waves resulting from the Hopf bifurcation. It would be interesting to see how the amplitude equations and the dynamics described by them change when both waves are taken into account.

Once the amplitude equations have been derived, they may be simulated and the results used to reconstruct the velocity vector and temperature field from their parts at each order. This is expected to yield results that are comparable to observations. The resulting temperature field could then be compared to the temperature fields shown in infrared photographs of Langmuir circulations on the ocean's surface, allowing the velocity field, and possibly other properties of the mixed layer, to be computed on the basis of the surface temperature distribution. A theoretical understanding of Langmuir circulation patterns might allow air-sea exchanges to be observed from space, which would be a useful tool for climate scientists.

One way to approach the pattern formation issues is the subject of chapter five. Instead of the full set of amplitude equations, a multi-modal analysis may be used to generate qualitatively correct results. Haeusser's [30] Landau coefficient is used to approximate the actual Landau coefficient, which is not expected to be far from Haeusser's result because, as shown in chapter four, changes in the Rayleigh number do not significantly change the linear results, and, as Haeusser shows, the critical parameters do not depend heavily on the Stokes drift. The actual growth rate is computed using the linearized system. These numbers provide sufficient

information for the computation of several unstable modes near critical, which are then superimposed to produce physical values of the temperature perturbation. The result is a series of stripes at an angle to the wind, as expected.

The temperature perturbation shows a downwind bias in the orientation of Y-junctions, in agreement with the observations of Farmer and Li [28] and the calculations of Bhaskaran and Leibovich [5]. Defects can not be localized without the full amplitude equations, however, each Y-junction corresponds to a perturbation temperature of zero. This zero may be due to a defect, or to other factors.

The link between defects and Y-junctions is of particular interest because it connects the theoretical amplitude equations with reality. However, it seems that this connection is not one-to-one; other factors, including the Lagrangian effects described by Bhaskaran and Leibovich, become important in determining whether or not a Y-junction forms at a defect. These other effects clearly influence the patterns formed, and point out a weakness in the ad hoc amplitude equation model of chapter five. The multi-mode model presented here does not treat defects the way that amplitude equations do (requiring that there be an equal number of positively and negatively charged defects), and the correspondence between zeros — the closest thing to defects appearing in this analysis — and Y-junctions is one-to-one, although the identification of Y-junctions remains subjective. Both Y-junctions and defects are important contributers to the patterns formed, and their connection remains an area for exploration.

The patterns formed by Langmuir circulations are similar to those formed by rotating convection, a simple pattern-forming system that can be used to model more complex systems. Physically, Langmuir circulation and rotating convection are linked by the two factors that relate them to geophysical phenomena, rotation and stratification, and by their importance in the environment. Convection occurs

as a mixing process in the atmosphere, ocean, and mantle, and Langmuir circulation is an important mixing process in the oceanic mixed layer. By studying these problems, it is possible to better understand how the fluid parts of the earth system interact, which should eventually lead to a better understanding of climate change.

APPENDIX A

SECULAR TERMS AT SECOND ORDER IN ROTATING CONVECTION

The third part of the right hand side of 2.29, which is proportional to $e^{ik_c x}$, could cause resonance in the form of a secular term at second order. In this section I show that this term does not exist, which is equivalent to saying that there is no slow timescale T_1 at order ϵ. For this to be true, the coefficient $\digamma$ in the equation $\frac{\partial A}{\partial T_1} = \digamma \nabla_\xi^2 A$ must be zero.

Following Newell and Whitehead's example for ordinary convection [53], I rewrite the system of equations in a self-adjoint form:

1. Apply the operator $\frac{\partial}{\partial t} - \nabla^2$ to the double curl equation, giving (for the linear problem — the nonlinear terms are unnecessary in this analysis because they produce no slow-derivative terms at second order).

$$\left(\frac{\partial}{\partial t} - \nabla^2\right)\left(\frac{\partial}{\partial t} - \mathrm{Pr}\nabla^2\right)\nabla^2 w + \left(\frac{\partial}{\partial t} - \nabla^2\right)\left(\mathrm{Pr}\mathcal{T}\frac{\partial \zeta}{\partial z} - \mathrm{PrRa}_c\nabla_h^2\theta\right) = 0 \tag{A.1}$$

2. Use the θ equation, $\frac{\partial \theta}{\partial t} - \nabla^2\theta - w = 0$, to eliminate θ, giving

$$\left(\frac{\partial}{\partial t} - \nabla^2\right)\left(\frac{\partial}{\partial t} - \mathrm{Pr}\nabla^2\right)\nabla^2 w + \mathrm{Pr}\mathcal{T}\left(\frac{\partial}{\partial t} - \nabla^2\right)\frac{\partial \zeta}{\partial z} - \mathrm{PrRa}_c\nabla_h^2 w = 0 \tag{A.2}$$

3. Assuming a stationary bifurcation, this equation becomes

$$\nabla^6 w - \mathcal{T}\nabla^2\frac{\partial \zeta}{\partial z} - \mathrm{Ra}_c\nabla_h^2 w = 0 \tag{A.3}$$

4. Apply $-\nabla^2$ to the ζ-equation, $-\mathrm{Pr}\nabla^2\zeta - \mathrm{Pr}\mathcal{T}w' = 0$, for a stationary bifurcation, giving

$$\nabla^4\zeta + \mathcal{T}\nabla^2\frac{\partial w}{\partial z} = 0 \tag{A.4}$$

5. The resulting system is

$$\begin{pmatrix} \nabla^6 - \mathrm{Ra}_c \nabla_h^2 & -\mathcal{T}\nabla^2 \frac{\partial}{\partial z} \\ \mathcal{T}\nabla^2 \frac{\partial}{\partial z} & \nabla^4 \end{pmatrix} \begin{pmatrix} w \\ \zeta \end{pmatrix} = \vec{0} \tag{A.5}$$

which is self-adjoint. The principle of exchange of stabilities holds: all eigenvalues are real because the bifurcation is assumed to be stationary.

The boundary conditions for this smaller system are:

$$w = w' = \zeta = \zeta'' = \mathcal{T}\zeta' - w'''' - 2k^2 w'' = 0 \tag{A.6}$$

for rigid boundaries or

$$w = w'' = \zeta' = w'''' = \zeta'' - k^2\zeta + \mathcal{T}w' = 0 \tag{A.7}$$

for stress-free boundaries.

The right hand side of the problem proportional to $\nabla_\xi^2 A$ is the second-order part of this operator, or

$$\begin{pmatrix} 3\nabla^4 - \mathrm{Ra}_c & -\mathcal{T}\frac{\partial}{\partial z} \\ \mathcal{T}\frac{\partial}{\partial z} & 2\nabla^2 \end{pmatrix} \nabla_\xi^2 \begin{pmatrix} w \\ \zeta \end{pmatrix} \tag{A.8}$$

Using the method of normal modes ($w_1 = A(\vec{X}, T)\hat{w}_1(z)e^{ik_c x}$, $\zeta_1 = A\hat{\zeta}_1 e^{ik_c x}$), I apply the solvability condition by dotting the right hand side with the adjoint eigenfunctions (which are w and ζ since the system is self-adjoint). After integrating with respect to x and y, I find (with $\nabla^2 = -k_c^2 + \frac{\partial^2}{\partial z^2}$)

$$\int_0^1 \left(\hat{w}_1(3\nabla^4 - \mathrm{Ra}_c)\hat{w}_1 - \mathcal{T}\hat{w}_1 \frac{\partial \hat{\zeta}_1}{\partial z} + \mathcal{T}\hat{\zeta}_1 \frac{\partial \hat{w}_1}{\partial z} + 2\hat{\zeta}_1 \nabla^2 \hat{\zeta}_1 \right) dz \tag{A.9}$$

which must equal zero for the order ϵ timescale to be neglected. I can use the vorticity equation and integration by parts to show that the last three terms cancel out. This leaves only

$$\int_0^1 \left(\hat{w}_1(3\nabla^4 - \mathrm{Ra}_c)\hat{w}_1\right) dz \tag{A.10}$$

For free boundaries this becomes $(3\nabla^4 - \mathrm{Ra}_c)w_1 = (3a_c^4 - \mathrm{Ra}_c) = 0$ using the fact that $\mathrm{Ra}_c = 3a_c^4$. Unfortunately, there is no such expression for rigid boundaries, and this derivation does not hold for the case of a Hopf bifurcation. Still, the timescale at order ϵ is not expected to contribute in these variations of the problem.

APPENDIX B

DETAILS OF THE DERIVATION OF THE MEAN DRIFT EQUATION FOR ROTATING CONVECTION

Here the mean drift equation for rotating convection with stress-free boundaries and a Hopf bifurcation, 3.63, is derived. The derivation for a stationary bifurcation, equation 2.57, is the same, requiring only that ω be set to zero.

The left hand side of the vorticity equation is:

$$\frac{\partial \zeta}{\partial t} - \mathrm{Pr}\nabla^2\zeta \tag{B.1}$$

which can be expanded to (at order $\epsilon^{7/2}$):

$$\frac{\partial \zeta_{3/2}}{\partial T} + \frac{\partial \zeta_{7/2}}{\partial t} - \mathrm{Pr}\left(\frac{\partial^2 \zeta_{3/2}}{\partial X^2} + \frac{\partial^2 \zeta_{5/2}}{\partial Y^2} + 2\frac{\partial^2 \zeta_{5/2}}{\partial X \partial x} + \frac{\partial^2 \zeta_{7/2}}{\partial z^2}\right) \tag{B.2}$$

This becomes $\mathrm{Pr}\frac{\partial^3 U}{\partial Y^3}$ after dropping all fast terms and fast derivatives, and recalling that $\zeta_{3/2}$ is zero. The time derivative in this equation is of higher order, and therefore is neglected in the final equation, although Zippelius and Siggia [73] elected to keep it. The slow part of the vorticity equation at order $\epsilon^{7/2}$ is

$$\mathrm{Pr}\frac{\partial^3 U}{\partial Y^3} = -(\vec{\nabla} \times (\vec{u} \cdot \vec{\nabla}\vec{u}))_{7/2} \cdot \hat{z} \tag{B.3}$$

The order $\epsilon^{7/2}$ parts of $(\vec{\nabla} \times (\vec{u} \cdot \vec{\nabla}\vec{u})) \cdot \hat{z}$ side that are proportional to e^0 are:

$$A^* \frac{\partial^3 A}{\partial Y^3}\left(-u'_{2ay} w^*_{1a} - u_{3/2ay} v^*_{1a}\right) + c.c. \tag{B.4}$$

$$\frac{\partial A^*}{\partial Y}\frac{\partial^2 A}{\partial Y^2}\left(-u'_{2ay} w^*_{1a} - u_{3/2ay} v^*_{1a} - u_{1a} v^*_{3/2ay} - u^*_{1a} v_{3/2ay}\right) + c.c. \tag{B.5}$$

$$\frac{\partial A^*}{\partial Y}\frac{\partial A}{\partial X}\left(-u'_{2ax} w^*_{1a} + v^{*'}_{3/2ay} w_{1a} - ik_c u_{1a} v^*_{3/2a} + v_{1a} v^*_{1a} + ik_c u^*_{3/2ay} v_{1a} - u_{1a} u^*_{1a}\right) + c.c. \tag{B.6}$$

$$A^* \frac{\partial^2 A}{\partial X \partial Y}\left(-u'_{2ax} w^*_{1a} + v^{*'}_{3/2ay} w_{1a} + ik_c u^*_{1a} v_{3/2a} + v_{1a} v^*_{1a} - ik_c u_{3/2a} v^*_{1a} - u_{1a} u^*_{1a}\right) + c.c. \tag{B.7}$$

$$B^* \frac{\partial^3 B}{\partial Y^3} \left(-u'_{2by} w^*_{1b} - u_{3/2by} v^*_{1b} \right) + c.c. \tag{B.8}$$

$$\frac{\partial B^*}{\partial Y} \frac{\partial^2 B}{\partial Y^2} \left(-u'_{2by} w^*_{1b} - u_{3/2by} v^*_{1b} - u_{1b} v^*_{3/2by} - u^*_{1b} v_{3/2by} \right) + c.c. \tag{B.9}$$

$$\frac{\partial B^*}{\partial Y} \frac{\partial B}{\partial X} \left(-u'_{2bx} w^*_{1b} + v^{*'}_{3/2by} w_{1b} - iku_{1b} v^*_{3/2b} + v_{1b} v^*_{1b} + iku^*_{3/2by} v_{1b} - u_{1b} u^*_{1b} \right) + c.c. \tag{B.10}$$

$$B^* \frac{\partial^2 B}{\partial X \partial Y} \left(-u'_{2bx} w^*_{1b} + v^{*'}_{3/2by} w_{1b} + iku^*_{1b} v_{3/2b} + v_{1b} v^*_{1b} - iku_{3/2b} v^*_{1b} - u_{1b} u^*_{1b} \right) + c.c. \tag{B.11}$$

where the functions u, v, and w are the velocity components with numerical subscripts referring to the order at which they appear and alphabetic subscripts referring to the amplitude (A or B) and derivative (none, X or Y) which they are associated with. For example, $u_{2ax} = \frac{\pi(i\omega + a_c^2)}{ik_c a_c^2 C} \cos \pi z$ is the coefficient of the $\frac{\partial A}{\partial X}$ term in u_2, without the exponential. Primes denote z-derivatives. The other important second-order velocity terms are:

$$u_{2bx} = \frac{\pi(-i\omega + a_c^2)}{ik_c a_c^2 C} \cos \pi z \tag{B.12}$$

$$u_{2ay} = -\frac{\pi(i\omega + a_c^2)}{k_c^2 a_c^2 C} \cos \pi z \tag{B.13}$$

$$u_{2by} = -\frac{\pi(-i\omega + a_c^2)}{k_c^2 a_c^2 C} \cos \pi z \tag{B.14}$$

Through careful algebra and the use of trigonometric identities, this right hand side can be simplified to equations 2.57 and 3.63. It is necessary to drop fast terms, retaining only those which are independent of z. For rigid boundaries, the form of this equation holds, but the numerical solutions for u must be used. This presents its own difficulties; it is impossible to confidently separate the part which is independent of depth for use in the second equation. Zippelius and Siggia [73] get around this difficulty by remarking that "the evaluation of the right-hand side should remain essentially unchanged except for some complicated functions of z, which we can eliminate by integration."

APPENDIX C

NUMERICAL METHODS

C.1 Linearized Problems

To solve the linearized problems in chapters two and four, I used Matlab's `bvp4c` function, described in detail in a paper by Shampine, Kierzenka, and Reichelt [62]. This function finds the relevant eigenvalues and their corresponding eigenfunctions, and can be incorporated into a loop to find the minimum of the neutral stability curve. `bvp4c` is a collocation method; it converts the differential equations into a set of nonlinear algebraic equations with the boundary conditions incorporated from the beginning.

A good initial guess must be provided because there are many different eigenvalues, which correspond to different eigenfunctions and points on the neutral stability curve. The critical values derived by Chandrasekhar [11] for rotating convection and by Haeusser [30] for Langmuir circulation and the simplest nontrivial initial guess for the eigenfunctions (setting each unknown and its derivative to one) gives satisfactory results for rotating convection and for Langmuir circulation when the Rayleigh number is small. For larger Rayleigh numbers, the results of the previous computation are used as the initial guess.

`bvp4c` seeks solutions with eigenvalues near a specified eigenvalue, given the critical wave-number and Rayleigh or Reynolds number. Matlab's `fminsearch` function, which finds the minimum of an unconstrained multivariable function, is used to maximize the eigenvalue's real part by varying the critical parameters. This solution is expected to have the same general shape as the previous solution, hence the use of the previous solution as the initial guess.

This finds one point on the neutral stability curve. To find the minimum of this

curve — the critical Rayleigh or Reynolds number — I use Matlab's `fminsearch` function again. This algorithm converges to the critical Rayleigh or Reynolds number relatively quickly when given a good initial guess. However, it does not converge as quickly to the critical wave number, and is even more slow to converge to the correct eigenvalue for a Hopf bifurcation. The frequency is particularly sensitive to small changes in Reynolds number, and making it necessary to find the critical Reynolds number at a higher accuracy to ensure that the frequency has converged.

Matlab's default tolerance of 10^{-4} proves sufficient for rotating convection, but needs to be refined for some points in the Langmuir circulation case. In these cases, I made a second pass with a lower tolerance (10^{-8}), with the result for each Rayleigh number in the first pass serving as an initial guess. Only every third Rayleigh number used in the first pass was also used in the second pass.

One weakness of this algorithm is that it can only find one eigenvalue at a time. Additional eigenvalues can be found by modifying the initial guess, but this requires a number of different initial guesses, and makes it impossible to be certain that all the eigenvalues were found. Therefore it is difficult to ensure that the desired eigenvalue is the one found by the algorithm. This may also affect the critical values found: if two eigenvalues with small real part are near each other, the algorithm may find one, but not the other. Continuation helps to minimize this problem.

Another weakness is the lack of speed. Because of the nested minimization, this code takes a long time to run. The need for a very good initial guess compounds this problem. For the Langmuir circulation problem only small steps between Rayleigh numbers may be taken. If the step is too large, the solution is likely to jump to a different eigenvalue, producing a higher critical Reynolds number.

C.2 Growth Rate

There are several ways to numerically compute the growth rate, σ. Two methods are used in this dissertation. One of these, which is used in chapter two, is to use the solvability condition, just as the other amplitude equation coefficients are computed. In chapter five another method, described here, is used.

I start with the critical values computed using the method in the previous section. Then I solve the linearized boundary value problem again, with a Reynolds number of $\mathrm{Re} = \mathrm{Re}_c + h$, where $h = 0.1$. The original eigenfunctions provide an initial guess, and no search is necessary because the parameters are fixed. This results in two eigenvalues, $i\omega_c$ and σ_2, which are the critical frequency and new eigenvalue, respectively. These values can be substituted into the first term of the Taylor series expansion of σ:

$$\sigma = \frac{\sigma_2 - i\omega}{h} (\mathrm{Re} - \mathrm{Re}_c) \tag{C.1}$$

The assumption that the eigenvalue grows linearly near the critical Reynolds number is implicitly made here, and figure C.1 confirms this.

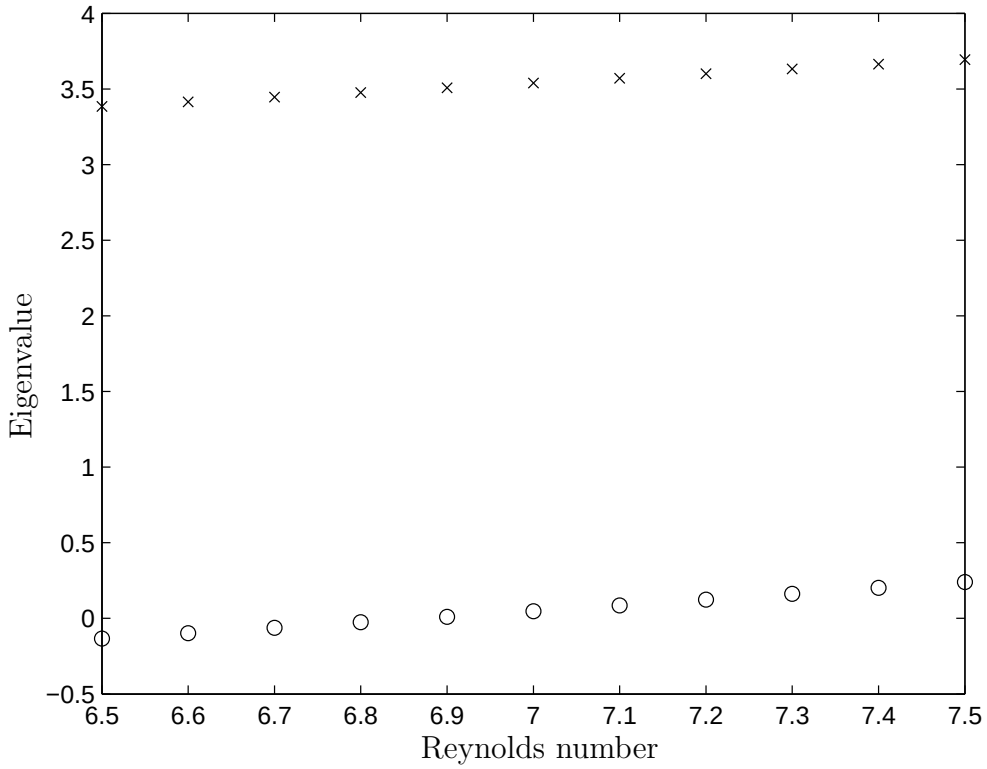

Figure C.1: Real (o) and imaginary (x) parts of the eigenvalue near the critical Reynolds number (6.87). The Rayleigh number is -5000 and the wave-number is at its critical value.

APPENDIX D

CRITICAL VALUES AND AMPLITUDE EQUATION COEFFICIENTS FOR ROTATING CONVECTION WITH RIGID BOUNDARIES

Table D.1: Amplitude equation coefficients for rotating convection with rigid boundaries and Pr = 1.

$\mathcal{T}$	Ra_c	k_c	$\frac{\sigma}{\alpha}$	$\frac{\lambda}{\alpha}$	$\frac{\delta}{\alpha}$	$\frac{\eta}{\alpha}$
3.16	1712.70	3.12	13.04	3.48	1.94	3.12
10.08	1757.10	3.16	13.36	3.57	1.95	3.16
17.00	1845.10	3.24	14.00	3.76	1.98	3.24
23.91	1971.70	3.34	14.90	4.03	2.00	3.34
30.83	2131.20	3.47	15.99	4.39	2.03	3.47
37.75	2318.30	3.61	17.22	4.81	2.06	3.61
44.66	2528.30	3.75	18.55	5.28	2.09	3.75
51.58	2749.80	3.86	19.83	5.73	2.12	3.86
58.50	3002.80	4.03	21.37	6.35	2.14	4.03
65.42	3261.90	4.16	22.80	6.92	2.17	4.16
72.33	3526.10	4.28	24.15	7.45	2.19	4.28
79.25	3807.70	4.42	25.64	8.10	2.20	4.42
86.17	4100.20	4.57	27.17	8.77	2.22	4.57
93.08	4401.50	4.70	28.64	9.41	2.23	4.70
100.00	4707.90	4.79	29.95	9.93	2.25	4.79

APPENDIX E

CRITICAL VALUES AND AMPLITUDE EQUATION COEFFICIENTS FOR ROTATING CONVECTION WITH A HOPF BIFURCATION AND FREE BOUNDARIES

Table E.1: Amplitude equation coefficients for rotating convection with a Hopf bifurcation and free boundaries.

Pr	$\mathcal{T}$	Ra_c	k_c	ω	v_g	σ	λ_a	λ_b	δ
0.025	25	1349.42	2.22	0.33	0.24	0.35-0.41i	88.04-8.08i	0.29-220.42i	0.08-0.09i
0.025	35	1350.88	2.23	0.59	0.19	0.35-0.24i	37.14-25.98i	0.29-124.43i	0.08-0.05i
0.025	45	1352.82	2.23	0.81	0.20	0.35-0.18i	21.11-23.77i	0.29-90.27i	0.08-0.04i
0.025	55	1355.25	2.23	1.03	0.21	0.35-0.15i	13.80-20.69i	0.29-71.69i	0.08-0.04i
0.025	65	1358.14	2.23	1.24	0.24	0.35-0.14i	9.82-18.11i	0.29-59.81i	0.08-0.03i
0.025	75	1361.51	2.24	1.44	0.26	0.36-0.13i	7.39-16.06i	0.30-51.50i	0.08-0.03i
0.025	85	1365.35	2.24	1.65	0.29	0.36-0.12i	5.81-14.42i	0.30-45.34i	0.08-0.03i
0.025	95	1369.65	2.25	1.85	0.31	0.36-0.12i	4.71-13.11i	0.30-40.59i	0.08-0.03i
0.025	105	1374.40	2.25	2.05	0.34	0.36-0.11i	3.92-12.03i	0.30-36.82i	0.08-0.03i
0.025	115	1379.60	2.26	2.25	0.37	0.36-0.11i	3.32-11.14i	0.30-33.75i	0.08-0.03i
0.025	125	1385.24	2.27	2.44	0.40	0.36-0.11i	2.87-10.39i	0.30-31.21i	0.08-0.03i
0.025	135	1391.31	2.27	2.64	0.42	0.36-0.11i	2.52-9.76i	0.30-29.08i	0.08-0.03i
0.025	145	1397.80	2.28	2.84	0.45	0.36-0.12i	2.24-9.22i	0.30-27.26i	0.08-0.03i
0.025	155	1404.71	2.29	3.03	0.48	0.36-0.12i	2.01-8.75i	0.30-25.69i	0.08-0.03i
0.025	165	1412.03	2.30	3.22	0.51	0.36-0.12i	1.82-8.34i	0.30-24.34i	0.08-0.03i
0.025	175	1419.75	2.31	3.42	0.54	0.36-0.12i	1.67-7.99i	0.30-23.15i	0.08-0.03i

Table E.1 (continued)

Pr	$\mathcal{T}$	Ra_c	k_c	ω	v_g	σ	λ_a	λ_b	δ
0.025	185	1427.85	2.32	3.61	0.57	0.37-0.12i	1.54-7.68i	0.30-22.10i	0.08-0.03i
0.025	195	1436.34	2.33	3.80	0.60	0.37-0.13i	1.43-7.41i	0.30-21.17i	0.08-0.03i
0.025	205	1445.19	2.34	3.99	0.63	0.37-0.13i	1.33-7.16i	0.30-20.34i	0.08-0.03i
0.025	215	1454.41	2.35	4.18	0.65	0.37-0.13i	1.25-6.95i	0.30-19.60i	0.08-0.03i
0.025	225	1463.98	2.36	4.37	0.68	0.37-0.14i	1.18-6.76i	0.30-18.93i	0.08-0.03i
0.025	235	1473.89	2.37	4.56	0.71	0.37-0.14i	1.12-6.59i	0.30-18.33i	0.08-0.03i
0.025	245	1484.14	2.38	4.75	0.74	0.37-0.14i	1.07-6.43i	0.31-17.78i	0.08-0.03i
0.025	255	1494.71	2.39	4.93	0.77	0.37-0.15i	1.02-6.30i	0.31-17.28i	0.08-0.03i
0.025	265	1505.60	2.40	5.12	0.80	0.38-0.15i	0.98-6.17i	0.31-16.83i	0.07-0.03i
0.025	275	1516.79	2.42	5.30	0.83	0.38-0.15i	0.94-6.06i	0.31-16.41i	0.07-0.04i
0.025	285	1528.29	2.43	5.48	0.86	0.38-0.16i	0.91-5.96i	0.31-16.03i	0.07-0.04i
0.025	295	1540.07	2.44	5.67	0.89	0.38-0.16i	0.88-5.87i	0.31-15.68i	0.07-0.04i
0.001	100	1316.38	2.22	0.08	0.01	0.01-0.00i	92.01-292.30i	0.01-910.83i	0.00-0.00i
0.016	100	1346.09	2.23	1.26	0.21	0.23-0.06i	6.19-18.90i	0.19-58.62i	0.05-0.02i
0.031	100	1392.34	2.27	2.39	0.40	0.44-0.16i	3.67-10.42i	0.36-31.86i	0.10-0.04i

Table E.1 (continued)

Pr	$\mathcal{T}$	Ra_c	k_c	ω	v_g	σ	λ_a	λ_b	δ
0.046	100	1453.17	2.31	3.47	0.59	0.65-0.28i	2.97-7.68i	0.53-23.01i	0.14-0.07i
0.061	100	1526.41	2.37	4.48	0.78	0.86-0.43i	2.76-6.44i	0.71-18.82i	0.17-0.10i
0.076	100	1609.97	2.43	5.44	0.96	1.08-0.60i	2.75-5.79i	0.88-16.52i	0.21-0.13i
0.091	100	1702.03	2.50	6.33	1.14	1.31-0.80i	2.86-5.43i	1.06-15.15i	0.24-0.17i
0.106	100	1801.08	2.57	7.17	1.32	1.55-1.02i	3.04-5.23i	1.24-14.31i	0.27-0.21i
0.121	100	1905.91	2.64	7.95	1.49	1.80-1.27i	3.27-5.13i	1.43-13.79i	0.30-0.25i
0.136	100	2015.56	2.71	8.68	1.66	2.06-1.54i	3.55-5.08i	1.62-13.48i	0.34-0.29i
0.151	100	2129.27	2.77	9.35	1.83	2.33-1.83i	3.85-5.07i	1.82-13.32i	0.37-0.33i
0.166	100	2246.43	2.84	9.99	2.00	2.61-2.14i	4.17-5.07i	2.03-13.26i	0.40-0.38i
0.181	100	2366.56	2.90	10.57	2.17	2.91-2.47i	4.52-5.08i	2.24-13.29i	0.43-0.42i
0.196	100	2489.28	2.96	11.11	2.34	3.21-2.83i	4.89-5.10i	2.46-13.38i	0.46-0.47i
0.211	100	2614.26	3.02	11.62	2.50	3.52-3.21i	5.27-5.12i	2.68-13.52i	0.49-0.52i
0.226	100	2741.25	3.07	12.08	2.67	3.85-3.61i	5.67-5.13i	2.91-13.70i	0.52-0.56i
0.241	100	2870.02	3.12	12.50	2.84	4.18-4.03i	6.07-5.14i	3.14-13.92i	0.55-0.61i
0.256	100	3000.40	3.18	12.88	3.02	4.52-4.48i	6.49-5.13i	3.38-14.18i	0.59-0.66i

Table E.1 (continued)

Pr	$\mathcal{T}$	Ra_c	k_c	ω	v_g	σ	λ_a	λ_b	δ
0.271	100	3132.24	3.22	13.23	3.19	4.87-4.95i	6.92-5.12i	3.62-14.47i	0.62-0.71i
0.286	100	3265.39	3.27	13.54	3.37	5.23-5.45i	7.35-5.10i	3.87-14.78i	0.65-0.77i
0.301	100	3399.76	3.32	13.81	3.56	5.60-5.98i	7.79-5.06i	4.12-15.13i	0.69-0.82i
0.316	100	3535.23	3.36	14.05	3.75	5.97-6.54i	8.23-5.01i	4.38-15.50i	0.72-0.88i
0.331	100	3671.73	3.40	14.25	3.94	6.35-7.12i	8.67-4.94i	4.64-15.91i	0.76-0.93i
0.346	100	3809.18	3.44	14.42	4.15	6.74-7.75i	9.12-4.86i	4.90-16.34i	0.79-0.99i
0.361	100	3947.51	3.48	14.55	4.36	7.14-8.40i	9.57-4.77i	5.17-16.81i	0.83-1.06i
0.376	100	4086.67	3.52	14.64	4.58	7.55-9.10i	10.01-4.66i	5.45-17.31i	0.87-1.12i
0.391	100	4226.59	3.55	14.70	4.82	7.96-9.84i	10.46-4.54i	5.73-17.86i	0.90-1.19i
0.406	100	4367.24	3.59	14.72	5.07	8.38-10.63i	10.90-4.40i	6.01-18.44i	0.94-1.26i
0.421	100	4508.57	3.62	14.71	5.33	8.80-11.48i	11.33-4.24i	6.29-19.07i	0.98-1.33i
0.436	100	4650.53	3.66	14.65	5.61	9.24-12.38i	11.76-4.07i	6.58-19.76i	1.03-1.41i
0.451	100	4793.11	3.69	14.55	5.91	9.68-13.36i	12.19-3.89i	6.87-20.51i	1.07-1.49i
0.466	100	4936.25	3.72	14.41	6.24	10.12-14.42i	12.60-3.69i	7.17-21.33i	1.11-1.57i
0.481	100	5079.93	3.75	14.23	6.60	10.57-15.57i	13.00-3.47i	7.47-22.23i	1.16-1.66i

APPENDIX F

CRITICAL VALUES FOR LANGMUIR CIRCULATIONS WITH THERMAL EFFECTS

Table F.1: Critical values for Langmuir circulation formation with Pr = 1, Ek = 1, $U_s(0) = 11.6$. When more than two sets of values for a given Rayleigh number is given, the first set of values has a tolerance of 10^{-4} and the second 10^{-8}. All cases with variations in latitude or wind direction have a tolerance of 10^{-6}.

ψ	ϕ	Ra	Re_c	k_x	k_y	ω
90	0	0	4.53	0.66	1.91	3.56
90	0	-0.1	4.53	0.66	1.90	3.54
90	0	-1	4.53	0.66	1.90	3.57
90	0	-1	4.53	0.67	1.92	3.56
90	0	-10	4.54	0.66	1.90	3.57
90	0	-100	4.63	0.64	1.86	3.49
90	0	-500	4.98	0.58	1.74	3.41
90	0	-500	4.98	0.59	1.74	3.39
90	0	-1000	5.33	0.54	1.63	3.35
90	0	-1500	5.62	0.50	1.56	3.33
90	0	-2000	5.86	0.47	1.49	3.30
90	0	-2000	5.86	0.47	1.50	3.31
90	0	-2500	6.07	0.45	1.45	3.28
90	0	-3000	6.26	0.44	1.43	3.35
90	0	-3500	6.43	0.43	1.41	3.35
90	0	-3500	6.43	0.42	1.40	3.34
90	0	-4000	6.59	0.42	1.39	3.35
90	0	-4500	6.74	0.41	1.37	3.40
90	0	-5000	6.87	0.40	1.38	3.50
90	0	-5000	6.87	0.40	1.37	3.47
90	0	-5500	7.00	0.40	1.35	3.42
90	0	-6000	7.12	0.39	1.35	3.51
90	0	-6500	7.23	0.39	1.35	3.54
90	0	-6500	7.23	0.39	1.34	3.54
90	0	-7000	7.34	0.39	1.37	3.66

Table F.1 (continued)

ψ	ϕ	Ra	Re_c	k_x	k_y	ω
90	0	-7500	7.44	0.38	1.33	3.58
90	0	-8000	7.54	0.38	1.33	3.62
90	0	-8500	7.63	0.38	1.33	3.64
90	0	-9000	7.72	0.37	1.32	3.66
90	0	-9500	7.80	0.37	1.33	3.73
90	0	-9500	7.80	0.38	1.36	3.80
90	0	-10000	7.89	0.37	1.33	3.76
90	0	-10500	7.96	0.37	1.33	3.79
90	0	-11000	8.04	0.38	1.35	3.89
90	0	-11000	8.04	0.37	1.34	3.83
90	0	-11500	8.12	0.38	1.35	3.89
90	0	-12000	8.19	0.37	1.34	3.91
90	0	-12500	8.26	0.37	1.34	3.92
90	0	-13000	8.32	0.38	1.37	4.07
90	0	-13500	8.39	0.38	1.40	4.17
90	0	-14000	8.45	0.38	1.39	4.12
90	0	-14500	8.51	0.38	1.37	4.12
90	0	-15000	8.57	0.37	1.36	4.11
90	0	-15500	8.63	0.37	1.36	4.12
90	0	-16000	8.69	0.37	1.36	4.13
90	0	-16500	8.75	0.38	1.38	4.22
90	0	-17000	8.80	0.38	1.40	4.34
90	0	-17500	8.85	0.39	1.42	4.37
90	0	-18000	8.91	0.38	1.40	4.36

Table F.1 (continued)

ψ	ϕ	Ra	Re_c	k_x	k_y	ω
90	0	-18500	8.96	0.37	1.38	4.31
90	0	-19000	9.01	0.37	1.37	4.30
90	0	-19500	9.06	0.37	1.37	4.33
90	0	-20000	9.10	0.37	1.38	4.37
45	0	-8000	7.47	0.38	1.34	3.65
45	30	-8000	7.47	0.38	1.34	3.63
45	60	-8000	7.49	0.38	1.33	3.61
45	90	-8000	7.52	0.38	1.33	3.59
45	120	-8000	7.55	0.38	1.33	3.65
45	150	-8000	7.59	0.39	1.35	3.67
45	180	-8000	7.61	0.39	1.35	3.62
45	210	-8000	7.61	0.38	1.33	3.65
45	240	-8000	7.59	0.38	1.34	3.68
45	270	-8000	7.56	0.38	1.34	3.67
45	300	-8000	7.52	0.38	1.34	3.67
45	360	-8000	7.47	0.38	1.34	3.65
67.5	0	-8000	7.51	0.37	1.32	3.61
45	0	-8000	7.47	0.38	1.34	3.63
22.5	0	-8000	7.38	0.38	1.36	3.70
10	0	-8000	7.20	0.37	1.35	3.66
5	0	-8000	6.99	0.37	1.46	4.08

BIBLIOGRAPHY

[1] Kapil M. S. Bajaj, Guenter Ahlers, and Werner Pesch. Rayleigh-Bénard convection with rotation at small Prandtl numbers. *Physical Review E*, 65:056309, 2002.

[2] Kapil M. S. Bajaj, Jun Liu, Brian Naberhuis, and Guenter Ahlers. Square patterns in Rayleigh-Bénard convection with rotation about a vertical axis. *Physical Review Letters*, 81(4):806–809, 1998.

[3] Andrew J. Bernoff. Finite amplitude convection between stress-free boundaries: Ginzburg-Landau equations and modulation theory. *European Journal of Applied Mathematics*, 5:267–282, 1994.

[4] M. Bestehorn, R. Friedrich, and H. Haken. The oscillatory instability of a spatially homogeneous state in large aspect ratio systems of fluid dynamics. *Zeitschrift für Physik B*, 72:265–275, 1988.

[5] Rajesh Bhaskaran and Sidney Leibovich. Eulerian and Lagrangian Langmuir circulation patterns. *Physics of Fluids*, 14(7):2557–2571, 2002.

[6] Eberhard Bodenschatz, Werner Pesch, and Guenter Ahlers. Recent developments in Rayleigh-Bénard convection. *Annual Review of Fluid Mechanics*, 32:709–776, 2000.

[7] Helmut R. Brand, Peter S. Lomdahl, and Alan C. Newell. Benjamin-Feir turbulence in convective binary fluid mixtures. *Physica D*, 23:345–361, 1986.

[8] Helmut R. Brand, Peter S. Lomdahl, and Alan C. Newell. Evolution of the order parameter in situations with broken rotational symmetry. *Physics Letters A*, 118(2):67–73, 1986.

[9] F. H. Busse and E. W. Bolton. Instabilities of convection rolls with stress-free boundaries near threshold. *Journal of Fluid Mechanics*, 146:115–125, 1984.

[10] S. Chandrasekhar. The instability of a layer of fluid heated below and subject to Coriolis forces. *Proceedings of the Royal Society A*, 217:306–27, 1953.

[11] S. Chandrasekhar. *Hydrodynamic and Hydromagnetic Stability*. Oxford University Press, Oxford, 1961. Republished in 1981 by Dover Publications, Inc., New York.

[12] S. Chandrasekhar and Donna D. Elbert. The instability of a layer of fluid heated below and subject to Coriolis forces II. *Proceedings of the Royal Society A*, 231:198–210, 1955.

[13] K.-H. Chiam, M. R. Paul, M. C. Cross, and H. S. Greenside. Mean flow and spiral defect chaos in Rayleigh-Bénard convection. *Physical Review E*, 67:056206, 2003.

[14] T. Clune. Unpublished description of calculations done using the Mathematica package "Pattern Selection". 1993.

[15] Thomas Clune and Edgar Knobloch. Pattern selection in rotating convection with experimental boundary conditions. *Physical Review E*, 47(4):2536–2550, 1993.

[16] S. M. Cox and S. Leibovich. Langmuir circulations in a surface layer bounded by a strong thermocline. *Journal of Physical Oceanography*, 23:1330–1345, 1993.

[17] S. M. Cox and P. C. Matthews. New instabilities in two-dimensional rotating convection and magnetoconvection. *Physica D*, 149:210–229, 2001.

[18] Stephen M. Cox, Sidney Leibovich, Irene M. Moroz, and Amit Tandon. Hopf bifurcations in Langmuir circulations. *Physica D*, 59:226–254, 1992.

[19] Stephen M. Cox, Sidney Leibovich, Irene M. Moroz, and Amit Tandon. Nonlinear dynamics in Langmuir circulations with O(2) symmetry. *Journal of Fluid Mechanics*, 241:669–704, 1992.

[20] A. D. D. Craik and S. Leibovich. A rational model for Langmuir circulations. *Journal of Fluid Mechanics*, 73(3):401–426, 1976.

[21] M. C. Cross and P. C. Hohenberg. Pattern formation outside of equilibrium. *Reviews of Modern Physics*, 65(3):851–1112, 1993.

[22] M. C. Cross and Alan C. Newell. Convection patterns in large aspect ratio systems. *Physica D*, 10:299–328, 1984.

[23] A. Davey, L. M. Hocking, and K. Stewartson. On the nonlinear evolution of three-dimensional disturbances in plane Poiseuille flow. *Journal of Fluid Mechanics*, 63(3):529–536, 1974.

[24] W. Decker and W. Pesch. Order parameter and amplitude equations for the Rayleigh-Bénard convection. *Journal de Physique II (France)*, 4:419–438, 1994.

[25] V. W. Ekman. On the influence of the Earth's rotation on ocean currents. *Arkiv für Matematik, Astronomi och Fysik*, 2:1–53, 1905.

[26] The Engineering Tool Box. Online resource, 2005. http://www.engineeringtoolbox.com/water-thermal-properties-d_162.html.

[27] A. J. Faller. Oceanic turbulence and the Langmuir circulations. *Annual Review of Ecology and Systematics*, 2:201–236, 1971.

[28] David Farmer and Ming Li. Patterns of bubble clouds organized by Langmuir circulation. *Journal of Physical Oceanography*, 25:1426–1440, 1995.

[29] Anand Gnanadesikan and Robert A. Weller. Structure and instability of the Ekman spiral in the presence of surface gravity waves. *Journal of Physical Oceanography*, 25:3148–3171, December 1995.

[30] Thomas Michael Haeusser. *Pattern formation in the oceanic Ekman-Langmuir layer*. PhD thesis, Cornell University, 1998.

[31] Dennis L. Hartmann. *Global Physical Climatology*, volume 56 of *International Geophysics*. Academic Press, San Diego, 1994.

[32] Martin van Hecke and Wim van Saarloos. Convection in rotating annuli: Ginzburg-Landau equation with tunable coefficients. *Physical Review E*, 55(2):R1259–R1262, 1997.

[33] Yuchou Hu, Robert E. Ecke, and Guenter Ahlers. Behavior of focus patterns in low Prandtl number convection. *Physical Review Letters*, 72(14):2191–2194, 1994.

[34] Yuchou Hu, Robert E. Ecke, and Guenter Ahlers. Convection under rotation for Prandtl numbers near 1: Linear stability, wave-number selection, and pattern dynamics. *Physical Review E*, 55(6):6928–6949, 1997.

[35] N. E. Huang. Surface drift currents in the ocean. *Journal of Fluid Mechanics*, 91:191–208, March 1979.

[36] Daniel D. Joseph. *Stability of Fluid Motions I*, volume 27 of *Springer Tracts in Natural Philosophy*. Springer-Verlag, New York, 1976.

[37] Koichi Kakimoto. Heat and mass transfer in semiconductor melts during single-crystal growth processes. *Journal of Applied Physics*, 77:1827–1842, 1995.

[38] A. Birl Kara, Peter A. Rochford, and Harley E. Hurlburt. An optimal definition for ocean mixed layer depth. *Journal of Geophysical Research*, 105(C7):16803–16821, July 2000.

[39] Kern E. Kenyon. Stokes drift for random gravity waves. *Journal of Geophysical Research*, 74(28):6991–6994, December 1969.

[40] E. Knobloch. Doubly diffusive waves. In N. E. Bixler and E. Spiegel, editors, *Double Diffusive Motions*, Joint ASCE/ASME Mechanics Conference, pages 17–25, Albuquerque, New Mexico, June 1985. Fluids Engineering Division, American Society of Mechanical Engineers.

[41] E. Knobloch and J. De Luca. Amplitude equations for travelling wave convection. *Nonlinearity*, 3:975–980, 1990.

[42] G. Küppers and D. Lortz. Transition from laminar convection to thermal turbulence in a rotating fluid layer. *Journal of Fluid Mechanics*, 35(3):609–620, 1969.

[43] L.D. Landau. On the problem of turbulence. *Comptes rendus de l'Académie des Sciences de l'U.R.S.S.*, 44:311–14, 1944. Reprinted in *Collected Papers*, edited by D. Ter Haar. Gordon and Breach, Science Publishers, New York, 1965. Pages 387–91.

[44] Irving Langmuir. Surface motion of water induced by wind. *Science*, 87(2250):119–123, 1938.

[45] S. Leibovich. Langmuir circulation and instability. In *Encyclopedia of Ocean Science*, pages 1453–1461. Academic Press, San Diego, 2001.

[46] S. Leibovich and G. Yang. Turbulent flow in natural water bodies driven by wind and surface waves. Unpublished manuscript, October 1996.

[47] Sidney Leibovich. The form and dynamics of Langmuir circulations. *Annual Review of Fluid Mechanics*, 15:391–427, 1983.

[48] Sidney Leibovich and Amit Tandon. Three-dimensional Langmuir circulation instability in a stratified layer. *Journal of Geophysical Research*, 98(C9):16501–16507, 1993.

[49] Ming Li and Chris Garrett. Is Langmuir circulation driven by surface waves or surface cooling? *Journal of Physical Oceanography*, 25:64–76, 1995.

[50] Yuanming Liu and Robert E. Ecke. Eckhaus-Benjamin-Feir instability in rotating convection. *Physical Review Letters*, 78(23):4391–4394, 1997.

[51] Carlos Martel, Edgar Knobloch, and José M. Vega. Dynamics of counter-propagating waves in parametrically forced systems. *Physica D*, 137:94–123, 2000.

[52] B. J. Matkowsky and V. Volpert. Stability of plane wave solutions of complex Ginzburg-Landau equations. *Quarterly of Applied Mathematics*, 51(2):265–281, June 1993.

[53] Alan C. Newell and J. A. Whitehead. Finite bandwidth, finite amplitude convection. *Journal of Fluid Mechanics*, 38(2):279–303, 1969.

[54] O. M. Phillips. *The Dynamics of the Upper Ocean*. Cambridge University Press, Cambridge, second edition, 1977.

[55] Willard J. Pierson, Jr. and Lionel Moskowitz. A proposed spectral form for fully developed wind seas based on the similarity theory of S. A. Kitaigorodskii. *Journal of Geophysical Research*, 69(4):5181–5190, December 1964.

[56] R. T. Pollard. Observations and theories of Langmuir circulations and their role in near surface mixing. In Martin Angel, editor, *A Voyage of Discovery: George Deacon 70th Anniversary Volume*, pages 235–251. Pergamon Press, Oxford, 1977.

[57] M. Revallo and D. Ševčovič. On the Ginzburg-Landau system of complex modulation equations for a rotating annulus with radial magnetical field. *Physica D*, 161:116–128, 2002.

[58] Hermann Riecke and Lorenz Kramer. The stability of standing waves with small group velocity. *Physica D*, 137:124–142, 2000.

[59] J. J. Sánchez-Álvarez, E. Serre, E. Crespo del Arco, and F. H. Busse.

Square patterns in rotating Rayleigh-Bénard convection. *Physical Review E*, 72:036307, 2005.

[60] J. D. Scheel. The amplitude equation for rotating Rayleigh-Bénard convection. *Physics of Fluids*, 19:104105, 2007.

[61] L. A. Segel. Distant side-walls cause slow amplitude modulation of cellular convection. *Journal of Fluid Mechanics*, 38:203–224, 1969.

[62] Lawrence F. Shampine, Jacek Kierzenka, and Mark W. Reichelt. Solving boundary value problems for ordinary differential equations in Matlab with bvp4c. October 2000. Available from the Mathworks website, http://www.mathworks.com/.

[63] Eric D. Siggia and Annette Zippelius. Pattern selection in Rayleigh-Bénard convection near threshold. *Physical Review Letters*, 47(2):835–839, 1981.

[64] G. G. Stokes. On the theory of oscillatory waves. *Transactions of the Cambridge Philosophical Society*, 8:441–455, 1849. Reprinted with additional notes in Stokes, George Gabriel, *Mathematical and Physical Papers*, volume 1. Cambridge University Press, Cambridge, 1880-1905.

[65] John William Strutt (Baron Rayleigh). On convection currents in a horizontal layer of fluid, when the higher temperature is on the under side. *Philosophical Magazine*, 32:529–546, 1916. Reprinted in *Scientific Papers*, Volume VI (1911–1919). Cambridge University Press, Cambridge, 1920.

[66] S. A. Thorpe. Langmuir circulation. *Annual Review of Fluid Mechanics*, 36:55–79, 2004.

[67] M. van Hecke. Unpublished calculation details.

[68] Martin van Hecke, Cornelis Storm, and Wim van Saarloos. Sources, sinks and wavenumber selection in coupled CGL equations and experimental implications for counter-propagating wave systems. *Physica D*, 134:1–47, 1999.

[69] José Eduardo Wesfried. Scientific biography of Henri Bénard (1874–1939). In *Dynamics of Spatio-Temporal Cellular Structures: Henri Bénard Centenary Review*, volume 207 of *Springer Tracts in Modern Physics*, pages 9–37. Springer Verlag, 2006.

[70] Virginia Westervelt. *Incredible Man of Science*. Simon & Schuster, Inc., New York, 1968.

[71] Wayne Wurtsbaugh. Langmuir streaks on Quake Lake, Montana. ASLO Image Library, http://www.aslo.org/photopost/index.php, September 2004.

[72] Yuan-Nan Young and Hermann Riecke. Mean flow in hexagonal convection: stability and nonlinear dynamics. *Physica D*, 163:166–183, 2002.

[73] Annette Zippelius and Eric D. Siggia. Stability of finite-amplitude convection. *Physics of Fluids*, 26(10):2905–2915, October 1983.